April 2018

Extending Spectrophotometric pHT Measurements in Coastal and Estuarine Environments

Nora Katherine Douglas
University of South Florida, noradouglas@mail.usf.edu

Extending Spectrophotometric pH_T Measurements in Coastal and Estuarine Environments

by

Nora K. Douglas

A dissertation submitted in partial fulfillment
of the requirements for the degree of
Doctor of Philosophy
College of Marine Science
University of South Florida

Major Professor: Robert H. Byrne, Ph.D.
Kristen N. Buck, Ph.D.
Richard A. Feely, Ph.D.
Pamela Hallock Muller, Ph.D.
Lisa L. Robbins, Ph.D.

Date of Approval:
April 5, 2018

Keywords: m-cresol purple, thymol blue, cresol red, indicator impurities, internal consistency

ACKNOWLEDGMENTS

I have been fortunate to work with a group of dedicated and talented scientists during the course of my graduate work, and my heartfelt gratitude is due each of them for the help they have given me and for making me a better scientist.

Foremost, I must thank my major professor, Dr. Robert Byrne, for taking me on as a student and advising me over the last six years. I am especially grateful for his guidance during latter part of my dissertation work, which I completed while working remotely and for which he possessed what I can only describe as a saint-like amount of patience. Thanks are also due to my dissertation committee: Dr. Kristen Buck, Dr. Richard Feely, Dr. Pamela Hallock Muller, and Dr. Lisa Robbins, for their insights and counsel throughout my doctoral work.

My graduate work would not have been possible without financial support from a University of South Florida Presidential Doctoral Fellowship through the Office of Graduate Studies. My work was also supported by two National Science Foundation grants, OCE 1220110 and OCE 1657894.

I am greatly indebted to the following Byrne lab personnel, past and present, for their technical expertise, training, assistance, and advice: Dr. Xuewu (Sherwood) Liu, Dr. Lori Adornato, Dr. James Patten, Dr. Kelly Quinn Deister, Dr. Mark Patsavas, Dr. Regina Easley, Dr. Bo Yang, Ms. Dominika Wojcieszek, Ms. Erin Cuyler, and Mr. Jon Sharp.

Dr. Tonya Clayton has given many hours of time to manuscript edits of Chapters Two and Three of this dissertation. For her helpful editorial comments, I am grateful, and I know that these chapters are far better because of her help.

During the course of my Ph.D. work, I was able to participate in the 2013 and 2016 NOAA West Coast Ocean Acidification cruises aboard the NOAA Ship *Fairweather*, *R/V Pt. Sur*, and NOAA Ship *Ronald H. Brown*. My thanks is given to the crews of these vessels, as well as to the chief scientists – Dr. Richard Feely, Dr. Adrienne Sutton, Mr. Dana Greeley, Dr. Simone Alin, and Mr. Julian Herndon – and scientific parties of both cruises. I would also like to thank Dr. Jessica Cross, whom I met during the 2013 cruise and who has become a good friend and mentor since then, as well as a great advocate for women in science.

My thanks are also due to the faculty and staff of the USF College of Marine Science, for all their efforts to train, teach, guide, and support students along the path toward scientific careers.

Less formally, I would like to thank Mr. John Gray and Ms. Jennifer Brizzolara for their generous hospitality at various times throughout the last two years. Additionally, I am grateful for all the friendships I have developed during my time at USF, especially with those in my incoming cohort from 2012. One of the greatest lessons I have learned in the last six years is the value of such a support network.

Finally, I must thank Jeremy Walch, James and Sue Douglas, and Jerry and Amy Walch for their boundless love and encouragement.

TABLE OF CONTENTS

LIST OF TABLES

LIST OF FIGURES

ABSTRACT

Nearshore and estuarine environments play a vital role in the cycling of carbon, but the effects of ocean acidification in estuarine waters have not been studied as extensively as in the open ocean. One reason for this is the limitation of pH measurement capabilities in low-salinity waters. Typically, pH in these environments has been measured using potentiometric methods that are subject to uncertainties on the order of 0.01. Spectrophotometric methods for measuring pH_T offer precision and accuracy superior to those of potentiometric methods. However, previous characterizations for purified sulfonephthalein indicators, used for marine spectrophotometric measurements, are not applicable to estuarine salinities. Some estuarine datasets using unpurified indicators exist, but the presence of dye impurities affects the accuracy of these characterizations. Colorimetric impurities are known to interfere with absorbance measurements and can cause errors in pH on the order of 0.02.

In this work, a mathematical model has been developed to correct spectrophotometric pH_T determined with unpurified m-Cresol Purple (mCP), the indicator used most widely for these measurements. The model accounts for absorbances of colorimetric impurities that interfere with absorbance by mCP. This corrective approach brings measurements made using unpurified mCP in synthetic solutions of 0.7 M NaCl into better agreement with those made using purified mCP: within ±0.004 pH units for all six indicators tested at $pH_T \leq 8.0$. The model is useful for both (a) research groups currently using unpurified mCP to measure pH_T, and (b) retrospective correction of historic pH_T datasets collected using unpurified mCP. The correction

requires only that a small sample of the unpurified mCP is saved for a single-point test at high pH_T (~12), and that historic absorbance measurements are archived for subsequent correction.

The principles of the corrective model were applied to an historic calibration of the mCP dissociation constant (K_I) at $0 \leq S \leq 40$ and $T = 298.15$ K using unpurified indicator. After correction of absorbances for dye impurities, recalculation of K_I was performed, and the recalculated values were combined with mCP K_I data for freshwater and seawater. The combined dataset was then refitted as a function of S and T. The resulting model is representative of mCP behavior across $0 \leq S \leq 40$ and $278.15 \leq T \leq 308.15$ K and produces $p(K_I e_2)$ values that are within ±0.004 of $p(K_I e_2)$ values from previously published purified mCP calibrations.

This refitting approach was also applied to pH_T determinations made with Thymol Blue (TB) and Cresol Red (CR), two sulfonephthalein indicators that have been previously used in waters outside the indicating range of mCP. The models, which were of the same form as the estuarine $p(K_I e_2)$ model for mCP, performed approximately as well as the mCP model: with the exception of one high-salinity, high-temperature TB datum, all residuals were within ±0.0043 of the previously published TB and CR calibrations.

Finally, an internal consistency analysis was performed using carbon chemistry data collected during two recent coastal ocean acidification research cruises. For pH_T measurements performed during both cruises, purified mCP was used, and corresponding measurements of total alkalinity (TA) and dissolved inorganic carbon (DIC) were conducted. Both cruises included excursions into the Columbia River, where low salinities prevent usage of the marine $p(K_I e_2)$ model for purified mCP. The Columbia River samples provided the opportunity to evaluate the internal consistency of pH_T measurements made in low-salinity waters using the refitted estuarine $p(K_I e_2)$ model. Although internal consistency agreement in the estuarine range is poor

compared to marine measurements, pH_T calculated using the new estuarine model compared well with pH_T calculated using the previously published estuarine mCP model. The poor internal consistency in the estuarine range, even when making state-of-the-art pH measurements, points toward the need for a more robust characterization of the carbonic acid dissociation constants in the estuarine salinity range. This characterization should take into account the contributions of organic acids to total alkalinity in nearshore waters.

CHAPTER ONE:

INTRODUCTION

1.1 Ocean Acidification: A Coastal and Estuarine Issue

Since the beginning of the Industrial Revolution around the year 1750, concentrations of atmospheric CO_2 have risen from 280 ppmv to more than 400 ppmv today [1]; this equates to an increase in the atmospheric carbon reservoir of 240 ± 10 Pg C (1 Pg C = 10^{15} g C) [1]. The global oceans have taken up about 30% of the CO_2 emitted during this time, increasing the oceanic carbon reservoir by 155 ± 30 Pg C (~0.41% of the pre-industrial oceanic carbon reservoir of 38,000 Pg C) [2–4]. Oceanic uptake mitigates the increase in atmospheric CO_2 concentrations. Unlike other atmospheric gases that simply remain in the dissolved gaseous state when exchanged with the oceans, CO_2 reacts with seawater and forms bicarbonate ion (HCO_3^-) and carbonate ion (CO_3^{2-}). These reactions produce hydrogen ions (H^+) and reduce the pH of the oceans, a process called ocean acidification (OA). Since the pre-industrial era, the pH of the oceans has decreased by 0.11, equivalent to a 26% increase in the hydrogen ion concentration, [H^+] [5–7]. In surface waters, pH is dropping at a rate of 0.0014 – 0.0024 yr^{-1} [5,8–14], while atmospheric CO_2 concentrations are increasing by ~2 ppm yr^{-1} [2].

The pH of the global surface ocean today is around 8.1 [5–7]; emission and mitigation of anthropogenic CO_2 will dictate the pH of the future oceans. Depending on the emissions and mitigation strategies employed now and into the coming decades, projected surface ocean pH at

the end of this century will be reduced by an additional 0.06–0.32 from recent (1985–2005) values [2,15].

Ocean acidification has deleterious effects on coastal and marine organisms, as lower-pH waters are less suited for calcifying organisms, many of which underpin marine ecosystems. Coastal environments, which include bays and estuaries where salinities may be lower than in the open ocean, are important not only for marine organisms, but also for human activity. These environments are centers of commercial and recreational fisheries, tourism, and transportation around the world. It is therefore important that these environments are monitored for changes in carbon chemistry in order to predict and prepare for ecological, economic, and cultural impacts.

Coastal environments are much more heterogeneous than the open ocean; as such, coastal environments need accurate, precise monitoring. Differences in physical oceanography (e.g., salinity, temperature, and pressure regimes; localized circulation patterns; upwelling or downwelling), geographic context (e.g., climate; tectonic regime; riverine inputs), and biological activity all differentiate coastal ecosystems from one another and the open ocean [16].

1.2 Marine CO_2 System Equilibrium

The addition of CO_2 to the atmosphere shifts the acid-base equilibrium of the oceans. When atmospheric CO_2 dissolves into the ocean, it partitions as follows [17]:

$$CO_{2\,(g)} \overset{K_0'}{\leftrightarrow} CO_2^* \tag{1.1}$$

where CO_2^* represents the combined concentrations of aqueous CO_2 and carbonic acid, H_2CO_3. H_2CO_3 is a minor species in the CO_2 equilibrium model, with a concentration <0.3% [16] that of dissolved CO_2 gas. K_0' is the Henry's Law constant for the dissolution of CO_2 into seawater and is defined as follows:

$$K_0' = \frac{[CO_2^*]}{f_{CO2}} \quad (1.2)$$

In Eq. (1.2), f_{CO2} is the CO_2 fugacity, a variable numerically very similar, but not identical, to the CO_2 partial pressure (see Section 1.3.3).

CO_2^* further reacts in seawater according to Eqs. (1.3) and (1.4), below:

$$CO_2^* \overset{K_1'}{\leftrightarrow} H^+ + HCO_3^- \quad (1.3)$$

$$HCO_3^- \overset{K_2'}{\leftrightarrow} H^+ + CO_3^{2-} \quad (1.4)$$

where the constants K_1' and K_2' are given according to Eqs. (1.5) and (1.6), respectively:

$$K_1' = \frac{[H^+]_T\,[HCO_3^-]_T}{[CO_2^*]} \quad (1.5)$$

$$K_2' = \frac{[H^+]_T\,[CO_3^{2-}]_T}{[HCO_3^-]_T} \quad (1.6)$$

where $[H^+]_T$, $[HCO_3^-]_T$, and $[CO_3^{2-}]_T$ represent the total concentrations of these ions. The equilibrium constants K_0', K_1', and K_2' have been parameterized by various research groups as functions of salinity (S), temperature (T), and pressure (P).

The marine CO_2 system equilibrium provides the primary buffer against dramatic changes in ocean acidity and enables the extensive oceanic uptake of CO_2. Dissolution of the $CaCO_3$ polymorphs aragonite and calcite, which are formed by calcifying organisms, can augment the marine supply of HCO_3^- and CO_3^{2-} according to the following reaction:

$$CaCO_{3\,(s)} \overset{K_{sp}'}{\leftrightarrow} Ca^{2+} + CO_3^{2-} \quad (1.7)$$

where K_{sp}' is the solubility product constant of either aragonite or calcite, defined according to Eq. (1.8):

$$K_{sp}' = [Ca^{2+}]_T\,[CO_3^{2-}]_T \quad (1.8)$$

The K_{sp}' values for aragonite and calcite differ from one another due to their differing solubilities; aragonite, the more soluble polymorph, has a K_{sp}' approximately 1.5 times that of calcite in seawater [16]. K_{sp}' for either polymorph is a function of salinity, temperature, and pressure. This difference of solubilities is due to structural differences in the crystal lattices of the two polymorphs and indicates that calcite-forming organisms are less susceptible than aragonite-forming organisms to shell dissolution in acidifying seawater. The corrosiveness of seawater with respect to either aragonite or calcite can be determined by calculating its saturation state (Ω), defined according to Eq. (1.9):

$$\Omega = \frac{[Ca^{2+}]_T\,[CO_3^{2-}]_T}{K_{sp}'} \tag{1.9}$$

Ω_A corresponds to the aragonite saturation state, calculated with the aragonite K_{sp}', and Ω_C corresponds to the calcite saturation state, calculated with the calcite K_{sp}'. For both polymorphs, the meaning of Ω is the same:

- Ω > 1 indicates that shell formation of that polymorph is thermodynamically favored.
- Ω < 1 indicates that shell dissolution of that polymorph is thermodynamically favored.
- Ω = 1 indicates that the water sample is at saturation with respect to that polymorph.

1.3 Marine CO_2 System Master Variables

To determine the state of the CO_2 system in a water sample, measurements of at least two of the following four CO_2 system master variables are required: dissolved inorganic carbon (DIC); total alkalinity (TA); CO_2 fugacity (f_{CO2}) or partial pressure (pCO_2); and pH. Thermodynamic relationships enable calculations of all other CO_2 system parameters from direct measurements of any pair of these four variables. Sections 1.3.1 to 1.3.4 describe the master variables in detail.

1.3.1 Dissolved Inorganic Carbon

Dissolved inorganic carbon (DIC, sometimes referred to as C_T, TCO_2, or ΣCO_2) is the sum of all inorganic carbon species in a seawater sample, defined as follows:

$$DIC = [CO_2{}^*] + [HCO_3^-]_T + [CO_3^{2-}]_T \quad (1.10)$$

DIC is considered a conservative quantity in seawater; it is unaffected by changes in temperature or pressure. However, it is highly affected by atmospheric exchange [17]. Typical oceanic DIC ranges from 1800–2300 μmol kg^{-1}, but it may be higher in localized environments [18]. DIC is measured coulometrically after acidifying with dilute H_3PO_4, which converts all carbonate species in solution to CO_2, and purging with N_2 gas. Accuracy and precision of ±1.5 μmol kg^{-1} are attainable using this method [18] and have been aided by the use of Certified Reference Materials (CRMs) distributed by the Dickson laboratory (UCSD-SIO) [19–21].

1.3.2 Total Alkalinity

Total alkalinity (TA, alternately referred to as A_T) is a quantitative measure of a water sample's acid-neutralizing capacity and is derived from titrations with strong acid. Like DIC, TA is a conservative quantity, independent of temperature and pressure. Unlike DIC and pH, TA is unaffected by gas exchange with the atmosphere. It is defined as the number of moles of protons equivalent to the excess of proton acceptors (conjugate bases of acids with $pK_a^0 \geq 4.5$ at T = 298.15 K) over proton donors (acids with $pK_a^0 < 4.5$ at T = 298.15 K) per kilogram of sample [21], where K_a^0 is the acid dissociation constant at zero ionic strength (i.e., in pure water). This relationship can be expressed mathematically as follows:

$$TA = [HCO_3^-]_T + 2[CO_3^{2-}]_T + [B(OH)_4^-]_T + [OH^-]_T + [HPO_4^{2-}]_T + 2[PO_4^{3-}]_T + [SiO(OH)_3{}^-]_T + [NH_3]_T + [HS^-]_T - [H^+]_f - [HSO_4^-]_T - [HF] - [H_3PO_4]_T + \cdots \quad (1.11)$$

The ellipsis in Eq. (1.11) represents minor species that can affect the alkalinity in a sample, such as dissolved organic matter (DOM) [23–26]. In the oligotrophic ocean, the assumption that minor organic species contribute negligibly to TA can generally be made, but in coastal, estuarine, and river water, organic alkalinity may be significant. Similarly, NH_3 and HS^- species may generally be neglected in the open ocean, but they become increasingly important contributors to TA in anoxic environments [18].

Typical seawater alkalinity is between 2000 and 2500 μmol kg^{-1} and can be measured using either closed-cell or open-cell titrimetric procedures [18]. During a titration, samples are acidified, and the pH is monitored either potentiometrically [18] or spectrophotometrically [26–30]. As with DIC, the use of CRMs promotes accurate measurements for TA; target accuracy and precision for TA measurements are ±3 μmol kg^{-1} [18].

1.3.3 CO_2 Partial Pressure and Fugacity

CO_2 partial pressure and fugacity (generally expressed in units of μatm) are two related parameters describing CO_2 gas concentrations for seawater samples. CO_2 partial pressure (pCO_2) refers to the pressure exerted by CO_2 in the gas phase that is in equilibrium with a seawater sample. pCO_2 is defined as follows:

$$pCO_2 = P \cdot xCO_2 \tag{1.12}$$

where P is the total pressure and the CO_2 mole fraction (xCO_2) is defined as the number of moles of CO_2 divided by the total moles of all gases in a mixture [17].

Partial pressure most appropriately describes ideal gases. Because CO_2 is a real gas that behaves non-ideally, CO_2 fugacity (f_{CO2}) is more appropriate to describe the behavior of CO_2 gas molecules. f_{CO2} takes into consideration attractions between gas molecules and any inelasticity of collisions between gas molecules [18,31]. For a given seawater sample, f_{CO2} will be slightly

smaller than pCO_2, but the difference between f_{CO2} and pCO_2 values is small when a gas mixture is dilute. Shipboard measurements of f_{CO2} and pCO_2 may be discrete or continuous, with analytical precisions of 10 and 2 μatm, respectively [18].

1.3.4 pH

Of greatest interest to the work in this dissertation is pH, described as a "master descriptive variable" [30] of the marine CO_2 system and defined generally in Eq. (1.13):

$$pH = -\log[H^+] \tag{1.13}$$

However, multiple pH scales exist for measurements in natural waters and are related in Eqs. (1.14) to (1.17), as follow in Table 1.1:

Table 1.1 pH scales used in the measurement of natural waters. Equations adapted from Zeebe and Wolf-Gladrow [16].

pH Scale	**Definition**	**Eq. #**
NBS	$pH_{NBS} = -\log a_{H^+}$	(1.14)
Free	$pH_f = -\log[H^+]_f$	(1.15)
Total	$pH_T = -\log[H^+]_T = -\log\left([H^+]_f + [HSO_4^-]_T\right)$	(1.16)
Seawater (SWS)	$pH_{SWS} = -\log\left([H^+]_f + [HSO_4^-]_T + [HF]\right)$	(1.17)

where a_{H+} is the hydrogen ion activity, $[H^+]_f$ is the free hydrogen ion concentration, $[H^+]_T$ is the total hydrogen ion concentration, [HF] is the hydrogen fluoride concentration, and $[HSO_4^-]_T$ is the total bisulfate ion concentration. Differences in pH scales are non-trivial for seawater measurements. Because pH_f is ~0.11 higher than pH_T and ~0.12 higher than pH_{SWS} for a typical seawater sample (S = 35, T = 298.15 K), pH measurements should always report the scale used for measurement [17]. For marine spectrophotometric pH analyses, the total scale is most frequently used [33–38], but much of the work performed by DeGrandpre and colleagues [39–

43] has measured spectrophotometric pH in freshwater on the free scale. When comparing pH measurements from multiple studies, is important to ensure that measurements are converted to the same scale [38].

pH measurements in natural waters may be performed using either (a) potentiometric electrodes, (b) ion-selective field effect transistors (ISFETs), or (c) spectrophotometric techniques. Potentiometric pH measurements using glass electrodes frequently involve calibrations on the NBS scale and offer a convenient means of measurement in real time. However, electrodes require frequent calibrations, and errors can arise due to liquid junction and asymmetry potentials [44]. Furthermore, the NBS scale is not generally well suited for seawater pH analyses and is more applicable in low-salinity environments. As such, precision of potentiometric pH measurements with glass electrodes is only about 0.01 [45].

ISFETs offer a useful alternative to glass electrodes for pH measurements in natural waters. Although ISFETs utilize the same principles of potentiometric methods, a high impedance amplifier provides improved precision [38,45–47]. Additionally, these sensors are more rugged than glass electrodes, require less frequent calibrations, and can be placed in the field for measurements over an extended period of time (on the order of multiple months [45). The Honeywell DuraFET sensor, the ISFET most often used in oceanography [48,49], has a short-term (on the order of hours) precision of 0.0005 and long-term (on the order of weeks to months) precision of 0.005 in a laboratory setting [46].

More precise than either glass electrodes or ISFETs, however, are spectrophotometric methodologies for measuring pH. Precision of spectrophotometric pH measurements is ±0.0004, with accuracies on the order of ±0.001. The principles underlying spectrophotometric pH measurements are discussed in Section 1.4.

1.4 Principles of Spectrophotometric pH Measurement

Spectrophotometric pH measurement methodologies for seawater were developed in the 1980s and 1990s [33,34,50,51] and have been subsequently refined with the use of purified indicators [36,37]. Samples are measured using a sulfonephthalein indicator, which behaves as a weak diprotic acid (H_2I) in solution and partitions as follows:

$$H_2I \overset{K_{I(1)}}{\longleftrightarrow} H^+ + HI^- \tag{1.18}$$

$$HI^- \overset{K_{I(2)}}{\longleftrightarrow} H^+ + I^{2-} \tag{1.19}$$

where $K_{I(1)}$ and $K_{I(2)}$ are the first and second dissociation constants for the indicator in solution. Because the first dissociation for sulfonephthalein indicators occurs at very low pH, virtually all of the indicator exists in its conjugate HI^- and I^{2-} forms, and considerations of H_2I and $K_{I(1)}$ can generally be excluded from analysis and calculations. Therefore, the remainder of this dissertation refers to $K_{I(2)}$ as simply K_I. K_I is defined as follows:

$$K_I = \frac{[H^+]_T\,[I^{2-}]_T}{[HI^-]_T} \tag{1.20}$$

The HI^- (acid) and I^{2-} (base) forms of sulfonephthalein indicators absorb at different wavelengths in the visible spectrum. The HI^- form absorbs strongly in the 430-440 nm range, while the I^{2-} form typically absorbs strongly in the 550–600 nm range. Measurements of absorbance can be made at the maximum-absorbing wavelengths (λ_1 and λ_2, for the acid and base peaks, respectively) for samples that have been injected with a sulfonephthalein indicator solution. The following relationships are then used to calculate pH:

$$e_1 = \frac{\lambda_2\varepsilon_{HI^-}}{\lambda_1\varepsilon_{HI^-}},\ e_2 = \frac{\lambda_2\varepsilon_{I^{2-}}}{\lambda_1\varepsilon_{HI^-}},\ e_3 = \frac{\lambda_1\varepsilon_{I^{2-}}}{\lambda_1\varepsilon_{HI^-}} \tag{1.21}$$

$$R = \frac{\lambda_2 A}{\lambda_1 A} \tag{1.22}$$

$$pH_T = -\log(K_I e_2) + \log\left(\frac{R - e_1}{1 - R\frac{e_3}{e_2}}\right) \quad (1.23)$$

where the e_x ratios are the ratios of the molar extinction coefficients (alternately referred to as the molar absorptivity coefficients) of the HI^- and I^{2-} indicator forms at λ_1 and λ_2, and ${}_{\lambda 1}A$ and ${}_{\lambda 2}A$ are the measured absorbances at the HI^- and I^{2-} peaks, respectively.

Because the indicator acts as a weak acid in solution, the equilibrium perturbation caused by the addition of indicator must also be accounted for. This can be done by sequential addition of indicator to a sample and regression of the resulting *R*-ratio [18].

1.5 Research Rationale

The major theme of this dissertation was to extend high-quality spectrophotometric pH_T models to estuarine and nearshore conditions where spectrophotometric models previously had not been well calibrated. The recent purification and characterization of the sulfonephthalein indicators m-Cresol Purple (mCP) [36,42,43,52] and Cresol Red (CR) [37,52] enable spectrophotometric pH_T models to be determined without systematic errors arising from impurity absorbances. However, historical measurements of spectrophotometric pH utilized unpurified indicators, and many research groups still make measurements with unpurified indicators. To improve measurements made with unpurified indicators, a corrective model was developed to account for impurity absorbances and was applied to a set of measurements made with unpurified mCP in synthetic solutions. This model was then applied to extant datasets measuring pH_T spectrophotometrically with unpurified indicators to correct for the contributions of impurities to absorbance measurements. Datasets were combined, and indicator thermodynamic behavior was reparameterized for applicability over temperate estuarine and marine conditions. Using absorbance measurements from two recent carbon cruises off the west coast of North

America, the reparameterized mCP model was used to evaluate the pH_T and CO_2 system internal consistency of the cruise datasets.

1.5.1 Improving Spectrophotometric pH_T Measurements Using Unpurified Indicators

Errors in spectrophotometric pH_T measurements can arise from the use of unpurified sulfonephthalein indicators [35,36,52–54]. The presence of colorimetric impurities spuriously increases the measured absorbance at the indicator's HI^- peak, resulting in a suppression of the calculated *R* and therefore the pH_T. Previous quantifications of this effect have found that colorimetric impurities can result in underestimations in pH_T on the order of 0.02 at pH ~8.1 [36,55]. Since the oceans have acidified by ~0.11 since the Industrial Revolution, underestimates of 0.02 represent an uncertainty of 20% and can have consequences for modeling of oceanic conditions. As an example, if two measurements of seawater pH are made – one with purified indicator and the other with unpurified indicator – for a typical surface seawater sample (S = 35, t = 16 °C, DIC = 2000 μmol kg^{-1}) and the resulting pH_T measurements are 8.1 and 8.08, this equates to a difference of 0.14 for Ω_A.

Due to the uncertainties that arise from use of unpurified indicators, it is recommended that spectrophotometric pH_T measurements are made with purified indicators whenever possible. However, the cost of purification can be prohibitive for some research groups, and historic measurements of pH_T prior to the development of purification techniques may contain systematic errors due to dye impurities. As such, quantification of impurities in batches of unpurified indicator can aid researchers who are using or have used unpurified indicators. A mathematical model has been developed and tested using six lots of unpurified m-Cresol Purple (mCP) indicator. Impurity-corrected pH_T was compared to corresponding pH_T measured with purified mCP and was found to be in good agreement. This corrective model enables more direct

intercomparison of pH_T measurements made with purified and unpurified mCP and promotes the goals of organizations such as the Global Ocean Acidification Observing Network (GOA-ON), which seeks to synthesize chemical and biological data over large spatial and temporal ranges to further our understanding of OA [56].

1.5.2 Extending Spectrophotometric pH_T Models to Estuarine Environments

Numerous studies have characterized the chemical and optical behavior of sulfonephthalein indicators for marine [33–37,50–52] and freshwater conditions [40–43,57]. However, far less data exist for these indicators in the estuarine salinity range [35,58,59], and none of these works were performed using purified indicator. Because the pH_T in estuarine and coastal environments can vary broadly and may not be appropriately measured using only one indicator, multiple sulfonephthalein indicators are needed to make measurements. In an effort to extend spectrophotometric pH measurement capabilities using purified indicators to the estuarine salinity range, published datasets and models for three indicators (m-Cresol Purple, Thymol Blue, and Cresol Red) were combined, mathematically corrected for the influence of impurities when possible, and refitted for redeterminations of $p(K_1e_2)$. These models exhibit agreement with existing models and enable use of these indicators for spectrophotometric pH_T measurements across a broad range of salinity and temperature: $0 \leq S \leq 40$ and $278.15 \leq T \leq 308.15$ K.

1.5.3 Assessing Coastal and Estuarine CO_2 System Internal Consistency

After developing a new $p(K_1e_2)$ model for mCP to measure spectrophotometric pH_T in coastal and estuarine environments, internal consistency of the CO_2 system was examined using field datasets from the 2013 and 2016 West Coast Ocean Acidification cruises (WCOA13 and WCOA16), which were conducted in support of the NOAA Ocean Acidification Program and its research and monitoring goals [60,61]. CO_2 system measurements on these cruises included DIC,

TA, and spectrophotometric pH_T. Internal consistency analysis of these datasets enabled investigation of how well pH_T determined using the new spectrophotometric $p(K_1e_2)$ model for mCP agreed with other CO_2 system parameters. Both cruise datasets included samples collected at $S < 20$ from the Columbia River, USA, which could not previously be characterized for pH_T using the purified mCP model of Liu et al. [36].

1.6 Overview of Dissertation

This dissertation presents four manuscripts as Chapters Two, Three, Four, and Five, with embedded tables and figures. References are listed at the end of each chapter.

- **Chapter Two** details a laboratory procedure to correct spectrophotometric pH_T measurements made with unpurified m-Cresol Purple for absorbances by colorimetric impurities. This manuscript has been published by *Marine Chemistry* [62].
- **Chapter Three** introduces a new model-based parameterization of the $p(K_1e_2)$ for m-Cresol Purple applicable to the range of salinities and temperatures observed in temperate estuaries and coastal marine environments. This manuscript has been published in *Marine Chemistry* [63].
- **Chapter Four** introduces model-based parameterizations for the $p(K_1e_2)$ of Thymol Blue and Cresol Red, analogous in form and salinity and temperature ranges to the parameterization of m-Cresol Purple introduced in Chapter Three. This manuscript will be submitted for publication.
- **Chapter Five** examines internal consistency of the CO_2 system in coastal and riverine environments using measurements collected during two recent coastal cruises along the west coast of North America. This manuscript will be submitted for publication.
- **Chapter Six** outlines future studies.

1.7 References

1. U.S. Department of Commerce, National Oceanic and Atmospheric Administration. "ESRL Global Monitoring Division – Global Greenhouse Gas Reference Network." NOAA.gov. http://www.esrl.noaa.gov/gmd/ccgg/trend/index.html. (Accessed April 4, 2018).

2. Ciais, P., Sabine, C., Bala, G., Bopp, L., Brovkin, V., Canadell, J., Chhabra, A., DeFries, R., Galloway, J., Heimann, M., Jones, C., Le Quéré, C., Myneni, R.B., Piao, S., Thornton, P., 2013. Carbon and Other Biogeochemical Cycles, in Stocker, T.F., Qin, D., Plattner, G.K., Tignor, M., Allen, S.K., Boschung, J., Nauels, N., Xia, Y., Bex V., Midgley, P.M. (eds.*), Climate Change 2013: The Physical Science Basis, Working Group I Contribution to the Fifth Assessment Report of the Intergovernmental Panel on Climate Change*. Cambridge University Press, Cambridge, United Kingdom, and New York, NY, USA. 106 pp.

3. Khatiwala, S., Tanhua, T., Mikaloff Fletcher, S., Gerber, M., Doney, S.C., Graven, H.D., Gruber, N., McKinley, G.A., Murata, A., Rios, A.F., Sabine, C.L., 2013. Global ocean storage of anthropogenic carbon. *Biogeosciences* **10**, 2169-2191.

4. Gattuso, J.P., Hansson, L., 2011. Ocean acidification: background and history, in Gattuso, J.P., Hansson, L. *Ocean Acidification*. Oxford University Press, Oxford, United Kingdom. 326 pp.

5. Rhein, M., Rintoul, S.R., Aoki, S., Campos, E., Chambers, D., Feely, R.A., Gulev, S., Johnson, G.C., Josey, S.A., Kostianoy, A., Mauritzen, C., Roemmich, D., Talley, L.D., Wang, F., 2013. Observations: Ocean, in Stocker, T.F., Qin, D., Plattner, G.K., Tignor, M., Allen, S.K., Boschung, J., Nauels, N., Xia, Y., Bex V., Midgley, P.M. (eds.*), Climate Change 2013: The Physical Science Basis, Working Group I Contribution to the Fifth Assessment Report of the Intergovernmental Panel on Climate Change*. Cambridge University Press, Cambridge, United Kingdom, and New York, NY, USA. 62 pp.

6. Orr, J.C., Fabry, V.J., Aumont, O., Bopp, L., Doney, S.C., Feely, R.A., Gnanadesikan, A., Gruber, N., Ishida, A., Joos, F., Key, R.M., Lindsay, K., Maier-Reimer, E., Matear, R., Monfray, P., Mouchet, A., Najjar, R.G., Plattner, G.-K., Rodgers, K.B., Sabine, C.L., Sarmiento, J.L., Schlitzer, R., Slater, R.D., Totterdell, I.J., Weirig, M.-F., Yamanaka, Y., Yool, A., 2005. *Nature* **437**(29), 681-686.

7. Feely, R.A., Doney, S.C., Cooley, S.R., 2009. Ocean acidification: Present conditions and future changes in a high-CO_2 world. *Oceanography* **22**(4), 36-47.

8. Bates, N.R., 2007. Interannual variability of the oceanic CO_2 sink in the subtropical gyre of the North Atlantic Ocean over the last two decades. *Journal of Geophysical Research: Oceans* **112**, C09013.

9. Bates, N.R., 2012. Multi-decadal uptake of carbon dioxide into subtropical mode water of the North Atlantic Ocean. *Biogeosciences* **9**, 2649-2659.

10. Santana-Casiano, J.M., González-Dávila, M., Rueda, M.J., Llinas, O., González-Dávila, E.F., 2007. The interannual variability of oceanic CO_2 parameters in the northeast Atlantic subtropical gyre at the ESTOC site. *Global Biogeochemical Cycles* **21**, GB1015.

11. Dore, J. E., Lukas, R., Sadler, D.W., Church, M.J., Karl, D.M., 2009. Physical and biogeochemical modulation of ocean acidification in the central North Pacific. *Proceedings of the National Academy of Science of the U.S.A.* **106**, 12235–12240.

12. Olafsson, J., Olafsdottir, S.R., Benoit-Cattin, A., Danielsen, M., Arnarson, T.S., Takahashi, T., 2009. Rate of Iceland Sea acidification from time series measurements. *Biogeosciences* **6**, 2661–2668.

13. González-Dávila, M., Santana-Casiano, J.M., Rueda, M.J., Llinas, O., 2010. The water column distribution of carbonate system variables at the ESTOC site from 1995 to 2004. *Biogeosciences*, **7**, 3067–3081.

14. Byrne, R.H., Mecking, S., Feely, R.A., Liu, X., 2010. Direct observations of basin-wide acidification of the North Pacific Ocean. *Geophysical Research Letters* **37**, L02601.

15. Collins, M., Knutti, R., Arblaster, J., Dufresne, J.-L., Fichefet, T., Friedlingstein, P., Gao, X., Gutowski, W.J., Johns, T., Krinner, G., Shongwe, M., Tebaldi, C., Weaver, A.J., Wehner, M., 2013. Long-term climate change: Projections, commitments and irreversibility, in Stocker, T.F., Qin, D., Plattner, G.K., Tignor, M., Allen, S.K., Boschung, J., Nauels, N., Xia, Y., Bex V., Midgley, P.M. (eds*.), Climate Change 2013: The Physical Science Basis, Working Group I Contribution to the Fifth Assessment Report of the Intergovernmental Panel on Climate Change*. Cambridge University Press, Cambridge, United Kingdom, and New York, NY, USA.

16. Barry, J.P., Widdicombe, S., Hall-Spencer, J.M., 2011. Effects of ocean acidification on marine biodiversity and ecosystem function, in Gattuso, J.P., Hansson, L. *Ocean Acidification*. Oxford University Press, Oxford, United Kingdom.

17. Zeebe, R.E., Wolf-Gladrow, D., 2001. CO_2 in Seawater: Equilibrium, Kinetics, Isotopes. Elsevier Science B.V., Amsterdam.

18. Dickson, A.G., Sabine, C.L., Christian, J.R. (Eds.), 2007. *Guide to Best Practices for Ocean CO_2 Measurements.* PICES Special Publication 3, 191 p.

19. Dickson, A.G., 2001. Reference materials for oceanic CO_2 measurements. *Oceanography* **14**(4), 21-22.

20. Dickson, A.G., Afghan, J.D., Anderson, G.C., 2003. Reference materials for oceanic CO_2 analysis: a method for the certification of total alkalinity. *Marine Chemistry* **80**(2-3), 185-187.

21. Bockmon, E.E., Dickson, A.G., 2015. An inter-laboratory comparison assessing the quality of seawater carbon dioxide measurements. *Marine Chemistry* **171**, 36–43.

22. Dickson, A.G., 1981. An exact definition of total alkalinity and a procedure for the estimation of alkalinity and total inorganic carbon from titration date. *Deep Sea Research Part A: Oceanographic Research Papers* **28**(6), 609-623.

23. Hernández-Ayon, J., Zirino, A., Dickson, A.G., Camiro-Vargas, T., Valenzuela-Espinoza, E., 2007. Estimating the contribution of organic bases from microalgae to the titration alkalinity in coastal seawaters. *Limnology and Oceanography: Methods* **5**(7), 225-232.

24. Muller, F.L, Bleie, B., 2008. Estimating the organic acid contribution to coastal seawater alkalinity by potentiometric titrations in a closed cell. *Analytical Chimica Acta* **619**(2), 183-191.

25. Hunt, C., Salisbury, J., Vandemark, D., 2011. Contribution of non-carbonate anions to total alkalinity and overestimation of pCO_2 in New England and New Brunswick rivers. *Biogeosciences* **8**(10), 3069-3076.

26. Yang, B., Byrne, R.H., Lindemuth, M., 2015. Contributions of organic alkalinity to total alkalinity in coastal waters: A spectrophotometric approach. *Marine Chemistry* **176**, 199-207.

27. Breland, J. A., Byrne, R. H., 1993. Spectrophotometric procedures for determination of sea water alkalinity using bromocresol green. *Deep Sea Research Part I: Oceanographic Research Papers* **40**(3), 629-641.

28. Yao, W., Byrne, R.H., 1998. Simplified seawater alkalinity analysis: Use of linear array spectrometers. *Deep Sea Research Part I: Oceanographic Research Papers* **45**(8), 1383-1392.

29. Martz, T.R., Dickson, A.G., DeGrandpre, M.D., 2006. Tracer monitored titrations: Measurement of total alkalinity. *Analytical Chemistry* **78**, 1817-1826.

30. Spaulding, R.S., DeGrandpre, M.D., Beck. J.C., Hart, R.D., Peterson, B., De Carlo, E.H., Drupp, P.S., Hammar, T.R., 2014. Autonomous in situ measurements of seawater alkalinity. *Environmental Science & Technology* **48**, 9573-9581.

31. Guggenheim, E.A., 1967. *Thermodynamics: An Advanced Treatment for Chemists and Physicists (5th ed.).* North-Holland, Amsterdam. 414 pp.

32. Byrne, R.H., 2014. Measuring ocean acidification: New technology for a new era of ocean chemistry. *Environmental Science & Technology* **48**, 5352-5360.

33. Clayton, T.D., Byrne, R.H., 1993. Spectrophotometric seawater pH measurements: Total hydrogen ion concentration scale calibration of m-cresol purple and at-sea results. *Deep-Sea Research, Part I* **40**, 2115-2129.

34. Zhang, H., Byrne, R.H., 1996. Spectrophotometric pH measurements of surface seawater at in-situ conditions: absorbance and protonation behavior of thymol blue. *Marine Chemistry* **52**, 17-25.

35. Mosley, L.M., Husheer, S.L.G., Hunter, K.A., 2004. Spectrophotometric pH measurement in estuaries using thymol blue and *m*-cresol purple. *Marine Chemistry* **91**, 175-186.

36. Liu, X., Patsavas, M.C., Byrne, R.H., 2011. Purification and characterization of meta-cresol purple for spectrophotometric seawater pH measurements. *Environmental Science & Technology* **45**, 4862-4868.

37. Patsavas, M.C., Byrne, R.H., Liu, X, 2013b. Physical-chemical characterization of purified cresol red for spectrophotometric pH measurements in seawater. *Marine Chemistry* **155**, 158-164.

38. Dickson, A.G., Camões, M.F., Spitzer, P., Fisicaro, P., Stoica, D., Pawlowicz, R. Feistel, R., 2015. Metrological challenges for measurements of key climatological observables. Part 3: seawater pH. *Metrologia* **53**(1), R26.

39. DeGrandpre, M.D., Baehr, M.M., Hammar, T.R., 1999. Calibration-free optical chemical sensors. *Analytical Chemistry* **71**, 1152-1159.

40. French, C.R., Carr, J.J., Dougherty, E.M., Eidson, L.A.K., Reynolds, J.C., DeGrandpre, M.D., 2002. Spectrophotometric pH measurements of freshwater. *Analytica Chimica Acta* **453**, 13-20.

41. Yuan, S., DeGrandpre, M.D., 2008. Evaluation of indicator-based pH measurements for freshwater over a wide range of buffer intensities. *Environmental Science & Technology* **42**, 6092-6099.

42. Lai, C.Z., DeGrandpre, M.D., Wasser, B.D., Branson, T.A., Clucas, D.S., Jaqueth, E.J., Benson, Z.D., Beatty, C.M., Spaulding, R.S., 2016. Spectrophotometric measurement of freshwater pH with purified meta-cresol purple and phenol red. *Limnology and Oceanography: Methods* **14**(12), 864-873.

43. Lai, C.Z., DeGrandpre, M.D., Wasser, B.D., Branson, T.A., Clucas, D.S., Jaqueth, E.J., Benson, Z.D., Beatty, C.M., Spaulding, R.S., 2017. Erratum: Spectrophotometric measurement of freshwater pH with purified meta-cresol purple and phenol red. *Limnology and Oceanography: Methods* **15**, 903.

44. Easley, R.A., Byrne, R.H., 2012. Spectrophotometric calibration of pH electrodes in seawater using purified m-cresol purple. *Environmental Science & Technology* **46**(9), 5018-5024.

45. Bresnahan Jr., P. J., Martz, T. R., Takeshita, Y., Johnson, K. S., LaShomb, M., 2014. Best practices for autonomous measurements of seawater pH with the Honeywell Durafet. *Methods in Oceanography* **9**, 44-60.

46. Martz, T.R., Connery, J.G., Johnson, K.S., 2010. Testing the Honeywell Durafet for seawater pH applications. *Limnology and Oceanography: Methods* **8**(5), 172-184.

47. Gonski, S.F., 2016. *An evaluation of the performance of an ISFET pH sensor in a dynamic estuarine system*. University of Delaware. http://udspace.udel.edu/bitstream/handle/19716/21486/2016_GonskiStephen_MS.pdf?sequence=1. (Accessed 4 February 2018).

48. Martz, T., McLaughlin, K., Weisberg, S.B., 2015. Best practices for autonomous measurement of seawater pH with the Honeywell Durafet pH sensor. Southern California Coastal Water Research Project. California Current Acidification Network (C-CAN) Technical Report 861. 20 pp.

49. Takeshita, Y., Martz, T.R., Johnson, K.S., Dickson, A.G., 2014. Characterization of an ion sensitive field effect transistor and chloride ion selective electrodes for pH measurements in seawater. *Analytical Chemistry* **86**(22), 11189-11195.

50. Robert-Baldo, G.L., Morris, M.J., Byrne, R.H., 1985. Spectrophotometric determination of seawater pH using phenol red. *Analytical Chemistry* **57**, 2564-2567.

51. King, D.W., Kester, D.R., 1989. Determination of seawater pH from 1.5 to 8.5 using colorimetric indicators. *Marine Chemistry* **26**, 5-20.

52. Patsavas, M.C., Byrne, R.H., Liu, X., 2013a. Purification of meta-cresol purple and cresol red by flash chromatography: Procedures for ensuring accurate spectrophotometric seawater pH measurements. *Marine Chemistry* **150**, 19-24.

53. Yao, W., Liu, X., Byrne, R.H., 2007. Impurities in indicators used for spectrophotometric seawater pH measurements: Assessment and remedies. *Marine Chemistry* **107**, 167-172.

54. Easley, R.A., Place, B.J., 2017. Mass spectra of sulfonephthalein pH indicator dyes and their impurities. *Journal of Research of the National Institute of Standards and Technology* **122**, 21.

55. Patsavas, M.C., 2014. *Improving spectrophotometric carbon system measurements.* University of South Florida. http://scholarcommons.usf.edu/etd/5095/. (Accessed 4 April 2018).

56. Newton, J.A., Feely, R.A., Jewett, E.B., Williamson, P., Mathis, J., 2014. Global Ocean Acidification Observing Network: Requirements and Governance Plan. http://www.goa-on.org/docs/GOA-ON_plan_print.pdf

57. Yao, W., Byrne, R.H., 2001. Spectrophotometric determination of freshwater pH using bromocresol purple and phenol red. *Environmental Science and Technology* **35**, 1197-1201.

58. Gabriel, M.D., Forja, J.M., Rubio, J.A., Gomez-Parra, A., 2005. Temperature and salinity dependence of molar absorptivities of thymol blue: Application to the spectrophotometric determination of pH in estuarine waters. *Ciencias Marinas* **31**(1B), 309-318.

59. Hammer, K., Schneider, B., Kulinski, K., Schulz-Bull, D.E., 2014. Precision and accuracy of spectrophotometric pH measurements at environmental conditions in the Baltic Sea. *Estuarine, Coastal and Shelf Science* **146**, 24-32.

60. Feely, R.A., Alin, S.R., Hales, B., Johnson, G.C., Byrne, R.H., Peterson, William; Liu, Xuewu; Greeley, Dana (2015). Dissolved inorganic carbon, total alkalinity, pH and other variables collected from profile and discrete sample observations using CTD, Niskin bottle, and other instruments from NOAA Ship Fairweather and R/V Point Sur in the U.S. West Coast California Current System during the 2013 West Coast Ocean Acidification Cruise (WCOA2013) from 2013-08-05 to 2013-08-28 (NCEI Accession 0132082). Version 2.2. NOAA National Centers for Environmental Information. Dataset.

61. Alin, S.R., Feely, R.A. Hales, B. Byrne, R.H., Cochlan, W., Liu, X.; Greeley, D., 2017. Dissolved inorganic carbon, total alkalinity, pH, dissolved oxygen, nutrients, and other variables collected from profile and discrete sample observations using CTD, Niskin bottle, and other instruments from Ronald H. Brown in the West Coast of North America from Canada to Mexico from 2016-05-08 to 2016-06-06 (NCEI Accession 0169412). Version 1.1. NOAA National Centers for Environmental Information. Dataset.

62. Douglas, N.K., Byrne, R.H., 2017a. Achieving accurate spectrophotometric pH measurements using unpurified meta-cresol purple. *Marine Chemistry* **190**, 66-72.

63. Douglas, N.K. Byrne, R.H., 2017b. Spectrophotometric pH measurements from river to sea: Calibration of mCP for $0 \leq S \leq 40$ and $278.15 \leq T \leq 308.15$ K. *Marine Chemistry* **197**, 64-69.

CHAPTER TWO:

ACHIEVING ACCURATE SPECTROPHOTOMETRIC pH MEASUREMENTS USING UNPURIFIED META-CRESOL PURPLE

Note to Reader

Portions of this chapter have been published [1] and are included with the permission of the publisher.

2.1 Abstract

For best accuracy, spectrophotometric characterizations of seawater pH are obtained using a purified pH-sensitive dye — usually meta-Cresol Purple (mCP) for typical ranges of seawater pH. In recognition of practical limitations, though, a straightforward method is here proposed to improve measurements made using unpurified mCP. The user first determines, for a particular lot of unpurified mCP, the absorbance contribution of indicator impurities at 434 nm ($_{434}A_{\text{imp}}$). Correction for this contribution is then mathematically applied to the measurements of seawater pH. We tested this approach using six unpurified lots of mCP and, for comparison, purified mCP in a synthetic experimental solution over the pH range 7.25–8.25. The $_{434}A_{\text{imp}}$ correction yielded substantial improvements in pH accuracy: on the order of 0.005 at low pH (~7.25) and 0.01 or more at higher pH (~8.25). The pH accuracy achieved by the corrective model was also examined relative to the Global Ocean Acidification Observing Network (GOA-ON) "weather" and "climate" goals for pH measurements (uncertainties of ±0.02 and ±0.003,

respectively). When previously published algorithms (appropriate for purified mCP) were used, none of the unpurified dyes met the more stringent "climate" goal in waters of pH > 7.6. With the algorithms proposed here (i.e., incorporating the lot-specific ${}_{434}A_{\text{imp}}$ correction), three of the six lots came into "climate" compliance over the full experimental pH_T range and two additional lots achieved "climate" compliance up to pH ~ 8.0. This protocol offers a simple, user-determined correction to significantly improve the accuracy of pH measurements made with unpurified mCP.

2.2 Introduction

High-quality CO_2 system measurements are essential for observing ocean acidification and interpreting its chemical and ecological effects. Additionally, understanding measurement quality is essential for insightful comparison of data sets. The United Nations General Assembly recently highlighted the importance of obtaining high-quality ocean measurements [2]. Toward that end, the establishment of the Global Ocean Acidification Observing Network (GOA-ON) has further promoted efforts to standardize measurement quality for the most frequently measured CO_2 system parameters: pH, total alkalinity (TA), and dissolved inorganic carbon (DIC).

In 2014 the GOA-ON released its guiding principles for data quality as a two-tiered set of goals: (1) "weather" goals, defined as "measurements of quality sufficient to identify relative spatial patterns and short-term variation," in order to "support mechanistic interpretation of the ecosystem response to and impact on local, immediate [ocean acidification] dynamics"; and (2) longer-term "climate" goals, defined as "measurements of quality sufficient to assess long term trends with a defined level of confidence," in order to "support detection of long-term anthropogenically-driven changes in hydrographic conditions and carbon chemistry over multi-

decadal timescales" [3]. These goals are to be achieved by constraining pH, TA, and DIC measurement uncertainties to thresholds that limit the uncertainty in calculated carbonate ion concentrations to ≤10% for the "weather" goal and ≤1% for the "climate" goal. For pH, these targets equate to a "weather" uncertainty goal of ±0.02 and a "climate" uncertainty goal of ±0.003.

To assess the quality of laboratory-based seawater CO_2 system measurements, including whether the GOA-ON goals are being met with current best practices, Bockmon and Dickson [4] used seawater standards to conduct an inter-laboratory comparison among more than 60 institutions around the world. Each laboratory measured TA, DIC, and pH. Data quality was evaluated by comparing each lab's measured values to the standard's "true" values. The differences between measured and true values were then used to determine whether the measurements met the GOA-ON goals. For the pH determinations, both spectrophotometric and potentiometric methods were assessed. Bockmon and Dickson found that of the three parameters evaluated, the pH determinations demonstrated the least consensus among the 60 laboratories. Laboratory-specific mean errors in the potentiometric pH measurements ranged from –0.1 to 0.05, and laboratory-specific mean errors in the spectrophotometric pH measurements ranged from –0.04 to 0.04 [4].

The use of unpurified pH-sensitive indicators is one potential source of error for spectrophotometric pH measurements. Uncharacterized impurities in an indicator solution may absorb light at the same wavelengths as the acid or base indicator species [5], thus affecting the pH calculated from the measured absorbances.

One of the most commonly used indicators for seawater analyses is meta-Cresol Purple (mCP), but high-performance liquid chromatography (HPLC) analyses show that commercially

available powders consistently include impurities that absorb significantly at 434 nm (the wavelength of maximum absorption for the acid species, HI^-) and negligibly at 578 nm (the wavelength of maximum absorption for the base species, I^{2-}) [5,6]. Because a sample's calculated pH is directly related to the ratio of these absorbances ($R = {}_{578}A/{}_{434}A$), these impurities spuriously lower the apparent sample pH. This confounding effect is most pronounced at pH >8.0 [5], when the absorbance by mCP is lower and the relative contribution of impurities to the measured absorbance is higher.

The use of purified mCP is now recommended for high-precision ocean-range pH measurements. However, purification requires the use of either HPLC [6] or flash chromatography [7] and a large volume of solvents. As a result, purified mCP is currently available from only a few academic labs. The inconvenience and cost of obtaining purified mCP may therefore limit some researchers' abilities to obtain sufficient quantities. In such cases — and for historical measurements made using unpurified mCP — a model to correct for impurities would be highly beneficial.

Liu et al. [6] used an empirical model to fit pH_T values obtained with unpurified mCP against values obtained with purified mCP. A major disadvantage of this approach is that it requires the user to make careful comparative pH_T measurements using both purified and unpurified mCP in a series of buffered seawater solutions. An alternative approach to the problem of indicator impurities is to quantify the absorbance contribution by the impurities and then correct for their influence on absorbance measurements. This approach circumvents the need for laborious comparisons against purified indicator over a range of pH.

In this work, a physical–chemical model was developed to allow users to reduce systematic pH measurement errors introduced by colored indicator impurities. The efficacy of

the method was assessed relative to measurements made using purified mCP. The influence of impurities and the benefit of the model correction were also examined relative to the GOA-ON "weather" and "climate" goals for ocean pH measurements. This corrective method can be used to (1) quantify the absorbance of spectrophotometrically interfering impurities in a solution of unpurified mCP, (2) correct for the use of unpurified mCP in seawater pH measurements (in the event that purified indicator is unavailable), and (3) correct historical seawater pH measurements made using unpurified mCP (provided that a sample of the original mCP powder is still available).

2.3 Theory

2.3.1 Spectrophotometric pH Measurements

In the decades since the development of procedures to use sulfonephthalein indicators to measure seawater pH [8–11], spectrophotometry has become a method of choice for chemical oceanographers investigating open-ocean pH. Spectrophotometry provides a number of advantages over potentiometry, including measurement speed and simplicity, good accuracy without empirical calibration, high levels of precision (±0.0004 units during shipboard analyses), and the ability to correct historical data (provided the original absorbance data and mCP powder are available [11]). Spectrophotometric methods can also be applied to underway and in situ analyses [12]. Additionally, spectrophotometric pH measurements are increasingly being used in laboratory studies concerning the effects of ocean acidification on marine organisms [13–18].

A number of sulfonephthalein indicators have been used for seawater pH measurements, with the choice of one over the other depending largely on each indicator's dissociation constant, K_I. The suite of seawater-relevant indicators includes Thymol Blue (pK_I ~8.6 [9,19]), Phenol Red (pK_I ~7.5 [8]), Cresol Red (pK_I ~7.8 [7,10]), and meta-Cresol Purple (pK_I ~8.0 [6,11]). Of these,

meta-Cresol Purple (mCP) is the most appropriate choice for open-ocean surface-to-deep pH profiles because its pK_I most closely matches the typical seawater pH range [11]. This indicator has now been used for thousands of at-sea pH observations, including measurements made during Joint Global Ocean Flux Study (JGOFS) and World Ocean Circulation Experiment (WOCE) cruises, as well as the more recent NOAA West Coast Ocean Acidification and East Coast Ocean Acidification cruises.

The same principles underlie all sulfonephthalein spectrophotometric pH measurements. When an indicator of the form H_2I is added to a seawater sample, the indicator acts as an acid and equilibrates into its HI^- and I^{2-} forms, with a negligible amount of H_2I remaining. The fact that these two ions absorb different wavelengths of visible light is the basis of the pH determination. For mCP, the absorbance maxima for HI^- and I^{2-} occur at 434 and 578 nm, respectively.

The ratio (R) of these absorbances (A) can be used to determine seawater pH on the total hydrogen ion concentration scale (pH_T) as follows:

$$R = \frac{{}_{\lambda_2}A}{{}_{\lambda_1}A} \tag{2.1}$$

where the λ_1 and λ_2 subscripts denote the wavelengths of the HI^- and I^{2-} absorbance maxima, respectively. For mCP, λ_1 and λ_2 are 434 and 578 nm, respectively. In conjunction with published indicator-specific constants, this measured R-ratio can be used to calculate seawater pH on the total hydrogen ion concentrations [11]:

$$\mathrm{pH_T} = -\log K_I + \log\left(\frac{R - e_1}{e_2 - R e_3}\right) \tag{2.2}$$

where K_I is the acid dissociation constant for the HI^- form of the indicator, expressed in terms of species concentrations ($K_I = [I^{2-}][H^+]_T[HI^-]^{-1}$). The terms e_1, e_2, and e_3 are molar absorbance ratios, defined as follows:

$$e_1 = \frac{{}_{578}\varepsilon_{HI}}{{}_{434}\varepsilon_{HI}}, \qquad e_2 = \frac{{}_{578}\varepsilon_{I}}{{}_{434}\varepsilon_{HI}}, \qquad e_3 = \frac{{}_{434}\varepsilon_{I}}{{}_{434}\varepsilon_{HI}} \tag{2.3}$$

where ${}_{\lambda}\varepsilon_i$ denotes the wavelength-specific molar absorptivity coefficient of species *i* (see [11] for additional details).

For the purified mCP model [6], the relationship between pH_T and pK_I is given in the following form:

$$\mathrm{pH_T} = p(K_I e_2) + \log\left(\frac{R - e_1}{1 - R\frac{e_3}{e_2}}\right) \tag{2.4}$$

where

$${}^{e_3}/_{e_2} = -0.020813 + 2.60262 \cdot 10^{-4} T + 1.0436 \cdot 10^{-4}(S - 35) \tag{2.5}$$

The values of the other terms in Eq. (2.4) are given in [6]. In Eq. (2.5), temperature (*T*) is expressed in Kelvin and salinity (*S*) is unitless. Eq. (2.4) is appropriate at $278.15 \leq T \leq 308.15$ and $20 \leq S \leq 40$.

2.3.2 Accounting for Impurity Effects on Spectrophotometric pH Measurements

According to the observations of Yao et al. [5] and Liu et al. [6], impurities in commercially available mCP contribute predominantly to the absorbance at 434 nm (and negligibly at 578 nm). With this assessment in mind, the following theoretical model is proposed for quantifying absorbance contributions from impurities in off-the-shelf mCP.

For unpurified mCP, the observed absorbance ratio (R_{obs}) can be defined as

$$R_{\mathrm{obs}} = {}_{578}A_{\mathrm{obs}}/{}_{434}A_{\mathrm{obs}} \tag{2.6}$$

where ${}_{578}A_{\mathrm{obs}}$ is the observed absorbance at 578 nm and ${}_{434}A_{\mathrm{obs}}$ is the observed absorbance at 434 nm. It is assumed that ${}_{434}A_{\mathrm{obs}}$ is composed of an absorbance contribution from mCP (${}_{434}A_{\mathrm{mCP}}$) plus an absorbance contribution from an impurity or suite of impurities (${}_{434}A_{\mathrm{imp}}$) such that

$${}_{434}A_{\mathrm{obs}} = {}_{434}A_{\mathrm{mCP}} + {}_{434}A_{\mathrm{imp}} \tag{2.7}$$

It is assumed that all absorbance contributions at λ = 578 nm are solely from mCP:

$$_{578}A_{\text{obs}} = {}_{578}A_{\text{mCP}} \tag{2.8}$$

Substituting Eqs. (2.7) and (2.8) into Eq. (2.6) yields

$$R_{\text{obs}} = \frac{{}_{578}A_{\text{mCP}}}{{}_{434}A_{\text{mCP}} + {}_{434}A_{\text{imp}}} \tag{2.9}$$

For a purified mCP solution:

$$R_{\text{pure}} = \frac{{}_{578}A_{\text{mCP}}}{{}_{434}A_{\text{mCP}}} \tag{2.10}$$

where R_{pure} is equivalent to the absorbance ratio obtained using purified indicator. By combining and rearranging the expressions for R_{obs} and R_{pure} (Eqs. (2.9) and (2.10), respectively), the following relations are obtained:

$$R_{\text{obs}} = \frac{R_{\text{pure}}}{\left(1 + \frac{{}_{434}A_{\text{imp}}}{{}_{434}A_{\text{mCP}}}\right)} \tag{2.11}$$

$$R_{\text{pure}} = R_{\text{obs}}\left(1 + \frac{{}_{434}A_{\text{imp}}}{{}_{434}A_{\text{mCP}}}\right) \tag{2.12}$$

By substituting terms from Eq. (2.7) into Eq. (2.12), the relation between R_{pure} and R_{obs} then becomes

$$R_{\text{pure}} = R_{\text{obs}}\left(1 + \frac{{}_{434}A_{\text{imp}}}{{}_{434}A_{\text{obs}} - {}_{434}A_{\text{imp}}}\right) \tag{2.13}$$

This statement posits that across the natural pH range of seawater tested by Liu et al. [6], R_{pure} can be calculated from R_{obs} if ${}_{434}A_{\text{imp}}$ is known.

To determine ${}_{434}A_{\text{imp}}$, we rely on the fact that at sufficiently high pH, the concentration of HI^- is negligible (i.e., essentially all mCP is in the I^{2-} form). Under these conditions, it follows that

$$R_{\text{pure}} = e_2/e_3 \tag{2.14}$$

Substituting Eq. (2.14) into Eq. (2.13) with algebraic rearrangement yields

$$\frac{R_{\mathrm{obs}}}{e_2/e_3} = \left(1 + \frac{{}_{434}A_{\mathrm{imp}}}{{}_{434}A_{\mathrm{obs}} - {}_{434}A_{\mathrm{imp}}}\right)^{-1} \tag{2.15}$$

$$\left(\frac{e_2/e_3}{R_{\mathrm{obs}}} - 1\right)({}_{434}A_{\mathrm{obs}} - {}_{434}A_{\mathrm{imp}}) = {}_{434}A_{\mathrm{imp}} \tag{2.16}$$

$${}_{434}A_{\mathrm{imp}} = \left(1 - {}^{e_3}/_{e_2} \cdot R_{\mathrm{obs}}\right) {}_{434}A_{\mathrm{obs}} \tag{2.17}$$

This ${}_{434}A_{\mathrm{imp}}$ term can be thought of as a correction factor that characterizes the contributions of indicator impurities to the sample absorbance measured at 434 nm.

The procedure for determining ${}_{434}A_{\mathrm{imp}}$ for a particular lot of unpurifed mCP is given in Table 2.1. Briefly, the overall steps are to prepare a high-pH NaCl solution and measure its baseline (no-dye) absorbances; add the unpurified mCP indicator and re-measure absorbances; use the baseline-corrected absorbances [20] to calculate R_{obs} using Eq. (2.6); and finally, use Eq. (2.17) to calculate the lot-specific correction factor ${}_{434}A_{\mathrm{imp}}$ for the indicator solution.

Table 2.1. Summary of ${}_{434}A_{\mathrm{imp}}$ corrective procedure for using unpurified mCP to determine seawater pH_T.

Objective	**Procedure**
Determine ${}_{434}A_{\mathrm{imp}}$ for a particular lot of unpurified mCP	1. Prepare a 0.7 M NaCl solution. 2. Add NaOH to adjust the pH to ~12 (final [NaOH] = 0.01 M; final ionic strength of solution = 0.71 M). 3. Warm a sample of the high-pH solution to 298.15 K in a thermostatted cell warmer. 4. Measure baseline (no-dye) absorbances of the sample at 434, 578, and 730 nm. 5. Add unpurified mCP to the sample cell. 6. Measure ${}_{434}A_{\mathrm{obs}}$, ${}_{578}A_{\mathrm{obs}}$, and ${}_{730}A_{\mathrm{obs}}$. 7. Use baseline-corrected ${}_{434}A_{\mathrm{obs}}$ and ${}_{578}A_{\mathrm{obs}}$ to calculate R_{obs} (Eq. 2.6). 8. Calculate e_3/e_2 (Eq. 2.5) with $S = 34.40$*. 9. Calculate the lot-specific value of ${}_{434}A_{\mathrm{imp}}$ (Eq. 2.17).
Use unpurified mCP and its ${}_{434}A_{\mathrm{imp}}$ to determine the pH_T of a seawater sample	1. Collect seawater sample and measure absorbances according to [20]. 2. Use baseline-corrected ${}_{434}A_{\mathrm{obs}}$ and ${}_{578}A_{\mathrm{obs}}$ to calculate R_{obs} (Eq. 2.6). 3. Use R_{obs} and the lot-specific value of ${}_{434}A_{\mathrm{imp}}$ to calculate R_{pure} (Eq. 2.13). 4. Use R_{pure} to calculate seawater pH_T (Eq. 2.4).

* The value of $S = 34.40$ corresponds to $I = 0.71$ M. For NaCl solutions of higher or lower ionic strength, the value of S should adjusted accordingly.

The procedure for determining seawater pH_T using the unpurified — but now characterized — mCP is also given in Table 2.1. Briefly, the overall steps are to use the standard protocol for spectrophotometric determinations of seawater pH_T [20] to obtain R_{obs} of the seawater sample (Eq. 2.6); use Eq. (2.13) to calculate R_{pure}; and finally, use Eq. (2.4) to calculate the impurity-corrected pH_T of the seawater sample.

2.4 Materials and Methods

Correction factors ($_{434}A_{imp}$) were first determined for six different lots of unpurified mCP. The utility of the proposed corrective model was then assessed by comparing, for a series of sample solutions, each sample's $pH_{T,pure}$ (obtained using purified mCP) to its $pH_{T,obs}$ (obtained using unpurified mCP, without the $_{434}A_{imp}$ correction) and $pH_{T,corr}$ (obtained using unpurified mCP, with the $_{434}A_{imp}$ correction). The usefulness of the correction factor in attaining the GOA-ON measurement goals was also assessed. The pH of all sample solutions was within the range of normal seawater ($7.25 \leq pH_T \leq 8.25$).

2.4.1 Preparation of Stock Solutions

A suite of six commercially purchased, unpurified mCP dyes was used to determine six lot-specific values of $_{434}A_{imp}$: Acros Organics lot #A0182569, Aldrich lot #11517KC, Kodak lot #C102024, MP Bio lot #1426K, Ricca lot #2107749, and TCI lot #FDP01. For comparison, purified mCP was also used. This mCP powder was purchased from Aldrich, lot #7005HH (unpurified), then flash-purified according to the procedure of Patsavas et al. [7]. Sodium salts of mCP (rather than the free acid form) were used due to their ease of dissolution.

The six solutions of 10 mM mCP (unpurified) were formulated, and their absorbance ratios were adjusted to $R = 1.6$ (±0.05) by addition of 0.1 M NaOH, diluted from 1 M NaOH (Fisher Scientific sodium hydroxide solution, 1 N, certified 0.995–1.005 N, lot #127455) with

MilliQ ultra-purified water (18.2 MΩ-cm molar resistivity). Over the course of the experiments, the *R*-ratios of the indicator solutions were periodically tested to ensure that CO_2 penetration into the dye had not occurred. Dissolution of CO_2 into the dye solution would lower its *R*-ratio and, in turn, would change the indicator's perturbation effect (i.e., the pH effect of adding the indicator to a seawater sample [20]). For these checks, a spectrophotometric cell with a 0.2 mm path length (Starna Scientific, Ltd.) was used.

For use in determining ${}_{434}A_{\text{imp}}$, a high-pH sodium chloride solution was prepared by adding 10 N NaOH (J.T. Baker, volumetric solution, lot #A43P05) to 0.7 M NaCl (Acros Organics, 99.5% for analysis, lot #A0318483) until a final concentration of 0.01 M NaOH was achieved. The final pH_T was ~12.

For use in assessing the utility of the correction factor ${}_{434}A_{\text{imp}}$ in the calculation of R_{pure} (Eq. 2.10), stock sample solutions of buffered sodium chloride were prepared: 0.7 M NaCl (Acros Organics sodium chloride, 99.5% for analysis, lot #A031843); 0.01 M 3-(*N*-morpholino)propanesulfonic acid (MOPS) buffer (Sigma MOPS, minimum 99.5% titration, lot #092K5443); and 0.01 M 3-[4-(2-Hydroxyethyl)-1-piperazinyl]propanesulfonic acid (EPPS) buffer (Acros Organics, 99% for biochemistry, lot #A0271122). The pH_T values of subsamples of this stock solution were then adjusted to values across the experimental range of about 7.25 to 8.25. For these adjustments, 0.7 M NaOH, diluted from 1 M NaOH (Fisher Scientific sodium hydroxide solution, 1 N, certified 0.995–1.005 N, lot #127455) with MilliQ ultra-purified water (18.2 MΩ-cm molar resistivity), was used. A new stock solution was prepared for each of the six tested dye lots; as the result, the adjusted pH_T varied slightly from one batch to another.

2.4.2 Determination of ${}_{434}\mathbf{A}_{imp}$ Correction Factors

For each lot of unpurified indicator, a value of ${}_{434}A_{\text{imp}}$ was determined in a unique batch of high-pH_T stock solution. Absorbances were recorded at 434, 578, and 730 nm before and after each of two 10 μL additions of 10 mM mCP. (The two indicator additions enable users to account for the pH perturbation caused by adding mCP to the sample. See [20] for detailed instructions regarding baseline corrections and perturbation corrections.) The value of R_{obs} was calculated using baseline-corrected absorbances in Eq. (2.6). Finally, values of T, S, R_{obs}, and ${}_{434}A_{\text{obs}}$ were used to calculate ${}_{434}A_{\text{imp}}$ (Eq. 2.17).

The absorbance measurements were carried out on a Varian Cary 400 UV/VIS spectrophotometer thermostatted with a Lauda Ecoline RE120 water bath. All measurements were performed at temperature $T = 298.15$ K and ionic strength $I = 0.70$–0.71 (equivalent to $S =$ 33.94–34.40). The resulting e_3/e_2 ratio (calculated using Eq. 2.5) was within the range of 0.05667 to 0.05672 for all experiments. The Varian Simple Reads software package was used for all absorbance measurements.

2.4.3 Use of ${}_{434}\mathbf{A}_{imp}$ for Determinations of $\mathbf{R}_{pure}$

To assess the utility of the six ${}_{434}A_{\text{imp}}$ correction factors, R_{pure} was determined for a series of buffered NaCl sample solutions over the pH_T range appropriate to natural seawater at $T =$ 298.15 K: approximately $7.25 \leq pH_T \leq 8.25$. The pH_T of each batch of stock experimental solution was initially adjusted to ~7.25, and baseline (no-dye) absorbances were measured. Two 10 μL additions of mCP solution were then added, and absorbances were measured at 434, 578, and 730 nm after each addition. The same procedure was repeated at pH_T ~7.50, 7.75, 8.00, and 8.25.

After adjusting the measured absorbance values to correct for baseline absorbances and the pH_T perturbation due to dye addition [20], the value of R_{obs} was calculated according to Eq. (2.6). A value of R_{pure} was then calculated using Eq. (2.13) with this R_{obs}, the lot-specific correction factor ${}_{434}A_{imp}$, and ${}_{434}A_{obs}$. Finally, to calculate $pH_{T,corr}$, the calculated value of R_{pure} was used in Eq. (2.4). According to the corrective model developed above, this value of $pH_{T,corr}$ should be equivalent to the value of $pH_{T,pure}$ that would be obtained using purified mCP.

To test this expectation, the $pH_{T,pure}$ of each batch of stock solution was determined using flash-purified mCP and the equations and constants of Liu et al. [6]. Finally, the two pH_T values were compared: $pH_{T,pure}$ (obtained using purified mCP) and $pH_{T,corr}$ (obtained using unpurified mCP and its lot-specific ${}_{434}A_{imp}$ correction).

Table 2.2 Summary of ${}_{434}A_{imp}$ correction factors. For all samples, [mCP] ≈ 3.3 μM and cell path length = 10 cm. The ${}_{434}A_{imp}$ values are calculated using Eq. (2.17).

mCP Lot	**${}_{434}A_{imp}$**
TCI lot #FDP01	2.977×10^{-3}
Aldrich lot #11517KC	4.413×10^{-3}
MP Bio lot #1426K	4.545×10^{-3}
Acros Organics lot #1426K	7.832×10^{-3}
Kodak lot #C102024	9.655×10^{-3}
Ricca lot #2107749	1.297×10^{-2}

2.5 Results

2.5.1 Determination of ${}_{434}A_{imp}$ Correction Factors

The results of the high-pH determinations of lot-specific ${}_{434}A_{imp}$ correction factors are summarized in Table 2.2. Each value is specific to a particular spectrophotometric pathlength (10 cm in this case) and final concentration of mCP (3.3 μM in this case). Among the six dye solutions tested, the TCI lot had the smallest impurity contribution to absorbance at 434 nm, and the Ricca lot had the largest. Impurities in a commercial lot of mCP may be present as a single

species or as multiple species. The value of ${}_{434}A_{\text{imp}}$ can be considered as the sum of absorbances for all impurities that absorb light at 434 nm.

2.5.2 Application of ${}_{434}\mathbf{A}_{imp}$ to Measurements of pH_T

Results for pH_T measured for the six batches of stock solution, each paired with a single lot of unpurified mCP, are summarized in Table 2.3 and Fig. 2.1. The findings are reported as pH_T residuals for the cases of no-correction (i.e., $pH_{T,obs}$ minus $pH_{T,pure}$) and with-correction (i.e., $pH_{T,corr}$ minus $pH_{T,pure}$). In Fig. 2.1, the dots show the mean residuals as a function of $pH_{T,pure}$: orange dots for no-correction (pH_T calculated without the ${}_{434}A_{\text{imp}}$ correction) and purple dots for with-correction (pH_T calculated with the ${}_{434}A_{\text{imp}}$ correction). Error bars represent the standard deviation for replicate samples. The results demonstrate that for the six dye lots tested, accounting for ${}_{434}A_{\text{imp}}$ consistently brings the pH_T measured with unpurified mCP into better agreement with the "true" pH_T (i.e., $pH_{T,pure}$). The improvement is as much as 0.01 at low pH and as much as 0.025 at higher pH.

The corrective model worked better for some dye lots than others. For three of the six lots (TCI, Aldrich, and Kodak), the ${}_{434}A_{\text{imp}}$ correction yielded $pH_{T,corr}$ values within ±0.003 units of $pH_{T,pure}$ across the full range of pH_T examined. For the other lots (Acros Organics, MP Bio, and Ricca), the ${}_{434}A_{\text{imp}}$ model performed relatively well at lower pH_T but was less effective when $pH_T > 8.0$. At the highest pH_T tested (~8.25), the model was able to bring the pH_T residuals for these three lots to within –0.0102, –0.0089, and –0.0051. These smaller residuals represent a significant improvement but are still larger than the high-pH residuals for the other three lots: –0.0006, 0.0008, and 0.0011 (for TCI, Aldrich, and Kodak, respectively).

Notably, the magnitude of ${}_{434}A_{\text{imp}}$ (Table 2.2) is not a definitive determinant of how well the corrective model will perform – i.e., how well $pH_{T,corr}$ will agree with $pH_{T,pure}$ (Table 2.3; Fig.

2.1). The Kodak lot, for example, had the second-largest ${}_{434}A_{\text{imp}}$ value but among the smallest pH_T residuals. Even an indicator lot with a relatively high concentration of impurities may provide high-quality pH_T values after application of the corrective model.

Table 2.3 Summary of pH_T values determined for each of the six stock solutions, using purified mCP ($pH_{T,pure}$), unpurified mCP without ${}_{434}A_{\text{imp}}$ correction ($pH_{T,obs}$), and unpurified mCP with ${}_{434}A_{\text{imp}}$ correction ($pH_{T,corr}$). Each batch of stock solution was paired with a single lot of unpurified mCP, as indicated by the Batch ID names.

Batch ID	**$pH_{T,pure}$**	**$pH_{T,obs}$**	**$pH_{T,corr}$**	**$pH_{T,obs} - pH_{T,pure}$ Residual**	**$pH_{T,corr} - pH_{T,pure}$ Residual**
TCI #FDP01	7.2563	7.2551	7.2579	–0.0012	0.0016
	7.4980	7.4956	7.4986	–0.0024	0.0006
	7.7290	7.7253	7.7290	–0.0037	9.96×10^{-6}
	8.0001	7.9946	7.9991	–0.0055	–0.0010
	8.3439	8.3355	8.3432	–0.0084	–0.0006
Aldrich #11517KC	7.2829	7.2774	7.2815	–0.0055	–0.0014
	7.5461	7.5401	7.5451	–0.0060	–0.0010
	7.7451	7.7379	7.7433	–0.0072	–0.0019
	8.0036	7.9968	8.0041	–0.0068	0.0005
	8.2714	8.2622	8.2722	–0.0092	0.0008
MP Bio #1426K	7.2211	7.2186	7.2227	–0.0025	0.0016
	7.4951	7.4934	7.4981	–0.0017	0.0030
	7.7267	7.7219	7.7267	–0.0048	–0.0001
	8.0266	8.0162	8.0240	–0.0104	–0.0026
	8.2767	8.2576	8.2678	–0.0192	–0.0089
Acros Organics #1426K	7.2274	7.2192	7.2270	–0.0082	–0.0004
	7.5211	7.5118	7.5197	–0.0093	–0.0014
	7.7622	7.7482	7.7589	–0.0140	–0.0032
	8.0191	8.0020	8.0154	–0.0171	–0.0038
	8.3231	8.2942	8.3130	–0.0290	–0.0102
Kodak #C102024	7.2861	7.2813	7.2885	–0.0048	0.0024
	7.5125	7.5073	7.5164	–0.0051	0.0039
	7.7479	7.7353	7.7476	–0.0126	–0.0004
	8.0188	8.0046	8.0179	–0.0142	–0.0009
	8.3324	8.3124	8.3335	–0.0200	0.0011
Ricca #2107749	7.2372	7.2268	7.2375	–0.0104	0.0004
	7.5257	7.5139	7.5262	–0.0119	0.0004
	7.7664	7.7505	7.7662	–0.0158	–0.0002
	8.0415	8.0210	8.0403	–0.0205	–0.0012
	8.3178	8.2848	8.3127	–0.0330	–0.0051

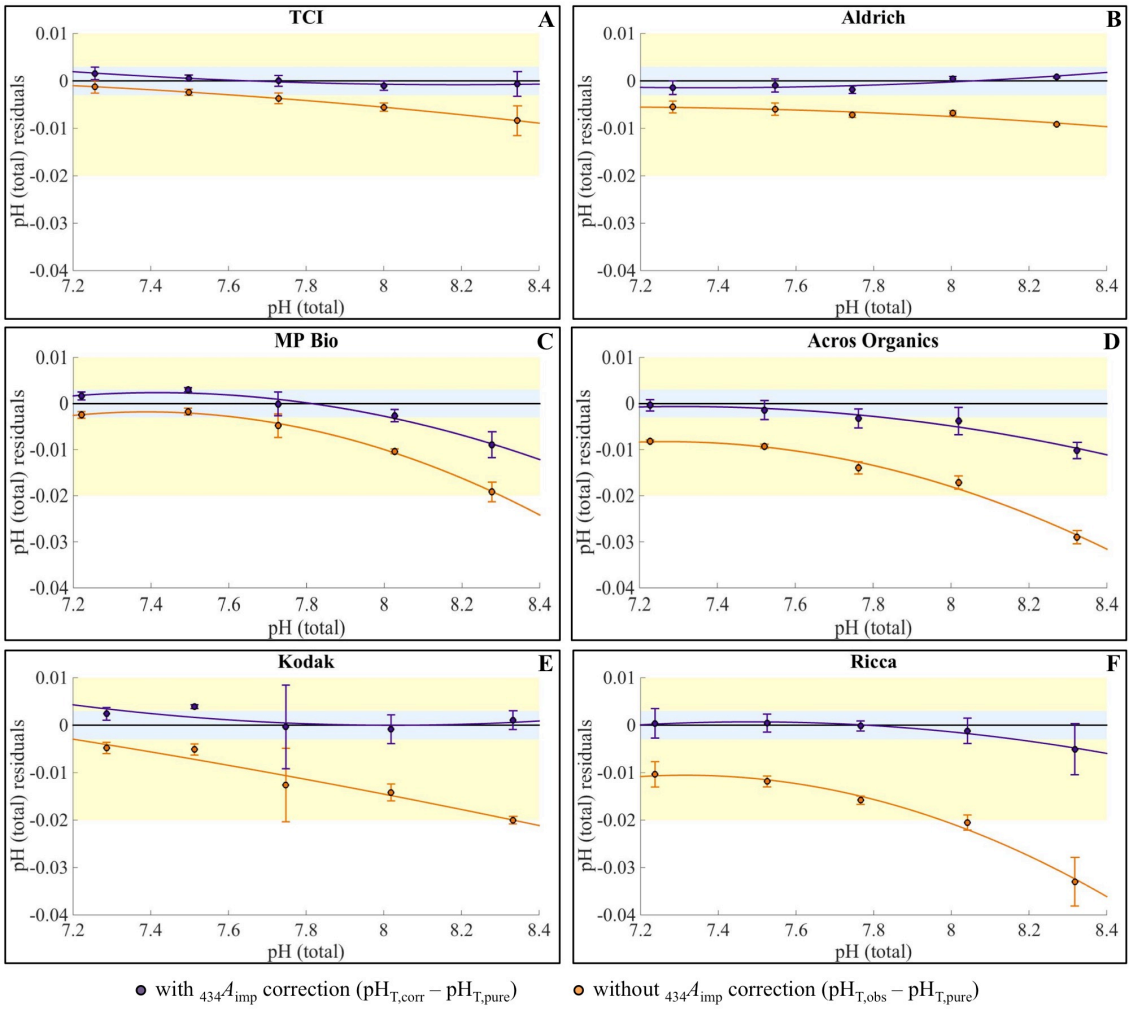

Fig. 2.1 Mean pH_T residuals (pH_T measured using unpurified mCP minus $pH_{T,pure}$) as a function of $pH_{T,pure}$. Differences are shown with and without $_{434}A_{imp}$ correction (purple and orange dots, respectively), for the six unpurified dyes: (A) TCI, (B) Aldrich, (C) MP Bio, (D) Acros Organics, (E) Kodak, and (F) Ricca. Error bars represent one standard deviation from the mean value. Interpolation lines are second-order polynomials ($r^2 > 0.94$ for all regressions). Shaded regions define the GOA-ON uncertainty goals: yellow represents the "weather" goal (±0.02), and blue represents the "climate" goal (±0.003).

2.5.3 Comparison with GOA-ON "Weather" and "Climate" Measurement Goals

Each indicator lot was also assessed to determine the pH range within which its measurement accuracy meets the GOA-ON "weather" and "climate" uncertainty goals for ocean pH measurements (Fig. 2.1). Deviations of $pH_{T,obs}$ and $pH_{T,corr}$ from $pH_{T,pure}$ (i.e., residuals) are here considered as contributions to measurement "uncertainty." In Fig. 2.1, the blue and yellow

shaded regions represent the GOA-ON measurement uncertainty goals. Residuals that fall within the yellow zone meet the "weather" goal (±0.02, shown up to +0.01 in Fig. 1), and those that fall within the blue zone meet the "climate" goal (±0.003).

For the "weather" goal, four of the six unpurified indicator lots provided uncorrected measurements ($pH_{T,obs}$) within the desired bounds over the entire range of experimental pH (TCI, Aldrich, MP Bio, and Kodak). The remaining two lots fell out of compliance with the goal at higher pH values. With the ${}_{434}A_{imp}$ correction (i.e., $pH_{T,corr}$), all six unpurified lots met the ±0.02 "weather" goal over the entire pH range.

For the more stringent "climate" goal, none of the unpurified mCP lots were able to provide uncorrected ($pH_{T,obs}$) measurements that were GOA-ON–compliant over the entire range of experimental pH. Two lots provided acceptable $pH_{T,obs}$ measurements at relatively low pH_T values (≤7.61; TCI and MP Bio). With the ${}_{434}A_{imp}$ correction, three of the six unpurified lots were able to meet the "climate" goal across the full experimental pH_T range (TCI, Aldrich, and Kodak). Every lot was in compliance for the more limited pH_T range of approximately 7.25 to 7.8. Up to pH 8.0, every lot provided $pH_{T,corr}$ measurements within ±0.004 of $pH_{T,pure}$, just outside the GOA-ON goal.

2.6 Discussion

The ${}_{434}A_{imp}$ protocol to assess and correct for the presence of colored impurities in off-the-shelf mCP powders significantly expands the availability of high-quality ocean pH measurements. Without application of the ${}_{434}A_{imp}$ corrective model, pH differences ranging from approximately –0.01 to –0.033 at pH_T ~8.25 could be expected for measurements made with unpurified mCP. When the ${}_{434}A_{imp}$ correction was applied, however, all six indicator lots showed

significant improvements in data quality, with all pH differences at pH_T ~8.25 minimized to approximately –0.01 or less.

2.6.1 Model Advantages

One way to correct for indicator impurities is to compare pH_T values obtained using unpurified versus purified mCP [21]. This approach, though, requires at least some amount of purified mCP and can be laborious, requiring two series of measurements over a range of pH (e.g., Fig. 2.1). The ${}_{434}A_{imp}$ correction method, in contrast, is simple to perform and can be used even when no purified mCP is available.

Another strength of the ${}_{434}A_{imp}$ correction method is its relative insensitivity to changes in temperature and salinity. In the Liu et al. [6] algorithm for computing pH_T from mCP absorbance ratios (Eq. 2.4), the term $K_I e_2$ is highly sensitive to changes in sample T and S. For example, the $S = 35$ value of e_2/e_3 at $T = 293.15$ K differs from the value at $T = 298.15$ K by only ~2% (Eq. 2.5), but the corresponding values of $K_I e_2$ differ by ~14% (see Liu et al. [6] for formula to calculate $K_I e_2$). The ${}_{434}A_{imp}$ term, in contrast, is insensitive to changes in S and T because colored impurities are not involved in H^+ exchange equilibria. This implies that the ${}_{434}A_{imp}$ correction can be applied to obtain a good approximation of R_{pure} over a wide range of temperature, salinity, and pressure.

2.6.2 Model Implications

Values of ${}_{434}A_{imp}$ are lot-specific [5]. Changes in synthesis techniques or reagents may result in different quantities or identities of impurities in mCP powders, even for different lots from a single vendor. It is therefore recommended that the procedure outlined in this study be used to characterize any lot of unpurified mCP that is to be used for pH measurements.

The Beer-Lambert Law states that a spectrophotometric absorbance measurement is directly proportional to the optical-cell path length multiplied by the concentration of the colorimetric species. Values of ${}_{434}A_{\text{imp}}$ determined for a particular set of experimental conditions can therefore be easily adjusted mathematically to apply to other conditions. For example, the values of ${}_{434}A_{\text{imp}}$ in Table 2.2 would be doubled for a change in dye concentration from 3.3 μM to 6.6 μM. Likewise, the ${}_{434}A_{\text{imp}}$ values would be halved for a change in pathlength from 10 cm to 5 cm.

It is important to note that Eq. (2.13) is appropriate only when ${}_{434}A_{\text{imp}}$ is independent of pH (i.e., when the impurities that contribute to absorbance at 434 nm do not act as acids or bases). The assumption of pH independence appears to be appropriate for all six of our indicator lots over the limited range of approximately $7.25 \leq \text{pH}_\text{T} \leq 8.00$ and seems to be particularly well justified for the lots produced by TCI, Aldrich, and Kodak.

This corrective model, though developed to account for mCP impurity absorbances, should also be applicable to other sulfonephthalein indicators. Patsavas et al. [7] observed that solutions of unpurified Cresol Red suffer from spurious impurity-associated absorbances at the wavelength of maximum absorption for the HI^- form (433 nm) and that the effect of impurity absorbances is greatest at higher pH (as is the case for unpurified mCP; Fig. 2.1). Use of the impurity correction model developed in this work should also improve the accuracy of pH measurements with Cresol Red.

Similarly, Liu et al. [6] noted that some lots of unpurified Thymol Blue indicator exhibit pH differences as large as 0.01, which were attributed to impurities. More recently, Lai et al. [22] modified the flash chromatography purification technique of Patsavas et al. [23] to purify Phenol Red for use in freshwater pH measurements, citing concerns about indicator impurities. Neither

of these studies elaborated on the wavelengths at which the impurities absorbed light, but both serve to highlight the potential for using a corrective model to account for impurity absorbances. In view of the simplicity of our corrective absorbance model, we recommend its application to measurements with any unpurified indicator that exhibits a pattern of pH residuals similar to those shown in Fig. 2.1.

2.7 Conclusions and Recommendations

For high-quality spectrophotometric pH measurements, purified indicator should always be the first choice. If purified mCP is unavailable or if the user's need does not justify the expense of purified mCP, application of the ${}_{434}A_{\text{imp}}$ corrective model is recommended. This method is convenient and inexpensive, and its application substantially improves the quality of pH_T analyses obtained using unpurified mCP.

Calculation of the ${}_{434}A_{\text{imp}}$ correction factor requires neither purified indicator nor laborious comparative measurements over a range of pH. Determination of ${}_{434}A_{\text{imp}}$ for a given lot of off-the-shelf mCP requires only that the user measure absorbances of a thermostatted sample at pH ~12 (Table 2.1). The value of ${}_{434}A_{\text{imp}}$ then calculated from Eq. (2.17) can be subsequently applied to all pH_T measurements made with that particular lot of indicator.

Properly stored crystalline mCP is highly stable. As a result, the ${}_{434}A_{\text{imp}}$ correction method may also be applied to historical measurements made with unpurified indicator — provided that the original absorbance data and a sample of the original mCP powder are available, as recommended [5–7]. If different indicator concentrations or spectrophotometric path lengths were used for the ${}_{434}A_{\text{imp}}$ determination compared to the original pH measurements, the Beer–Lambert Law can be used to calculate a value of ${}_{434}A_{\text{imp}}$ appropriate to the original experimental conditions.

To date, little is known about the shelf life of mCP solutions. It is therefore recommended that indicator solutions be consumed within a few weeks after preparation. Whenever possible, solutions of mCP should be made fresh for each application, to minimize the chance of dye breakdown or microbial contamination. These processes have not been extensively studied but could conceivably, over extended periods of time, alter the level or nature of mCP impurities.

The corrective procedure outlined here is meant as guidance for researchers using unpurified mCP for seawater pH measurements. This ${}_{434}A_{\text{imp}}$ model can enable scientists using unpurified mCP to make seawater pH measurements that fit within the GOA-ON guidelines.

2.8 Acknowledgments

The authors gratefully acknowledge financial support from the National Science Foundation, project number OCE 1220110. N.K. Douglas was supported by a Presidential Doctoral Fellowship from the University of South Florida Office of Graduate Studies. The authors wish to thank Dr. Xuewu Liu and Dr. Bo Yang for technical assistance, Dr. Tonya Clayton for valuable editorial support, and two anonymous reviewers for helpful and insightful comments.

2.9 References

1. Douglas, N.K., Byrne, R.H. (2017a). Achieving accurate spectrophotometric pH measurements using unpurified meta-cresol purple. *Marine Chemistry* **190**, 66-72.
2. United Nations General Assembly resolution 68/70, Oceans and the law of the sea, A/RES/68/70 (9 December 2013), available from undocs.org/A/RES/68/70.
3. Newton, J.A., Feely, R.A., Jewett, E.B., Williamson, P., Mathis, J., 2014. Global Ocean Acidification Observing Network: Requirements and Governance Plan. http://www.goa-on.org/docs/GOA-ON_plan_print.pdf
4. Bockmon, E.E., Dickson, A.G., 2015. An inter-laboratory comparison assessing the quality of seawater carbon dioxide measurements. *Marine Chemistry* **171**, 36–43.
5. Yao, W., Liu, X., Byrne, R.H., 2007. Impurities in indicators used for spectrophotometric seawater pH measurements: Assessment and remedies. *Marine Chemistry* **107**, 167–172.

6. Liu, X., Patsavas, M.C., Byrne, R.H., 2011. Purification and characterization of meta-cresol purple for spectrophotometric seawater pH measurements. *Environmental Science & Technology* **45**, 4862–4868.

7. Patsavas, M.C., Byrne, R.H., Liu, X., 2013a. Purification of meta-cresol purple and cresol red by flash chromatography: Procedures for ensuring accurate spectrophotometric seawater pH measurements. *Marine Chemistry* **150**, 19–24.

8. Robert-Baldo, G.L., Morris, M.J., Byrne, R.H., 1985. Spectrophotometric determination of seawater pH using phenol red. *Analytical. Chemistry* **57**, 2564–2567.

9. Byrne, R.H., 1987. Standardization of standard buffers by visible spectrophotometry. *Analytical Chemistry* **59**(10), 1479–1481.

10. Byrne, R.H., Breland, J.A., 1989. High precision multiwavelength pH determinations in seawater using cresol red. *Deep-Sea Research* **36**(5), 803–810.

11. Clayton, T.D., Byrne, R.H., 1993. Spectrophotometric seawater pH measurements: total hydrogen ion concentration scale calibration of m-cresol purple and at-sea results. *Deep Sea Research I* **40**(10), 2115–2129.

12. Liu, X., Wang, Z.A., Byrne, R.H., Kaltenbacher, E.A., Bernstein, R.E., 2006. Spectrophotometric measurements of pH in-situ: Laboratory and field evaluations of instrumental performance. *Environmental Science & Technology* **40**, 5036–5044.

13. Dore. J.E., Lukas, R., Sadler, D.W., Church, M.J., Karl, D.M., 2009. Physical and biogeochemical modulation of ocean acidification in the central North Pacific. *Proceedings of the National Academy of Sciences of the United States of America* **106**(30), 12235-12240.

14. Passow, U., 2012. The abiotic formation of TEP under different ocean acidification scenarios. *Marine Chemistry* **128**, 72-80.

15. Torstensson, A., Chierici, M., Wulff, A., 2012. The influence of increased temperature and carbon dioxide levels on the benthic/sea ice diatom *Navicula directa*. *Polar Biology* **35**, 2015-214.

16. Bramanti, L., Movilla, J., Guron, M., Calvo, E., Gori, A., Dominguez-Carrió, C., Grinyó, J., Lopez-Sanz, A., Martinez-Quintana, A., Pelejero, C., Ziveri, P., Rossi, S., 2013. Detrimental effects of ocean acidification on the economically important Mediterranean red coral (*Corallium rubrum*). *Global Change Biology* **19**: 1897–1908.

17. Tatters, A.O., Roleda, M.Y., Schnetzer, A., Fu, F., Hurd, C.L., Boyd, P.W., Caron, D.A., Liu, A.A.Y., Hoffmann, L.J., Hutchins, D.A., 2013. Short- and long-term conditioning of a temperate marine diatom community to acidification and warming. *Philosophical Transactions of the Royal Society B* **368**, 14 p.

18. Frieder, C.A., Gonzalez, J.P., Bockmon, E.E., Navarro, M.O., Levin, L.A., 2014. Can variable pH and low oxygen moderate ocean acidification outcomes for mussel larvae? *Global Change Biology* **20**, 754-764.

19. Zhang, H., Byrne, R.H., 1996. Spectrophotometric pH measurements of surface seawater at in-situ conditions: Absorbance and protonation behavior of thymol blue. *Marine Chemistry* **52**, 17–25.

20. Dickson, A.G., Sabine, C.L., Christian, J.R. (Eds.), 2007. Guide to best practices for ocean CO_2 measurements. PICES Special Publication 3, 191 p.

21. Fajar, N.M., García-Ibáñez, M.I., SanLeón-Bartolomé, H., Álvarez, M., Pérez, F.F., 2015. Spectrophotometric measurements of the carbonate ion concentration: Aragonite saturation states in the Mediterranean Sea and Atlantic Ocean. *Environmental Science & Technology* **49**, 11679–11687.

22. Lai, C.Z., DeGrandpre, M.D., Wasser, B.D., Brandon, T.A., Clucas, D.S., Jaqueth, E.J., Benson, Z.D., Beatty, C.M., Spaulding, R.S., 2016. Spectrophotometric measurement of freshwater pH with purified meta-cresol purple and phenol red. *Limnology and Oceanography: Methods* **14**(12), 864-873.

23. Patsavas, M.C., Byrne, R.H., Liu, X., 2013b. Physical-chemical characterization of purified cresol red for spectrophotometric pH measurements. *Marine Chemistry* **155**, 158-164.

CHAPTER THREE:

SPECTROPHOTOMETRIC pH MEASUREMENTS FROM RIVER TO SEA:

CALIBRATION OF mCP for $0 \leq S \leq 40$ AND $278.15 \leq T \leq 308.15$ K

Note to Reader

Portions of this chapter have been published [1] and are included with the permission of the publisher.

3.1 Abstract

The indicator meta-cresol purple (mCP) has been widely used for spectrophotometric pH measurements in seawater and has been recently used in freshwater as well. Previous works have not, however, provided the comprehensive characterization of purified mCP (equilibrium and spectral behavior) required for pH measurements across the full ranges of temperature (T) and salinity (S) found in temperate estuaries. This work provides, for the first time, a comprehensive S- and T-dependent model for spectrophotometric pH measurements appropriate to freshwater, estuarine water, and seawater. Our model combines previous characterizations of the behavior of (a) purified mCP in pure water ($S = 0$), (b) purified mCP in seawater ($20 \leq S \leq 40$), and (c) unpurified mCP at 298.15 K and $0 \leq S \leq 40$, herein corrected for the effects of impurities. Using the ratio (R) of mCP absorbances at 578 nm and 434 nm, the summary equations for calculations of pH on the total proton concentration scale for the conditions of $0 \leq S \leq 40$ and $278.15 \leq T \leq 308.15$ K are as follows:

$\mathrm{pH_T} = \mathrm{p}(K_\mathrm{I} e_2) + \log\left(\frac{R - e_1}{1 - R\frac{e_3}{e_2}}\right)$, where

$e_1 = -0.007762 + 4.5174 \times 10^{-5}\, T$

$e_3/e_2 = -0.020813 + 2.60262 \cdot 10^{-4}\, T + 1.0436 \cdot 10^{-4}\, (S - 35)$

$\mathrm{p}(K_\mathrm{I} e_2) = 5.561224 - 0.547716\, S^{0.5} + 0.123791\, S - 0.0280156\, S^{1.5} + 0.00344940\, S^2$

$-0.000167297\, S^{2.5} + 52.640726\, S^{0.5}\, T^{-1} + 815.984591\, T^{-1}$

This new model, appropriate for use with purified mCP, produces pH values that are within ±0.004 of those obtained using previously published data and purified-mCP models for pure water and seawater.

3.2 Introduction

Spectrophotometric procedures remain largely underutilized for pH investigations of low-salinity waters ($S < 20$), although such methods are widely employed in open-ocean work [2–8]. Because many important pH-dependent chemical processes occur in low-S environments such as lakes [9–11] and estuaries [12–14], high-quality spectrophotometric pH measurements are essential for understanding the role of these environments in chemical cycling.

In the decades since the initial physical–chemical characterization of meta-cresol purple (mCP) for use in seawater [7], this sulfonephthalein dye has become the most widely used indicator for marine spectrophotometric pH measurements. Recently, mCP purification procedures [8, 15–18] have alleviated earlier concerns about the effects of colorimetric impurities on measurement accuracy [1,19–21]. Efforts to employ spectrophotometric methods with a variety of indicators in freshwater environments have included the works of Yao and Byrne [12], French et al. [22], Liu et al. [23], Yuan and DeGrandpre [24], and Lai et al. [17,18].

However, only two studies have been performed to allow for the use of mCP in estuaries [19,25], and both were conducted using unpurified mCP.

Mosley et al. [19] used unpurified mCP to develop an S-dependent pK_I relationship for mCP across the range $0 \leq S \leq 40$ at $T = 298.15$ K (where K_I is the dissociation constant of the indicator for the reaction $HL^- \Leftrightarrow H^+ + L^{2-}$). Hammer et al. [25] subsequently combined the S-dependent pK_I of Mosley et al. [19] and the T-dependent terms of Clayton and Byrne [7] to create a model applicable to the Baltic Sea. However, the use of unpurified mCP can produce pH measurement errors on the order of 0.015 or larger [21]. Such measurements can be corrected retrospectively to improve accuracy when original measurements are archived and a sample of the stock indicator is preserved [21], but a comprehensive, generally applicable model for purified mCP is preferable.

There are currently no characterizations of purified mCP over the wide range of S relevant to estuaries. Although pK_I for purified mCP has recently been characterized at $S = 0$ over a range of T [17,18] the resulting measurement algorithm, which is based on the procedures of Yao and Byrne [12], is subject to the limitations of the Davies [26] equation for prediction of ion activity coefficients at ionic strengths substantially greater than zero [27]. Consequently, a spectrophotometric pH measurement model is needed to facilitate the seamless use of mCP across aquatic and marine environments, from $S = 0$ to $S = 40$.

In the present work, using procedures similar to the pH-correction methods of Douglas and Byrne [21], it is shown that previously determined pK_I values for mCP at $0 \leq S \leq 40$ at $T = 298.15$ K [19] can be corrected for the effects of indicator impurities. These corrected pK_I values are then combined with the pH measurement algorithms for freshwater [17,18] and seawater [8] to produce a comprehensive and seamless model for mCP-based measurements of total proton

scale pH (pH_T) over the salinity range of 0 to 40 and the temperature range of 278.15 to 308.15 K.

Spectrophotometric pH of a water sample is determined using the following relationship [4,7,28]:

$$pH_T = pK_I + \log\left(\frac{R - e_1}{e_2 - R e_3}\right) \quad (3.1)$$

where $pH_T = -\log [H^+]_T$, R is the ratio of the spectrophotometric absorbances ($_{\lambda}A$) at the indicator's base-form (I^{2-}) and acid-form (HI^-) absorbance peaks ($R = {}_{578}A/{}_{434}A$), and the terms e_1, e_2, and e_3 (referred to generally as e_x) are HI^- and I^{2-} molar absorptivity ratios at selected wavelengths.

Liu et al. [8] characterized the physical–chemical properties of HPLC-purified mCP in seawater and determined the T and S dependence of the e_x ratios and K_I. Their refined pH_T equation is given in the following form [8,29]:

$$pH_T = p(K_I e_2) + \log\left(\frac{R - e_1}{1 - R\frac{e_3}{e_2}}\right) \quad (3.2)$$

Additional information regarding the $p(K_I e_2)$, e_1, and e_3/e_2 terms can be found in Liu et al. [8].

HPLC tests of off-the-shelf mCP have revealed that colorimetric impurities interfere with the absorbance of the HI^- peak at 434 nm, thus spuriously lowering the pH_T calculated from Eqs. (3.1) and (3.2) [8,20]. With this observation in mind, Douglas and Byrne [21] developed the following model to correct for absorbance contributions from impurities in commercially available mCP:

$$R_{pure} = R_{obs}\left(1 + \frac{{}_{434}A_{imp}}{{}_{434}A_{obs} - {}_{434}A_{imp}}\right) \quad (3.3)$$

where R_{pure} is the R-ratio that would have been measured with purified mCP; R_{obs} is the R-ratio actually observed with unpurified mCP; ${}_{434}A_{imp}$ is the 434 nm absorbance due to colorimetric

impurities alone (experimentally determined for each lot of commercial mCP); and ${}_{434}A_{\text{obs}}$ is the 434 nm sample absorbance observed using unpurified mCP. The ${}_{434}A_{\text{imp}}$ term is determined by measuring absorbances of the unpurified mCP in solutions at high pH (~12), where the concentration of HI^- is negligible and all mCP is in the basic I^{2-} form. Measurements of absorbance ratios under these conditions can be used to reveal the small spectral influence of impurities in the presence of the dominant spectral signature of the I^{2-} species. The ${}_{434}A_{\text{imp}}$ model assumes that any impurities in the dye solution do not participate in acid-base H^+ exchange equilibria and instead behave as inert chemical species in the sample; Douglas and Byrne [21] found this assumption to be appropriate over the range $7.25 \leq \text{pH}_\text{T} \leq 8.00$ for the six lots of unpurified mCP used to test the ${}_{434}A_{\text{imp}}$ model, i.e., Eq. (3.3).

In this work, the equations developed by Douglas and Byrne [21] were extended to correct previously published experimentally determined pK_I values for the effects of indicator impurities. The procedures developed for retrospective refinements of pK_I values were then applied to the data set of Mosley et al. [19].

3.3 Theory

Correction of previously published pK_I values that were obtained using unpurified mCP can be performed using the following mathematical relationship for the spectral behavior of the indicator and the colorimetric impurities found in a dye solution: ${}_{434}A_{\text{obs}} - {}_{434}A_{\text{mCP}} = {}_{434}A_{\text{imp}}$ (Eq. (7) of Douglas and Byrne [21].

Dividing Eq. (7) of Douglas and Byrne [21] by ${}_{578}A$ results in the following expression:

$$\frac{{}_{434}A_{\text{obs}}}{{}_{578}A} - \frac{{}_{434}A_{\text{mCP}}}{{}_{578}A} = \frac{{}_{434}A_{\text{imp}}}{{}_{578}A} \tag{3.4}$$

Eq. (3.4) can be rewritten as

$$(R_{\text{obs}})^{-1} - \left(R_{\text{pure}}\right)^{-1} = \frac{{}_{434}A_{\text{imp}}}{{}_{578}A} \tag{3.5}$$

From algebraic rearrangement of the fundamental equation that relates mCP absorbances to mCP molar absorptivities, dissociation constants, and pH (Eq. (5c) of Clayton and Byrne [7]), ${}_{578}A$ can be expressed as follows:

$$ {}_{578}A = \frac{{}_{578}\varepsilon_{\mathrm{I}} + {}_{578}\varepsilon_{\mathrm{HI}} \cdot {K_{\mathrm{I}}}^{-1} \cdot [\mathrm{H}^+]_{\mathrm{T}}}{1 + {K_{\mathrm{I}}}^{-1} * [\mathrm{H}^+]_{\mathrm{T}}} \cdot l \cdot [\mathrm{mCP}]_{\mathrm{T}} \tag{3.6} $$

where ${}_{578}\varepsilon_{\mathrm{I}}$ and ${}_{578}\varepsilon_{\mathrm{HI}}$ are the molar absorptivity coefficients for mCP at 578 nm for the I^{2-} and HI^{-} forms of mCP, respectively; $[\mathrm{H}^+]_{\mathrm{T}}$ is the total hydrogen ion concentration; l is the spectrophotometric cell pathlength; $[\mathrm{mCP}]_{\mathrm{T}}$ is the total concentration of mCP; and K_{I} is the dissociation constant of mCP (equivalent to the inverse of the formation constant, which was used by Clayton and Byrne [7]).

From the Beer-Lambert Law, ${}_{434}A_{\mathrm{imp}}$ is given as follows:

$$ {}_{434}A_{\mathrm{imp}} = {}_{434}\varepsilon_{\mathrm{imp}} \cdot l \cdot c \cdot [\mathrm{mCP}]_{\mathrm{T}} \tag{3.7} $$

where ${}_{434}\varepsilon_{\mathrm{imp}}$ is the molar absorptivity coefficient of impurities and c is the constant of proportionality between the concentration of impurities and the concentration of mCP indicator in an unpurified dye solution. Combining Eqs. (3.6) and (3.7) and then rearranging, the term on the right side of Eq. (3.5) can be written as

$$ \frac{{}_{434}A_{\mathrm{imp}}}{{}_{578}A} = \frac{\theta\,(1 + {K_{\mathrm{I}}}^{-1}\ [\mathrm{H}^+]_{\mathrm{T}})}{({}_{578}\varepsilon_{\mathrm{I}}/{}_{578}\varepsilon_{\mathrm{HI}}) + {K_{\mathrm{I}}}^{-1}\ [\mathrm{H}^+]_{\mathrm{T}}} \tag{3.8} $$

where θ is defined as:

$$ \theta = \frac{{}_{434}\varepsilon_{\mathrm{imp}}\, c}{{}_{578}\varepsilon_{\mathrm{HL}}} \tag{3.9} $$

Because the numerator of θ includes the molar absorptivity coefficient of impurities and depends on the proportionality constant c, values of θ are specific to every source of indicator, i.e., specific to a particular batch of synthesized mCP. If more than one dye source were used during the course of a series of measurements, more than one value of θ would be needed. Our

work assumes that a single dye solution was used for the experiments of Mosley et al. [19] and that one value of θ is sufficient for the impurity correction.

Finally, using the definitions of e_1 and e_2, Eqs. (3.5) and (3.8) can be combined to calculate R_{pure} from R_{obs}, the molar absorptivity ratios, and the known $[H^+]_T$ values of buffer solutions:

$$(R_{obs})^{-1} - (R_{pure})^{-1} = \frac{\theta\,(1 + {K_I}^{-1}\,[H^+]_T)}{{e_2}/{e_1} + {K_I}^{-1}\,[H^+]_T} \quad (3.10)$$

Eq. (3.10) allows for the calculation of θ, an inherent characteristic of the unpurified indicator used by Mosley et al. [19], from four known or calculable variables: (1) the K_I results of Mosley et al. [19] at each measured pH_{tris} for samples with $20 \le S \le 40$; (2) the e_x values of Clayton and Byrne [7], used by Mosley et al. [19]; (3) the Mosley et al. [19] R_{obs} values and pH_T measurement algorithm; and (4) R_{pure} results calculated from the model of Liu et al. (2011), to correspond to the buffers (i.e., $[H^+]_T$ values) used by Mosley et al. [19] within the range of conditions ($20 \le S \le 40$) relevant to the model of Liu et al. [8].

Subsequently, using the average value of θ determined in these calculations, Eq. (3.10) can be used to provide R_{pure} values for each of the buffers used by Mosley et al. [19]. Finally, using these R_{pure} values in conjunction with the S- and T-dependent e_1 and e_3/e_2 equations of Liu et al. [8], impurity-corrected values of $p(K_I e_2)$ can be determined (rederived) from the data of Mosley et al. [19]. These impurity-corrected values can then be combined with the algorithms for freshwater [17,18] and seawater [8] to provide a model that enables the use of mCP for pH measurements in waters of $0 \le S \le 40$ and $278.15 \le T \le 308.15$ K.

3.4 Methods

3.4.1 Obtaining Impurity-Corrected mCP p($K_I e_2$*) Values for* $0 \leq S \leq 40$ *at* $T = 298.15$ *K*

Data inputs came from Table 2 of Mosley et al. [19], adapted here in Table 3.1. The pH of each tris buffer solution is given on the total pH scale (mol kg-soln^{-1}). All calculations were performed using the MATLAB 2014b software program.

Table 3.1 Inputs (based on Table 2 of Mosley et al. [19]) and corresponding impurity-corrected outputs of R_{pure} and mCP pK_I values.

Inputs: from Mosley et al. (2004) data				**Outputs: Corrected values**	
S	**pH$_{tris}$**	**pK_I**	***R*$_{obs}$**	***R*$_{pure}$**	**pK_I**
0.06	8.0739	8.5626	0.697940	0.706456	8.5570
0.13	8.0737	8.5301	0.748921	0.758204	8.5244
0.27	8.0734	8.4849	0.825775	0.836251	8.4791
0.54	8.0728	8.4349	0.919031	0.931016	8.4289
1.01	8.0720	8.3803	1.031932	1.045833	8.3741
1.50	8.0712	8.3393	1.124683	1.140230	8.3329
2.00	8.0706	8.3069	1.203511	1.220509	8.3003
3.04	8.0694	8.2635	1.316040	1.335192	8.2567
4.03	8.0685	8.2305	1.408035	1.429021	8.2234
4.98	8.0677	8.2060	1.479686	1.502143	8.1988
7.51	8.0664	8.1556	1.638732	1.664600	8.1480
10.00	8.0660	8.1209	1.758759	1.787328	8.1130
14.99	8.0670	8.0738	1.940166	1.973030	8.0655
20.02	8.0706	8.0419	2.084332	2.125679	8.0321
20.26	8.0708	8.0425	2.082658	2.130824	8.0311
24.98	8.0763	8.0195	2.204901	2.230895	8.0136
30.01	8.0842	8.0094	2.285215	2.328938	7.9998
30.03	8.0842	8.0060	2.300660	2.329143	7.9998
35.02	8.0941	8.0013	2.367986	2.416186	7.9911
35.04	8.0941	7.9997	2.375464	2.416303	7.9910
39.99	8.1058	7.9975	2.441260	2.490691	7.9873
39.99	8.1058	7.9975	2.441260	2.490691	7.9873

The following procedure was used to calculate new p($K_I e_2$) values from the data of Mosley et al. [19] for $0 \leq S \leq 40$ at $T = 298.15$ K:

1. Using Eq. (3.1), R_{obs} was calculated for each row of data in Table 3.1 (i.e., across all salinities). The pH$_{tris}$ and pK_I data of Mosley et al. [19] were used to calculate R_{obs}. Consistent with the original assumptions of Mosley et al. [19], the molar absorptivity (e_x)

ratios of Clayton and Byrne [7] were used in these calculations: $e_1 = 0.00691$, $e_2 = 2.2220$, and $e_3 = 0.1331$.

2. For the subset of Table 3.1 data with $S \geq 20$, R_{pure} was calculated using Eq. (3.2). R_{pure} is the value that theoretically would have been obtained had Mosley et al. [19] used purified mCP. For each sample with $S \geq 20$, values of $p(K_I e_2)$, e_1, and e_3/e_2 were calculated according to the equations of Liu et al. [8]. The pH_{tris} data in Table 2 of Mosley et al. [19] were used.

3. Using Eq. (3.10) and calculated values of R_{obs} and R_{pure} for the subset of Table 3.1 data with $S \geq 20$, θ values were calculated, and the mean value of θ (hereafter referred to as $\overline{\theta}$) was determined. For this calculation, K_I values (calculated from pK_I in Table 2 of Mosley et al. [19], $[H^+]_T$ (calculated from pH_{tris} in Table 2 of Mosley et al. [19]), and the ratio $e_2/e_1 = 2.2220/0.00691 = 321.56295$ were used.

4. For the subset of Table 3.1 data with $S < 20$, Eq. (3.10) and $\overline{\theta}$ were used to calculate the quantity $(R_{obs})^{-1} - (R_{pure})^{-1}$, from which R_{pure} values could be calculated. For this calculation, $\overline{\theta}$ (from Step 3), K_I values (calculated from pK_I in Table 2 of Mosley et al., [19]), $[H^+]_T$ (calculated from pH_{tris} in Table 2 of Mosley et al. [19]), the ratio $e_2/e_1 = 321.56295$, and R_{obs} values (calculated in Step 1) were used.

5. For the entire range of salinity, Eq. (3.1) and the R_{pure} values (resulting from Steps 2 and 4) were used to calculate K_I and pK_I values for each sample. The R_{pure} values used in this step were obtained from Step 4 for samples with $S < 20$ and in Step 2 for samples with $S \geq 20$. The pH_{tris} values from Table 2 of Mosley et al. [19] and the e_x values of Clayton and Byrne [7] were utilized in Eq. (3.1).

6. Steps 3–5 were repeated using the new K_I values for Steps 3 and 4. This procedure was performed iteratively until pK_I, $\overline{\theta}$, and R_{pure} no longer changed from one iteration to the next, i.e., no value changed by $>10^{-6}$ between subsequent iterations. (Values stabilized after three iterations; typically $\overline{\theta} \approx 1.387$).

7. Using $e_2 = 2.2220$, the value assumed by Mosley et al. [19], and the final pK_I values from Step 6, new values of p($K_I e_2$) were determined.

3.4.2 Deriving a New Model for p($K_I e_2$) Across a Range of S *and* T

In order to incorporate T dependence into our algorithm, the impurity-corrected p($K_I e_2$) values calculated in Step 7 above (based on the $T = 298.15$ K data of Mosley et al. [19]) were combined with the temperature-dependent freshwater model [17,18] and the salinity and temperature-dependent marine model [8]. A best-fit algorithm for p($K_I e_2$) across the ranges $0 \le S \le 40$ and $278.15 \le T \le 308.15$ K was thereby determined as follows:

8. For $S = 0$ and $281.15 \le T \le 303.15$ K, values of e_2 and pK_I were calculated using the equations found in Tables 2 and 3 of Lai et al. [17,18] at temperature intervals of 2 K. These values of e_2 and pK_I were then used to calculate p($K_I e_2$) values. Values of p($K_I e_2$) were then calculated as the difference of pK_I and $\log_{10}(e_2)$. The number of S–T combinations and corresponding p($K_I e_2$) values determined in this step (n_{Lai}) is 12.

9. For $20 \le S \le 40$ and $278.15 \le T \le 308.15$ K, values of p($K_I e_2$) were calculated according to the equations of Liu et al. [8] at 4-unit salinity intervals and 5 K temperature intervals. The number of S–T combinations and corresponding p($K_I e_2$) values determined in this step (n_{Liu}) is 42.

10. These p($K_I e_2$) values were combined with the impurity-corrected p($K_I e_2$) values derived from the data of Mosley et al. [19] (Table 3.1). The number of *S*–*T* combinations and corresponding p($K_I e_2$) values for the corrected Mosley data ($n_{Mosley,corr}$) is 22.

11. To ensure that all three data sets (each with a different number of data points) were given equal consideration in the multivariate polynomial fit for p($K_I e_2$), each p($K_I e_2$) value was assigned a weight, W_{source}, that was inversely proportional to the size of the source data set. W_{Lai} was arbitrarily assigned a value of 1, whereupon $W_{Liu} = 0.28571$ and $W_{Mosley,corr} = 0.54545$. For example, each p($K_I e_2$) value calculated using the model of Lai et al. [17,18] was weighted by a factor of 3.5 relative to the p($K_I e_2$) values calculated using the Liu et al. [8] model ($n_{Liu} = 3.5(n_{Lai})$). The Lai-derived p($K_I e_2$) values were arbitrarily assigned a weight of 1 ($W_{Lai} = 1$). The Liu-derived p($K_I e_2$) values were therefore given a weight (W_{Liu}) of 0.28571, and the impurity-corrected Mosley-derived p($K_I e_2$) values were given a weight ($W_{Mosley,corr}$) of 0.54545.

12. A multivariate polynomial fit of the p($K_I e_2$) data was performed using the MATLAB *stepwiselm* tool, with $S^{0.5}$ and T^{-1} serving as the independent variables for fifth- and first-order polynomials (including an *S*-*T* interaction term) and the data were weighted according to Step 10 above. The full data set used for this fit is summarized in Appendix B. The *stepwiselm* tool generates a polynomial fit of the independent variables, up to the highest-order polynomial specified by the user, by adding or removing terms by stepwise regression, using *F*-test results to determine whether or not a term is added ($p \leq 0.05$ for the addition of a term) or removed ($p \geq 0.10$ for the removal of a term). This process continues until no more terms can be added or removed from the model, and the model is considered to be optimized.

3.5 Results

3.5.1 New p($K_I e_2$) Model Parameterization

The results of the R_{obs} calculations and the iterative calculations of R_{pure} and K_I (here reported as pK_I values) are shown in Table 3.1. The final values of R_{pure} are 0.009–0.049 higher than their corresponding R_{obs} values, consistent with the improvements that Douglas and Byrne [21] obtained when applying the ${}_{434}A_{imp}$ correction to their absorbance data. The final corrected values of pK_I are 0.0056–0.0114 lower than the original results of Mosley et al. [19]. Smaller differences between the original (input) and impurity-corrected (output) pK_I values are generally observed at low salinities. This pattern is expected because the larger difference between pH_{tris} and pK_I at low ionic strength (with pH being less than pK_I) increases the HI^-/I^{2-} concentration ratio and thereby minimizes the influence of impurity absorption on the pH calculations [21]. The new fit for p($K_I e_2$) as a function of S and T is given in Table 2 ($r^2 \geq 0.9999$), along with the e_x parameterizations [8] needed to calculate pH_T. Although the Liu et al. [8] e_x parameterizations were obtained only over a marine salinity range, they are assumed to apply over the full estuarine range for the purposes of these calculations.

Residuals of p($K_I e_2$), expressed as differences between the p($K_I e_2$) characterizations derived from prior studies and the values calculated according to the new model (Table 3.2), are shown in Fig. 3.1 as a function of salinity, and the temperatures of the data are color coded. The new estuarine model fits the p($K_I e_2$) values within ±0.004 across the full range of temperature and salinity conditions. The Mosley et al. [19] dataset contained multiple samples at $S \sim 20$, 30, 35, and 40. Because the paired p($K_I e_2$) values at these salinities were in very close agreement, the paired residuals overlap and appear as only a single star at each salinity (Fig. 3.1).

Table 3.2 Estuarine pH_T model and parameterizations for $0 \leq S \leq 40$ and $278.15 \leq T \leq 308.15$ K.

Model	**Source**	**Equation**	**Test values (S = 35, T = 298.15 K, R = 1)**
pH_T	Liu et al. (2011)	$pH_T = p(K_1e_2) + \log\left(\frac{R - e_1}{1 - R\frac{e_3}{e_2}}\right)$	7.66993
e_1	Liu et al. (2011)	$e_1 = -0.007762 + 4.5174 * 10^{-5}\, T$	0.00571
e_3/e_2	Liu et al. (2011)	$e_3/e_2 = -0.020813 + 2.60262 * 10^{-4}\, T + 1.0436 * 10^{-4}\,(S - 35)$	0.05678
$p(K_1e_2)$	This work	$p(K_1e_2) = 5.561224 - 0.547716\, S^{0.5} + 0.123791\, S - 0.0280156\, S^{1.5} + 0.00344940\, S^2 - 0.000167297\, S^{2.5} + 52.640726\, S^{0.5}\, T^{-1} + 815.984591\, T^{-1}$	7.64703

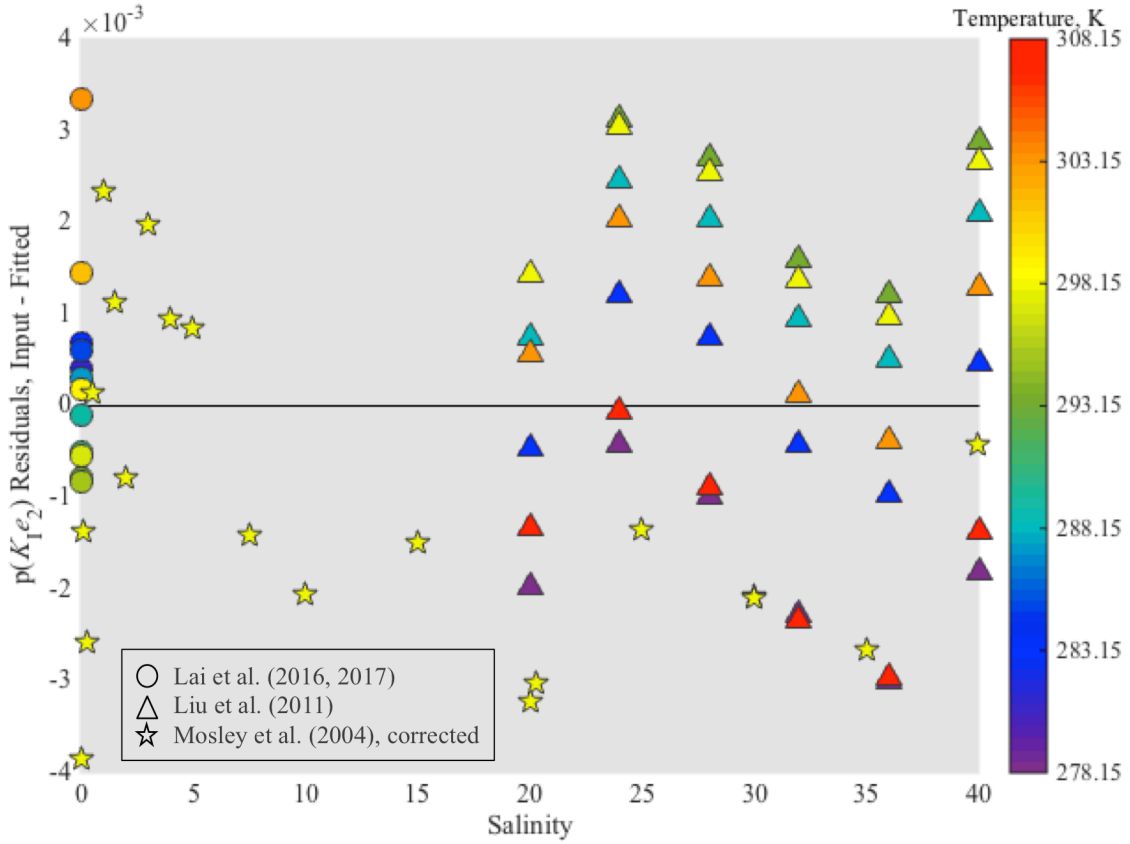

Fig. 3.1 Residuals for the new pK_1e_2 model (given in Table 3.2) as a function of salinity. Residuals are calculated as model input (as shown in the figure legend) minus the fitted values given by the new estuarine model. Colors represent temperature.

3.5.2 Comparisons of pH_T Within the Freshwater and Marine Salinity Ranges

Using the freshwater ($S = 0$) model of Lai et al. [17,18], the marine ($20 \leq S \leq 40$) model of Liu et al. [8], and the estuarine ($0 \leq S \leq 40$) model of this study (Table 3.2), pH_T values were calculated across each model's applicable ranges of S and T for R-ratios ranging between 0.2 and 2.0. The pH_T values calculated in this manner ranged from 6.8 to 8.8. The pH residuals, defined as $\Delta pH_T = pH_T$(Lai or Liu model) – pH_T(estuarine model), are identical to the $p(K_1e_2)$ residuals shown in Fig. 3.1 within ±0.0006. Consequently, as for the $p(K_1e_2)$ residuals, the pure and marine water pH_T residuals are within approximately ±0.004, independent of the R-ratio. The residuals of pH_T and $p(K_1e_2)$ are strongly correlated because the influence of variations in the modeled e_1 and e_3/e_2 terms (Eq. (3.2)) is comparatively small.

3.6 Discussion

This work provides, for the first time, a model appropriate for obtaining impurity-free spectrophotometric mCP-based pH measurements across the full range of river-to-sea salinities. The model described in Table 2 combines information from three independent studies of the molecular characteristics of mCP, including one that was herein corrected for the effects of indicator impurities. The new pH_T model agrees well with the empirical freshwater models of Lai et al. [17,18] (approximately ±0.003 for zero ionic strength and $281.15 \leq T \leq 303.15$ K), the empirical marine model of Liu et al. [8] (approximately ±0.003 pH units for $20 \leq S \leq 40$ and $278.15 \leq T \leq 308.15$ K), and the impurity-corrected estuarine data of Mosley et al. [19] (approximately ±0.004 for $0 \leq S \leq 40$ and $T = 298.15$ K). Given that different methodologies were used for these three different studies, we consider this agreement to be very good. The ±0.004 internal consistency of the composite estuarine pH model should be sufficient to reliably monitor the often-large pH variability observed in estuarine environments (e.g., [8]).

It is important to be aware that spectrophotometric pH measurements made in freshwater present challenges not encountered for measurements in seawater [12]. For example, adding mCP to a sample solution causes pH perturbations [7,17,30] that are inversely proportional to the solution's buffer intensity [31]. Because the total alkalinity (TA) of marine water is consistently on the order of ~2000 μM, the buffer intensity of seawater leads to relatively small indicator-induced pH perturbations. In freshwater, though, the alkalinity and buffer intensity are commonly much lower, so mCP perturbation effects are generally much larger.

To minimize this perturbation effect, the *R* of the indicator solution can be adjusted to match that of the sample solution as closely as possible by the addition of acid or base to raise or lower the indicator solution *R*-ratio. One can also apply a perturbation correction in which stepwise indicator additions are performed in order to linearly extrapolate observed pH values (or *R* values) to a pH appropriate to near-zero concentrations of mCP [7,19,30]. For very weakly buffered samples (e.g., freshwater), the use of a long-pathlength spectrophotometric cell (10 cm or longer) is recommended to minimize the amount of indicator required to be added [20,24,30].

Such measures are important for improving the accuracy and precision of pH measurements, but the optimal precision or accuracy for a given undertaking should be assessed in the context of project aims and also of the temporal and spatial variability of the system under investigation. For example, accurate indicator-addition perturbation corrections are essential for rigorous measurements of open-ocean pH, where demands for precision on the order of 0.001 or better are standard. In a spatially heterogeneous system, however, where large pH variations (i.e., > 0.01 pH units) occur on a scale of several meters, pH precisions of ±0.001 may be excessively burdensome and a pH perturbation correction may not be warranted. If accuracy better than ±0.01 is desired, perturbation corrections are recommended [17] and likely essential.

Another matter of considerable concern for pH measurements at very low ionic strength is the large influence of salinity on pH measurement accuracy. For salinities between 0 and 1 at T = 298.15 K, the p(K_1e_2) of mCP changes by more than 0.2. As such, accurate and precise salinity or ionic strength measurements are essential for making accurate and precise pH measurements at low ionic strength. Accurate pH measurements in freshwater at very low ionic strengths additionally require careful specification of the ionic composition of the measured medium. Freshwater generally lacks the constancy of composition of seawater (i.e., constant concentration ratios for major seawater ions). Therefore, conductivity measurements may not provide a highly reliable measure of ionic strength. The issue of composition constancy further complicates comparisons between measurements made on different pH scales (i.e., free versus total) at low ionic strengths. Additional useful discussion of this point can be found in Lai et al. [17].

With the creation of the estuarine pH model, there are now two models appropriate for mCP pH measurements in fresh waters: Lai et al. [17,18] and this work. There are also two models appropriate for measurements in marine systems, S = 20 to 40: Liu et al. [8] and this work. For salinities between those conditions—i.e., the full range of estuarine conditions—this work fills an important gap. The new estuarine pH_T model is appropriate for both in situ measurements and the calibration of electrometric pH-measuring devices because it includes the influences of T and S over wide ranges.

3.7 Acknowledgments

The authors wish to thank Luke M. Mosley, Shamus L.G. Husheer, and Keith A. Hunter for their careful investigation of mCP characteristics, published as Mosley et al. [19], and for the inclusion of their full data set in a form that can be used by others. The authors also thank Xuewu Liu, Mark C. Patsavas, Chun-Ze Lai, Michael D. DeGrandpre, Brandon D. Wasser, Taymee A.

Brandon, Daniel S. Clucas, Emma J. Jaqueth, Zachary D. Benson, Corry M. Beatty, and Reggie S. Spaulding for their mCP characterizations, published as Liu et al. [8] and Lai et al. [17,18], which were used extensively throughout this work. Insightful and helpful editorial comments from Tonya Clayton are greatly appreciated. The comments of Michael DeGrandpre and one anonymous reviewer significantly improved our work. Special thanks is also given to Michael DeGrandpre for providing an advance copy of the erratum for the published work of Lai et al. [17], cited throughout this document as Lai et al. [18], prior to its publication. This work was supported by the National Science Foundation, project numbers OCE 1220110 and OCE 1657894. N.K. Douglas was also supported by a Presidential Doctoral Fellowship from the University of South Florida Office of Graduate Studies.

3.8 References

1. Douglas, N.K., Byrne, R.H., 2017b. Spectrophotometric pH measurements from river to sea: Calibration of mCP for $0 \leq S \leq 40$ and $278.15 \leq T \leq 308.15$ K. *Marine Chemistry* **197**, 64-69.
2. Robert-Baldo, G.L., Morris, M.J., Byrne, R.H., 1985. Spectrophotometric determination of seawater pH using phenol red. *Analytical Chemistry* **57**, 2564-2567.
3. Byrne, R.H., Robert-Baldo, G., Thompson, S.W., Chen, C.T.A., 1988. Seawater pH measurements: an at-sea comparison of spectrophotometric and potentiometric methods. *Deep Sea Research, Part A: Oceanographic Research Papers* **35**(8), 1405-1410.
4. Byrne, R.H., Breland, J.A., 1989. High precision multi-wavelength pH determinations in seawater using cresol red. *Deep-Sea Research, Part I* **36**, 803-810.
5. King, D.W., Kester, D.R., 1989. Determination of seawater pH from 1.5 to 8.5 using colorimetric indicators. *Marine Chemistry* **26**, 5-20.
6. Breland, J. A., Byrne, R. H., 1993. Spectrophotometric procedures for determination of sea water alkalinity using bromocresol green. *Deep Sea Research Part I: Oceanographic Research Papers* **40**(3), 629-641.
7. Clayton, T.D., Byrne, R.H., 1993. Spectrophotometric seawater pH measurements: Total hydrogen ion concentration scale calibration of m-cresol purple and at-sea results. *Deep-Sea Research, Part I* **40**, 2115-2129.
8. Liu, X., Patsavas, M.C., Byrne, R.H., 2011. Purification and characterization of meta-cresol purple for spectrophotometric seawater pH measurements. *Environmental Science & Technology* **45**, 4862-4868.

9. Maberly, S.C., 1996. Diel, episodic and seasonal changes in pH and concentrations of inorganic carbon in a productive lake. *Freshwater Biology* **35**(3), 579-598.

10. Dean, W.E. and Gorham, E., 1998. Magnitude and significance of carbon burial in lakes, reservoirs, and peatlands. *Geology* **26**(6), pp.535-538.

11. Alin, S.R., Johnson, T.C., 2007. Carbon cycling in large lakes of the world: A synthesis of production, burial, and lake‐atmosphere exchange estimates. *Global Biogeochemical Cycles* **21**(3).

12. Yao, W., Byrne, R.H., 2001. Spectrophotometric determination of freshwater pH using bromocresol purple and phenol red. *Environmental Science and Technology* **35**, 1197-1201.

13. Feely, R.A., Alin, S.R., Newton, J., Sabine, C.L., Warner, M., Devol, A., Krembs, C., Maloy, C., 2010. The combined effects of ocean acidification, mixing, and respiration on pH and carbonate saturation in an urbanized estuary. *Estuarine, Coastal and Shelf Science* **88**(4), 442-449.

14. Hales, B., Suhrbier, A., Waldbusser, G.G., Feely, R.A., Newton, J.A., 2017. The carbonate chemistry of the "fattening line," Willapa Bay, 2011–2014. *Estuaries and Coasts* **40**(1), 173-186.

15. Patsavas, M.C., Byrne, R.H., Liu, X., 2013a. Purification of meta-cresol purple and cresol red by flash chromatography: Procedures for ensuring accurate spectrophotometric seawater pH measurements. *Marine Chemistry* **150**, 19-24.

16. DeGrandpre, M.D., Spaulding, R.S., Newton, J.O., Jaqueth, E.J., Hamblock, S.E., Umansky, A.A., Harris, K.E., 2014. Consideration for the measurement of spectrophotometric pH for ocean acidification and other studies. *Limnology and Oceanography: Methods* **12**, 830-839.

17. Lai, C.Z., DeGrandpre, M.D., Wasser, B.D., Branson, T.A., Clucas, D.S., Jaqueth, E.J., Benson, Z.D., Beatty, C.M., Spaulding, R.S., 2016. Spectrophotometric measurement of freshwater pH with purified meta-cresol purple and phenol red. *Limnology and Oceanography: Methods* **14**(12), 864-873.

18. Lai, C.Z., DeGrandpre, M.D., Wasser, B.D., Branson, T.A., Clucas, D.S., Jaqueth, E.J., Benson, Z.D., Beatty, C.M., Spaulding, R.S., 2017. Erratum: Spectrophotometric measurement of freshwater pH with purified meta-cresol purple and phenol red. *Limnology and Oceanography: Methods*, **15**(10), 903.

19. Mosley, L.M., Husheer, S.L.G., Hunter, K.A., 2004. Spectrophotometric pH measurement in estuaries using thymol blue and *m*-cresol purple. *Marine Chemistry* **91**, 175-186.

20. Yao, W., Liu, X., Byrne, R.H., 2007. Impurities in indicators used for spectrophotometric seawater pH measurements: Assessment and remedies. *Marine Chemistry* **107**, 167-172.

21. Douglas, N.K., Byrne, R.H., 2017a. Achieving accurate spectrophotometric pH measurements using unpurified meta-cresol purple. *Marine Chemistry* **190**, 66-72.

22. French, C.R., Carr, J.J., Dougherty, E.M., Eidson, L.A.K., Reynolds, J.C., DeGrandpre, M.D., 2002. Spectrophotometric pH measurements of freshwater. *Analytica Chimica Acta* **453**, 13-20.

23. Liu, X., Wang, Z.A., Byrne, R.H., Kaltenbacher, E.A., Bernstein, R.E., 2006. Spectrophotometric measurements of pH in-situ: laboratory and field evaluations of instrumental performance. *Environmental Science & Technology* **40**, 5036–5044.

24. Yuan, S., DeGrandpre, M.D., 2008. Evaluation of indicator-based pH measurements for freshwater over a wide range of buffer intensities. *Environmental Science & Technology* **42**, 6092-6099.

25. Hammer, K., Schneider, B., Kulinski, K., Schulz-Bull, D.E., 2014. Precision and accuracy of spectrophotometric pH measurements at environmental conditions in the Baltic Sea. *Estuarine, Coastal and Shelf Science* **146**, 24-32.

26. Davies, C.W., 1962. *Ion association*. Butterworths.

27. Millero, F.J. and Schreiber, D.R., 1982. Use of the ion pairing model to estimate activity coefficients of the ionic components of natural waters. *American Journal of Science* **282**(9), 1508-1540.

28. Byrne, R.H., 1987. Standardization of standard buffers by visible spectrometry. *Analytical Chemistry* **59**, 1479-1481.

29. Zhang, H., Byrne, R.H., 1996. Spectrophotometric pH measurements of surface seawater at in-situ conditions: absorbance and protonation behavior of thymol blue. *Marine Chemistry* **52**, 17-25.

30. Dickson, A.G., Sabine, C.L., Christian, J.R. (Eds.), 2007. *Guide to best practices for ocean CO_2 measurements*. PICES Special Publication 3.

31. Stumm, W., Morgan, J.J., 1981. *Aquatic chemistry*. J. Wiley & Sons.

.

CHAPTER FOUR:

CHARACTERIZATION OF THYMOL BLUE AND CRESOL RED FOR SPECTROPHOTOMETRIC pH MEASUREMENTS ACROSS $0 \leq S \leq 40$ AND $278.15 \leq T \leq 308.15$ K

4.1 Abstract

Because the pH of natural waters in fresh, estuarine, and marine environments can vary widely, accurate spectrophotometric measurements in these environments require a suite of pH indicators suited to a broad range of pH. Although the indicator meta-Cresol Purple (mCP) has been characterized across a wide range of salinity and temperature, other indicators, with pH ranges that complement that of mCP, have not been as well characterized. To broaden the environmental applications of sulfonephthalein pH indicators, parameterizations of Thymol Blue (TB) and Cresol Red (CR) have been performed across the range $0 \leq S \leq 40$ and $278.15 \leq T \leq 308.15$ K using compilations of data from studies of these indicators over the last 20 years. Indicator dissociation characteristics, i.e., $p(K_I e_2)$, were fitted as functions of salinity and temperature. Modeled fits for both indicators fit extant data with $r^2 > 0.999$ and RMSEs < 0.003. Using the new $p(K_I e_2)$ models and previously published parameterizations of molar extinction coefficient ratios (e_x), pH_T can be calculated from absorbance ratio measurements over a considerably expanded range of environmental conditions. The new models provide $p(K_I e_2)$ values that are within ±0.0065 units of $p(K_I e_2)$ values calculated using previously published

models for TB and within ±0.0025 for CR. Our models provide an additional step toward robust, molecularly-based pH measurements across a broad range of salinity and temperature regimes.

4.2 Introduction

The characterization and use of sulfonephthalein indicators to measure seawater pH have become established practices in the oceanographic community over the past 30 years [1–13]. Additionally, to measure freshwater pH spectrophotometrically, a number of indicator studies have been performed at zero or near-zero ionic strength [14–20]. However, far fewer spectrophotometric pH studies have been performed in the estuarine salinity range ($S < 20$) [21–24]. As such, spectrophotometric techniques remain largely underutilized in these environments [23,25]. Instead, researchers largely rely upon potentiometric methods to measure pH in estuaries. While potentiometric devices are easy to transport and use in the field [25,26], they require periodic calibration and offer lower precision than spectrophotometric methods (±0.01 for glass electrodes, versus ±0.0004 to ±0.001 for spectrophotometric measurements) [8,11,13,27,28]. Because estuaries are dynamic biogeochemical environments where many important pH-dependent processes occur, accurate and precise characterizations of pH in these waters are highly valuable.

In the previous work of Douglas and Byrne [23], spectrophotometric pH data from three studies [11,19–21] across a range of salinity and temperature were combined to generate a new model for meta-Cresol Purple (mCP) applicable to temperate natural waters ($0 \leq S \leq 40$, $278.15 \leq T \leq 308.15$ K). Calculations of pH_T using the new model agree within ±0.004 of pH_T calculated using preexisting models, and the new model provides coverage over a range of salinities and temperatures where the preexisting models were not considered applicable.

The Douglas and Byrne [23] mCP model provides an additional step toward robust spectrophotometric pH measurements across estuarine conditions. However, because freshwater and estuaries exhibit wide ranges of pH, it is important that additional sulfonephthalein indicators are available for use in waters with conditions that are outside the indicating range of mCP. Sulfonephthalein indicators are generally considered most appropriate for $(pK_I - 1) \leq pH \leq (pK_I + 0.3)$ where K_I is the second dissociation constant for the diprotic form of the indicator [12]. Using this rule of thumb, approximate pH ranges for measurements with three commonly used sulfonephthalein indicators are given in Table 4.1 for Thymol Blue (TB), mCP, and Cresol Red (CR) in seawater ($S = 35$) and freshwater at $T = 298.15$ K. Multiple indicators are required to measure pH when a single indicator is insufficient for the environment being studied [29,30]. To extend spectrophotometric pH measurements to a variety of aquatic environments, comprehensive models should be developed for the chemical and spectral properties of all sulfonephthalein dyes over a range of salinity and temperature that encompasses freshwater, estuarine and marine conditions.

Table 4.1 Approximate pH ranges for spectrophotometric measurements by three sulfonephthalein indicators ($T = 298.15$ K), as $(pK_I - 1) \leq pH \leq (pK_I + 0.3)$.

Indicator	**Freshwater pH range ($S = 0$)**	**Seawater pH range ($S = 35$)**
Thymol Blue	8.1 – 9.4	7.5 – 8.8
m-Cresol Purple	7.7 – 9.0	7.0 – 8.3
Cresol Red	7.4 – 8.7	6.7 – 8.0

As shown in Fig. 4.1, sulfonephthalein indicators have strong structural similarities. All act as weak diprotic acids in solution, with the first dissociation ($H_2I \Leftrightarrow H^+ + HI^-$) occurring at very low pH, so that effectively all indicators exist as either HI^- and I^{2-} in natural waters. Solutions with comparatively high HI^- concentrations appear yellow in color, and higher-pH samples, with higher relative concentrations of I^{2-}, are either reddish-purple or blue-green. The

HI^- form of the indicator absorbs strongly at wavelengths 430–440 nm (with the maximum absorbing wavelength referred to as λ_1, according to the nomenclature of Clayton and Byrne [8]), and I^{2-} forms absorb most strongly between 550–600 nm (λ_2), depending on the indicator. Table 4.2 lists λ_1 and λ_2 values for TB, mCP, and CR.

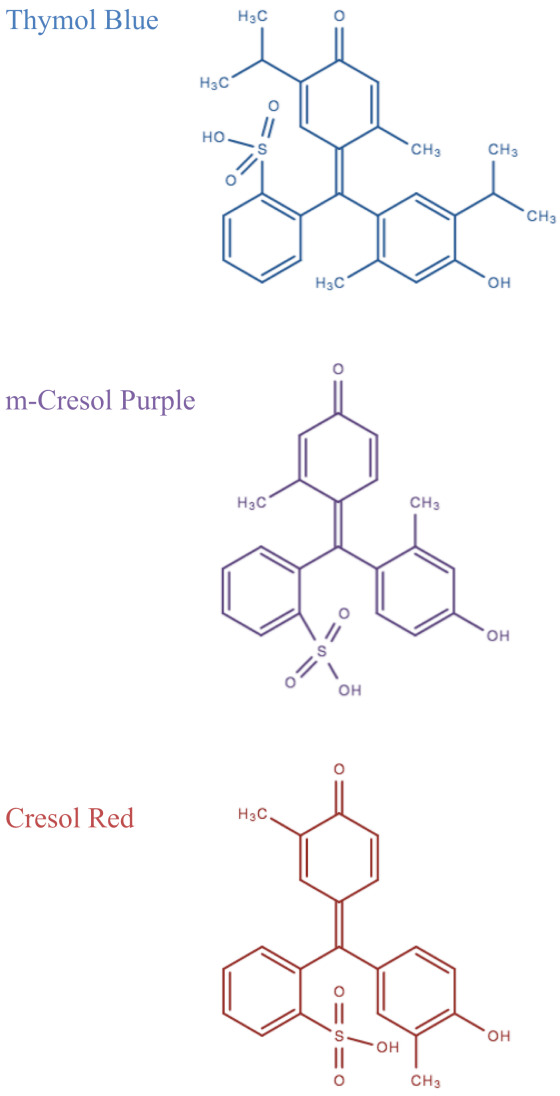

Fig. 4.1 Chemical structures of Thymol Blue, m-Cresol Purple, and Cresol Red.

Table 4.2 λ_1 and λ_2 values for three sulfonephthalein indicators.

Indicator	**λ_1 (nm)**	**λ_2 (nm)**	**Source**
Thymol Blue	435	596	[10,21]
m-Cresol Purple	434	578	[8,11,19–21]
Cresol Red	433	573	[4,12]

Calibrations of sulfonephthalein indicators for spectrophotometric pH measurements rely on absorbance ratio measurements (R) to determine sample pH, according to the following relationship [2,4,8,10]:

$$\mathrm{pH_T} = \mathrm{p}K_\mathrm{I} + \log\left(\frac{R - e_1}{e_2 - Re_3}\right) \quad (4.1)$$

where $\mathrm{pH_T} = -\log [\mathrm{H^+}]_\mathrm{T}$ (i.e., total hydrogen ion concentration scale), R is the perturbation-corrected ratio [8,31] of the spectrophotometric absorbances ($_\lambda A$) at an indicator's base-form ($\mathrm{I^{2-}}$) and acid-form ($\mathrm{HI^-}$) absorbance peaks ($R = {}_{\lambda 2}A/{}_{\lambda 1}A$), and the terms e_1, e_2, and e_3 (referred to generally as e_x) are $\mathrm{HI^-}$ and $\mathrm{I^{2-}}$ molar extinction coefficient ratios at selected wavelengths. Zhang and Byrne [10] and Liu et al. [11] showed that Eq. (4.1) could be equivalently written as follows:

$$\mathrm{pH_T} = \mathrm{p}(K_\mathrm{I}e_2) + \log\left(\frac{R - e_1}{1 - R\frac{e_3}{e_2}}\right) \quad (4.2)$$

This form of the $\mathrm{pH_T}$ equation was adopted by Liu et al. [11] and Patsavas et al. [12] in characterizations of mCP and Cresol Red (CR), as well as by Douglas and Byrne [23] in their estuarine model for mCP. It offers the advantage of eliminating one variable from the equation, thereby reducing some sources of error in e_x characterizations.

4.3 Model Parameterizations

Because the family of sulfonephthalein indicators has strong chemical similarities, it should be expected that TB and CR characterizations can be performed using analytical procedures similar to those used for mCP. In the previous work of Douglas and Byrne [23],

published mCP parameterizations were combined to create a new polynomial fit applicable over the salinity (S) and temperature (T) range of temperate estuaries. The Douglas and Byrne [23] polynomial has the general form

$$p(K_I e_2) = a_0 + a_1 S^{0.5} + a_2 S + a_3 S^{1.5} + a_4 S^2 + a_5 S^{2.5} + a_6 T^{-1} + a_7 S^{0.5} T^{-1} \quad (4.3)$$

The previous model of Douglas and Byrne [23] is updated here to reflect the correct application of datasets' weighting factors, which were misapplied in the original manuscript. This correction alters the p($K_I e_2$) values given by Douglas and Byrne [23] by only 0.0002, considerably less than the level of imprecision of spectrophotometric pH analyses. The revised p($K_I e_2$) model for mCP is given as

$$\mathrm{p}(K_I e_2)_{mCP} = 5.567924 - 0.551542\, S^{0.5} + 0.126183\, S - 0.0290566\, S^{1.5} + 0.00363148\, S^2 - 0.000178371\, S^{2.5} + 53.204901\, S^{0.5}\, T^{-1} + 814.078293\, T^{-1} \quad (4.4)$$

A test value for the Eqn. (4.4) polynomial is provided in Appendix C.

In this work datasets published over the past two decades are combined to quantitatively describe the indicating properties of two additional sulfonephthalein indicators, TB and CR, that are useful for measurements of spectrophotometric pH outside the useful indicating range of mCP. Prior to fitting the p($K_I e_2$) characteristics of these indicators as a function of S and T, the TB data of Zhang and Byrne [10] were corrected using the updated Tris pH algorithm of DelValls and Dickson [32], which supersedes the Tris model of Dickson [33]. The new p($K_I e_2$) models generated for TB and CR were then used to calculate pH_T across a range of salinities and temperatures ($0 \leq S \leq 40$ and $278.15 \leq T \leq 308.15$ K) for R-ratios between 0.25 and 2.25. The pH_T values generated with the new models are then compared to pH_T values that are obtained using previously published models. Table 4.3 summarizes the datasets used in these analyses.

Table 4.3 Summary of datasets used for creation of TB and CR models. For e_x values that are f(S,T), S = 35 and T = 298.15 K for values listed.

Data Source	S	T (°C)	# of data (n)	Weights (W)	Pure dye? (Y/N)	e_x's f(S,T) or constants (C)?	e_1	e_2	e_3	e_3/e_2
Thymol Blue										
Zhang and Byrne [10]	30-40	5-35	26	0.8462	N	f(T)	0.0035	2.3856	0.1391	0.0583
Mosley et al. [21]	0-40	25	22	1	N	f(T)				
Cresol Red										
Yuan and DeGrandpre [16]	0	10-25	4	1	N	C	0.0033	2.8521	0.1046	0.0367
Patsavas et al. [12]	20-40	5-35	32	0.125	Y	f(S,T)	0.0013	n/a	n/a	0.0323

4.4 Methods

4.4.1 Compiling and Treating Individual Datasets

4.4.1.1 Thymol Blue

Yao et al. [34] observed that the lot of TB used by Zhang and Byrne [10] was relatively low in impurities, but because no p($K_I e_2$) model for purified TB is yet available, the constituent datasets cannot be rigorously treated for impurity absorbances. However, another correction to the datasets must be made: DelValls and Dickson [32] point out that pK_I's based on the Tris characterization of Dickson [33] — derived from the work of Ramette et al. [35] — are likely erroneous. Two methods of correction are available: (1) Addition of 0.0047 (the mean pH_{Tris} difference quoted in DelValls and Dickson [32]) to all pK_I's of Zhang and Byrne [10]; or (2) Recalculation of the pH_{Tris} for the samples reported in Table 2 of Zhang and Byrne [10] according to DelValls and Dickson's Tris parameterization, with subsequent recalculation of pK_I. Because Zhang and Byrne [10] report R for each measured sample, the second choice, which is more rigorous, was employed. Using the S and T data in Table 2 of Zhang and Byrne [10], pH_{Tris}

was calculated using Eq. (18) of DelValls and Dickson [32], which is applicable to 0.04 mol kg^{-1} Tris in seawater. Using (a) the recalculated pH_{Tris} values, (b) the Zhang and Byrne [10] e_1, e_2, and e_3 formulations, and (c) the R-ratios given in Table 2A of Zhang and Byrne [10], pK_I for each sample was recalculated.

For the Mosley et al. [21] data inputs, estuarine pK_I data at $T = 298.15$ K was directly available in Table 2 of Mosley et al. [21]. Because the 0.04 mol kg^{-1} Tris parameterization of DelValls and Dickson [32] does not extend to $S < 20$, Mosley et al. [21] developed a new parameterization for Tris buffer pH_T across the range $0 \leq S \leq 40$ at $T = 298.15$ K, with results consistent within ±0.002 of the DelValls and Dickson [32] Tris characterization.

The $p(K_I e_2)$ values for both datasets were calculated using the T-dependent e_2 formulation of Zhang and Byrne [10].

4.4.1.2 Cresol Red

For the Yuan and DeGrandpre [16] data inputs, pK_I was calculated for $S = 0$ and $T =$ 283.15–303.15 K at intervals of 5 K, according to Eq. (5) of Yuan and DeGrandpre [16]. Although the parameterization is appropriate to the free hydrogen ion concentration scale, the conversion at $S = 0$ is implicit, and the pK_I calculated is applicable to the total scale. Yuan and DeGrandpre [16] report their e_x values at $T = 293.15$ K. Because no temperature dependence was reported for the e_x values, the constant values they reported have been used for all calculations using their pK_I model. Values of $p(K_I e_2)$ for all Yuan and DeGrandpre [16] modeled data were calculated using their reported value of e_2 (2.8521).

For the Patsavas et al. [12] data, $p(K_I e_2)$ values were calculated using S and T data from Table 3 of Patsavas et al. [12] and the Patsavas et al. [12] $p(K_I e_2)$ parameterization.

4.4.2 Deriving New Models for p(K_1e_2) Across a Range of S *and* T

The compiled p(K_1e_2) datasets for each indicator were fitted as empirical multivariate polynomial functions of $S^{0.5}$ and T^{-1}, including an interactive term, using the *stepwiselm* function in MATLAB. Data were weighted according to the assigned values given in Table 4.3. Further details regarding the weighting algorithm are found in Douglas and Byrne [23]. The *stepwiselm* tool generates a polynomial fit, up to the highest-order polynomial specified by the user (in this case, fifth- and first-order polynomials for $S^{0.5}$ and T^{-1}, respectively), by adding or removing terms by stepwise regression, using *F*-test results to determine whether a term is added ($p \leq 0.05$ for the addition of a term) or removed ($p \geq 0.10$ for the removal of a term). This process continues until no more terms can be added or removed from the model.

4.4.3 Comparing pH_T Test Values Using New and Existing Models

The polynomial fits for p(K_1e_2) for the two indicators were considered to be applicable across $S = 0–40$ and $T = 278.15–308.15$ K. To compare (a) pH_T values calculated using Eq. (4.2) with the new p(K_1e_2) parameterizations and (b) pH_T values calculated using the previously published models, comparative calculations were performed for each of the indicators across the applicable *S* and *T* ranges, at intervals of 5 for *S* and 5 K for *T*. For these calculations, *R* values ranging from 0.25–2.25 (at intervals of 0.25) were used. The e_x values used in Eq. (4.2) with the new p(K_1e_2) parameterizations were chosen as follows:

- For TB, the Zhang and Byrne [10] e_x parameterizations were adopted. This set was chosen because the e_x's were parameterized as functions of temperature and were used by both Zhang and Byrne [10] and Mosley et al. [21].

- For CR, the Patsavas et al. [12] parameterizations of e_x were used. In addition to its e_x characterization as functions of both salinity and temperature, this dataset was chosen because it was obtained using purified CR.

To account for Zhang and Byrne's use of the Dickson [33] Tris characterizations, 0.0047 was added to the pH_T values directly calculated using the Zhang and Byrne [10] algorithm. Comparisons of pH_T were then made for each model over its applicable salinity and temperature range.

4.5 Results

4.5.1 New p(K_1e_2) Model Parameterizations

Following the form of Eq. (4.3), the new parameterizations for TB and CR p(K_1e_2) are given by Eqs. (4.5) and (4.6):

$$\mathrm{p}(K_1e_2)_{TB} = 6.315793 - 0.508094\,S^{0.5} + 0.108027\,S - 0.0231101\,S^{1.5} + 0.00266553\,S^2 - 0.000119833\,S^{2.5} + 50.119275\,S^{0.5}\,T^{-1} + 732.625732\,T^{-1} \quad (4.5)$$

$$\mathrm{p}(K_1e_2)_{CR} = 5.462784 - 0.439300\,S^{0.5} + 0.0352495\,S - 0.00168501S^{1.5} + 54.213148\,S^{0.5}\,T^{-1} + 733.877224\,T^{-1} \quad (4.6)$$

Table 4.4 summarizes the new *S*- and *T*-dependent fits for p(K_1e_2) for TB and CR and provides test values for both. Both models had $r^2 > 0.999$, and RMSE ≤ 0.0054. Using the *stepwiselm* function, higher-order terms (S^2 and $S^{2.5}$) were eliminated from the CR model; the full suite of terms was retained in the TB model.

Fig. 4.2 shows the salinity dependencies of p(K_1e_2) for mCP, TB and CR at $T = 298.15$ K calculated using Eqs. (4.4), (4.5), and (4.6). Although this figure only shows p(K_1e_2) at a single temperature, the overall shape of the models is very closely similar for other temperatures.

Table 4.4 Summary of new p(K_1e_2) fit coefficients and statistics.

	Thymol Blue	**Cresol Red**
p(K_1e_2) model fitting terms		
Intercept	6.315793	5.462784
$S^{0.5}$	-0.508094	-0.439300
T^{-1}	732.625732	733.877224
$S^{0.5}\ T^{-1}$	50.119275	54.213148
S	0.108027	0.0352495
$S^{1.5}$	-0.0231101	-0.00168501
S^2	0.00266553	0
$S^{2.5}$	-0.000119833	0
p(K_1e_2) test value (S = 35, T = 298.15 K)	8.154129	7.285847
p(K_1e_2) model statistics		
p(K_1e_2) model r^2	0.9998	1.0000
p(K_1e_2) model RMSE	0.0025	0.0005
p(K_1e_2) model residuals range	Z&B: -0.0065 – 0.0033 Mosley: -0.0015 – 0.0035	Y&D: -0.000124 – 0.00167 Patsavas: -0.0025 – 0.0023

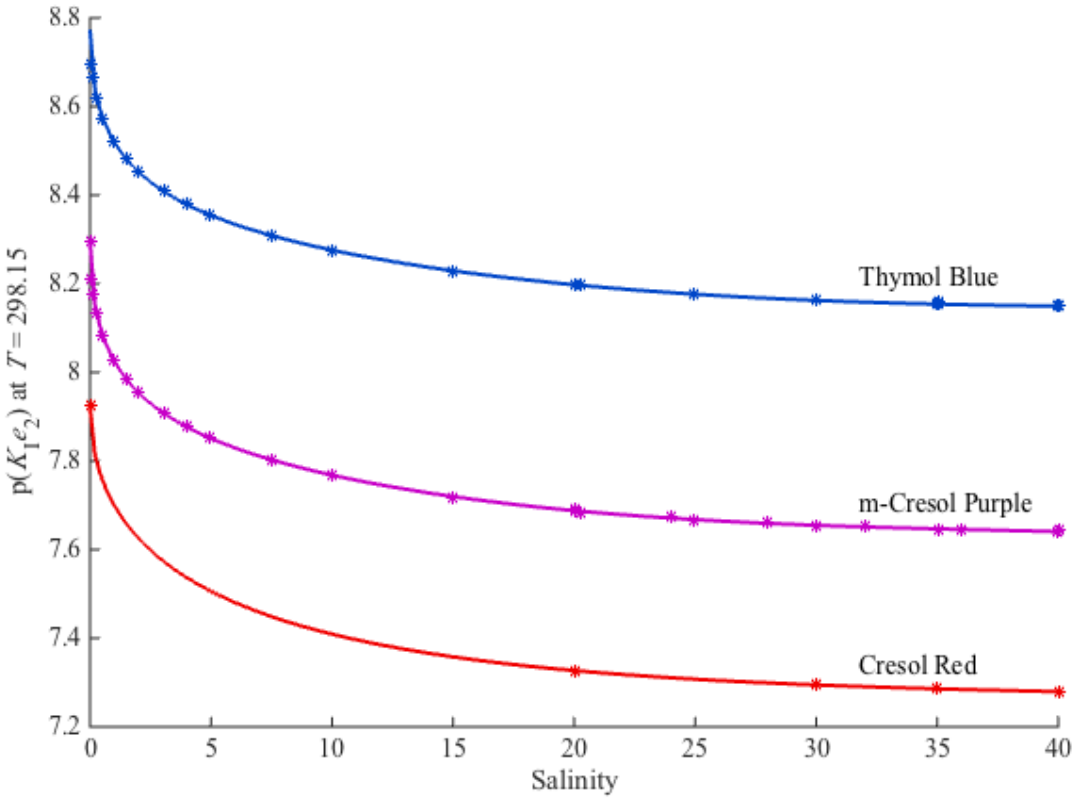

Fig. 4.2 New fits for p(K_1e_2) as functions of S for T = 298.15 K. Fit for p$(K_1e_2)_{mCP}$ is from Douglas and Byrne [23].

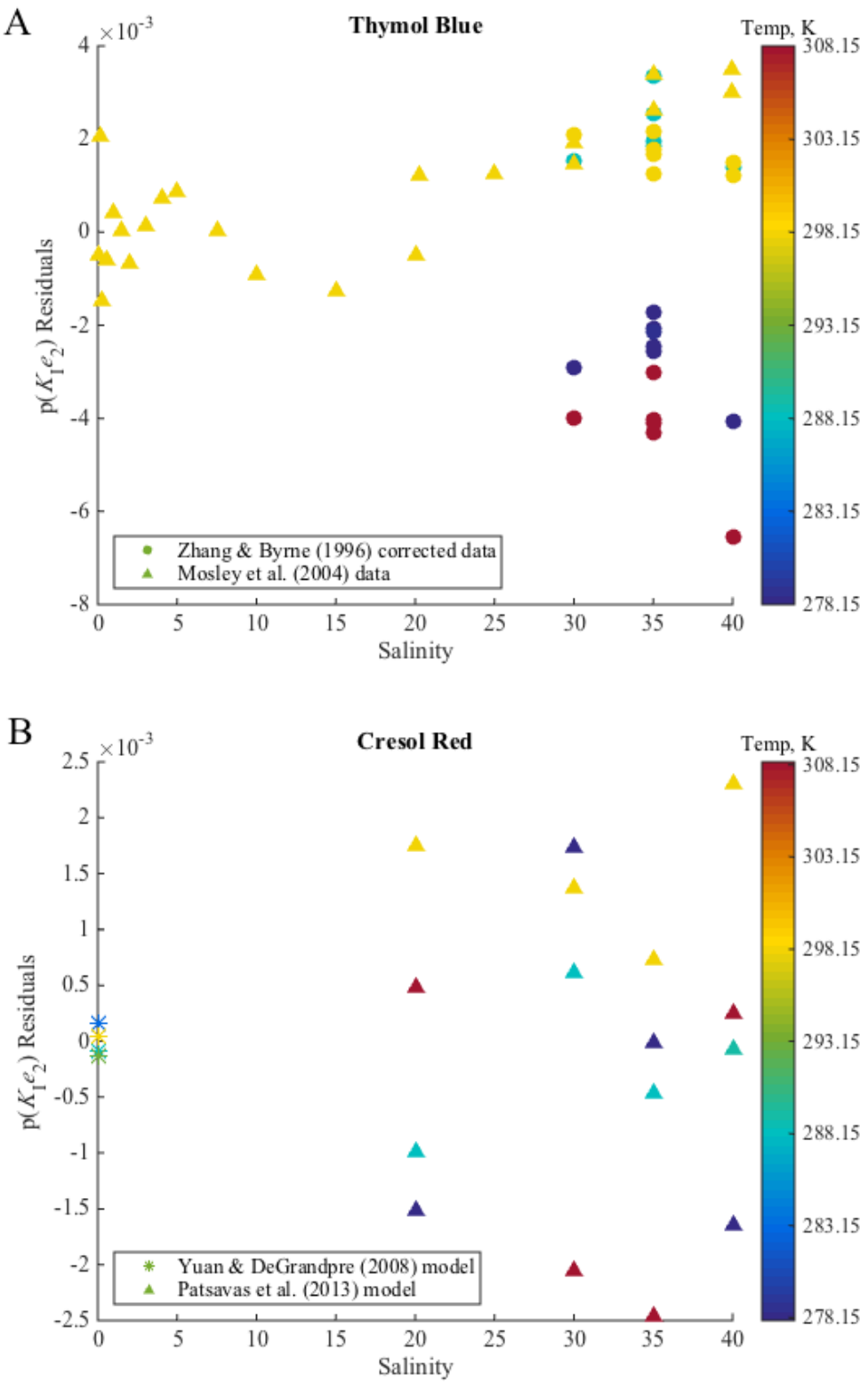

Fig. 4.3 Residuals for the new pK_1e_2 models, given in 4.4, Eqs. (4.5) and (4.6), as a function of salinity, for (A) TB and (B) CR. Residuals are calculated as model input (as shown in the figure legend) minus the fitted values given by the new models. Colors represent temperature.

Residuals of $p(K_1e_2)$, expressed as differences between the $p(K_1e_2)$ characterizations derived from prior studies and the values calculated according to Eqs. (4.5) and (4.6), are shown as a function of salinity in Fig. 4.3. Note that the residuals are color coded with respect to temperature. The ranges of residuals for each constituent dataset are summarized in Table 4.4.

The TB and CR models performed approximately as well as the Douglas and Byrne [23] mCP model. For TB, all residuals are within ±0.0043 with the exception of one high-salinity, high-temperature datum (S = 40, T = 308.15 K) from Zhang and Byrne [10] that differed by -0.0065. The model for CR also effectively minimized residuals, with an RMSE (±0.0005) approximately equal to the precision of spectrophotometric pH methods (±0.0004). Because the residuals for the S = 0 data [16] were all within ±0.0002, it can be assumed that the errors in the model derive from the parameterization's S-dependent terms, and not the terms that are dependent on T.

4.5.2 Comparing Modeled pH_T Across a Range of R, S, and T

Table 4.5 reports root mean squares of the differences between pH_T (hereafter abbreviated RMS ΔpH_T) calculated using the published models and the new models (Eqs. 4.5 and 4.6) within the applicable (S,T) ranges (at intervals of 5 for S and 5 K for T). Table 4.5a reports these differences for the full applicable T range for each model, and Table 4.5b reports differences for T = 298.15 K, at which most spectrophotometric pH measurements are made.

For TB, because the Zhang and Byrne [10], Mosley et al. [21], and estuarine (Eq. 4.5) models all use the e_x characterizations of Zhang and Byrne [10], ΔpH_T values are attributable to different parameterizations of pK_I or, in the case of Eq. (4.5), $p(K_1e_2)$. pH_T calculated with Eqs. (4.2) and (4.5) agrees well with both the Mosley et al. [21] modeled pH_T and the Tris-corrected Zhang and Byrne [10] modeled pH_T over most of the models' S and T ranges.

Table 4.5 RMS ΔpH_T, the root mean square of ($pH_{T\ (source\ model)} - pH_{T\ (D\&B)}$), for all applicable S of source models and (*a*) all applicable T of source models, and (*b*) $T = 298.15$ K only.

R	**Thymol Blue**		**Cresol Red**	
	Z&B	**Mosley**	**Y&D**	**Patsavas**
Table 4.5a RMS ΔpH_T for applicable S and T ranges of source models				
0.25	0.0025	0.0039	0.0030	0.0014
0.50			0.0004	
0.75			0.0011	
1.00			0.0022	
1.25			0.0032	
1.50			0.0041	
1.75			0.0051	
2.00			0.0060	
2.25			0.0069	
Table 4.5b RMS ΔpH_T for $T = 298.15$ K and applicable S ranges of source models				
0.25	0.0017	0.0039	0.0029	0.0019
0.50			0.0005	
0.75			0.0007	
1.00			0.0016	
1.25			0.0024	
1.50			0.0032	
1.75			0.0040	
2.00			0.0047	
2.25			0.0055	

With the exception of $S = 0$ and $S = 40$, all pH_T values calculated with (a) the TB $p(K_1e_2)$ parameterization of Eq. (4.5) and (b) the Mosley et al. [21] TB model (all at $T = 298.15$ K) were within ±0.003. Further assessment of the ΔpH_T results revealed that model comparisons agree within ±0.004 for $0.02 < S < 37.6$ at $T = 298.15$ K. The difference at near-zero salinity is likely due to the large changes in $p(K_1e_2)$ that are not well constrained by the available data for TB, as the lowest salinity measured in the work of Mosley et al. [21] is $S = 0.06$. For pH_T calculated with the model of Zhang and Byrne [10], with the addition of 0.0047 to account for their use of the Dickson [33] Tris algorithm, ΔpH_T values agree within ±0.004 at all T for $S < 37.6$ and within ±0.004 for all S when $T = 298.15$ K.

For CR, differences in pH_T calculated with the new model (Eqs. (4.2) and (4.6)) and the model of Patsavas et al. [12] are due only to differences in characterizations of $p(K_I e_2)$. All pH_T values calculated using the new $p(K_I e_2)$ model (Eq. 4.6) are within ±0.0024 of the corresponding pH_T calculated using the Patsavas et al. [12] model. Differences in pH_T calculated using Eqs. (2) and (6) and the model of Yuan and DeGrandpre [16] are due to differences in both $p(K_I e_2)$ and e_x characterizations. ΔpH_T as calculated (a) by the Yuan and DeGrandpre [16] model and (b) using Eqs. (4.2) and (4.6) are largest at higher *R*-ratios: at $R = 2.25$, the root mean squared ΔpH_T at $R = 2.25$ (0.0055) is about twice as large as its corresponding value at $R = 0.25$ (0.0029). However, if a slightly lower e_3 value, such as the value (0.09025) used by Byrne and Breland [4] for seawater, is used in lieu of the Yuan and DeGrandpre [16] e_3 value (0.1046), the resulting pH_T agrees much better with pH_T as calculated using Eqs. (2) and (6), and the magnitude of RMS ΔpH_T no longer corresponds with the *R*-ratio, varying between 0.0005 ($R = 1.00$) and 0.0036 ($R = 0.25$). We suspect this result arises from colorimetric impurities in the CR dye used by Yuan and DeGrandpre [16]. See Section 4.6.1 for more information about this effect.

4.6 Discussion

4.6.1 Influence of e_x Choice on pH_T

In their estuarine model for the $p(K_I e_2)$ of mCP, Douglas and Byrne [23] chose to use the e_x parameterizations of Liu et al. [11] because they had been obtained using purified indicator and were applicable across a wide range of *S* and *T* ($S = 20–40$, $T = 278.15–308.15$ K). The assumption was stated that the e_x parameterizations of Liu et al. [11] would be applicable in the estuarine and freshwater range as well. This assumption was adequate for pH_T agreement within ±0.004, the magnitude of which was principally accounted for by differences in $p(K_I e_2)$. The same assumptions should be made for the e_x choices in the TB and CR models.

The choice of the Zhang and Byrne [10] T-dependent e_x parameterizations for TB was sensible for the estuarine model, as both input datasets [10,21] made use of these parameterizations. The choice of the Patsavas et al. [12] e_x algorithms for CR is analogous to the choice of the Liu et al. [11] e_x algorithms for mCP. Both the Patsavas et al. [12] and Liu et al. [11] e_x parameterizations were determined using purified indicator and were characterized as functions of salinity and temperature over a broad range of S and T. Additionally, the Patsavas et al. [12] algorithms have the same form as those of Liu et al. [11].

Colorimetric impurities affect not only determinations of an indicator's pK_I, but also determinations of its e_x ratios. Of particular concern is the determination of e_3, a ratio of the indicator's molar extinction coefficients at the short (430–440 nm range) wavelength (i.e., λ_1), given as follows:

$$e_3 = \frac{{}_{\lambda 1}\varepsilon_I}{{}_{\lambda 1}\varepsilon_{HI}} \tag{4.7}$$

To determine e_3, absorbances are measured at high pH (~12) for ${}_{\lambda 1}\varepsilon_I$ and low pH (~4) for ${}_{\lambda 1}\varepsilon_{HI}$. At pH = 12, virtually all of the indicator will be in the I^{2-} form, which absorbs only weakly at the short wavelength. Because colorimetric impurities absorb most strongly in the λ_1 range, the importance of λ_1-range absorbances by impurities will be enhanced in high-pH solutions, spuriously increasing the determined ${}_{\lambda 1}\varepsilon_I$. It therefore follows that impurities lead to inflated values of e_3. This agrees with the observation that use of an e_3 slightly smaller than the value used by Yuan and DeGrandpre [16] improves agreement between pH_T calculated with the new CR model and that of Yuan and DeGrandpre [16].

4.6.2 Future Work

The models presented here represent a step toward more robust p($K_I e_2$) parameterization for sulfonephthalein indicators, but they should be considered provisional models until additional

data can be collected to improve model fits. For mCP and TB, the data of Mosley et al. [21] provide an estuarine dataset at $T = 298.15$ K, but more data for all indicators are needed in the estuarine salinity range over a broad range of temperatures. Data to be generated should especially include $0 < S < 5$, as $p(K_1e_2)$ changes dramatically over this narrow salinity range.

It is quite important that purification techniques are developed for all indicators. While purified mCP and CR have been made available by the Byrne lab [11,36], and the DeGrandpre laboratory has developed techniques for purification of phenol red (PR) [19,20], TB purification techniques have been developed only recently, and purification techniques for bromocresol purple (BCP) are not yet available. Models and measurements using sulfonephthalein indicators are subject to systematic errors unless they are based on use of purified forms.

Toward the goal of improving spectrophotometric pH measurements made with purified indicator, NIST (National Institutes of Standards and Technology) currently has a program to characterize the pH response of purified mCP reference material. Based on Harned cell measurements, mCP characterizations and pH uncertainty budgets will be developed for $5 \leq S \leq 45$ and $278.15 \leq T \leq 323.15$ K.

4.7 Acknowledgments

The authors wish to thank Michael D. DeGrandpre, Keith A. Hunter, Shamus L.G. Husheer, Xuewu Liu, Luke M. Mosley, Mark C. Patsavas, Shigui Yuan, and Huining Zhang, for the authorship of the following studies used to develop our new models: Zhang and Byrne [10], Mosley et al. [21], Yuan and DeGrandpre [16], and Patasvas et al. [12]. This work was supported by the National Science Foundation, project numbers OCE 1220110 and OCE 1657894. N.K. Douglas was also supported by a Presidential Doctoral Fellowship from the University of South Florida Office of Graduate Studies.

4.8 References

1. Robert-Baldo, G.L., Morris, M.J., Byrne, R.H., 1985. Spectrophotometric determination of seawater pH using phenol red. *Analytical Chemistry* **57**, 2564-2567.
2. Byrne, R.H., 1987. Standardization of standard buffers by visible spectrometry. *Analytical Chemistry* **59**, 1479-1481.
3. Byrne, R.H., Robert-Baldo, G., Thompson, S.W., Chen, C.T.A., 1988. Seawater pH measurements: an at-sea comparison of spectrophotometric and potentiometric methods. *Deep Sea Research, Part A: Oceanographic Research Papers* **35**(8), 1405-1410.
4. Byrne, R.H., Breland, J.A., 1989. High precision multi-wavelength pH determinations in seawater using cresol red. *Deep-Sea Research, Part I* **36**, 803-810.
5. King, D.W., Kester, D.R., 1989. Determination of seawater pH from 1.5 to 8.5 using colorimetric indicators. *Marine Chemistry* **26**, 5-20.
6. Breland, J.A., Byrne, R.H., 1992. Determination of sea water alkalinity by direct equilibration with carbon dioxide. *Analytical Chemistry* **64**, 2306-2309.
7. Breland, J. A., Byrne, R. H., 1993. Spectrophotometric procedures for determination of sea water alkalinity using bromocresol green. *Deep Sea Research Part I: Oceanographic Research Papers* **40**(3), 629-641.
8. Clayton, T.D., Byrne, R.H., 1993. Spectrophotometric seawater pH measurements: Total hydrogen ion concentration scale calibration of m-cresol purple and at-sea results. *Deep-Sea Research, Part I* **40**, 2115-2129.
9. Bellerby,R.G.J., Turner, D.R., Millward, G.E., Worsfold, P.J., 1995. Shipboard flow injection determination of sea water pH with spectrophotometric detection. *Analytica Chimica Act*a **309**, 259-270.
10. Zhang, H., Byrne, R.H., 1996. Spectrophotometric pH measurements of surface seawater at in-situ conditions: absorbance and protonation behavior of thymol blue. *Marine Chemistry* **52**, 17-25.
11. Liu, X., Patsavas, M.C., Byrne, R.H., 2011. Purification and characterization of meta-cresol purple for spectrophotometric seawater pH measurements. *Environmental Science & Technology* **45**, 4862-4868.
12. Patsavas, M.C., Byrne, R.H., Liu, X, 2013b. Physical-chemical characterization of purified cresol red for spectrophotometric pH measurements in seawater. *Marine Chemistry* **155**, 158-164.
13. Hammer, K., Schneider, B., Kulinski, K., Schulz-Bull, D.E., 2014. Precision and accuracy of spectrophotometric pH measurements at environmental conditions in the Baltic Sea. *Estuarine, Coastal and Shelf Science* **146**, 24-32.
14. Yao, W., Byrne, R.H., 2001. Spectrophotometric determination of freshwater pH using bromocresol purple and phenol red. *Environmental Science and Technology* **35**, 1197-1201.

15. French, C.R., Carr, J.J., Dougherty, E.M., Eidson, L.A.K., Reynolds, J.C., DeGrandpre, M.D., 2002. Spectrophotometric pH measurements of freshwater. *Analytica Chimica Acta* **453**, 13-20.

16. Yuan, S., DeGrandpre, M.D., 2008. Evaluation of indicator-based pH measurements for freshwater over a wide range of buffer intensities. *Environmental Science & Technology* **42**, 6092-6099.

17. DeGrandpre, MD., Spaulding, R.S., Newton, J.O., Jaqueth, E.J., Hamblock S.E., Umansky, A.A., Harris, K.E. (2014). Considerations for the measurement of spectrophotometric pH for ocean acidification and other studies. *Limnology and Oceanography: Methods* **12**, 830-839.

18. Spaulding, R.S., DeGrandpre, M.D., Beck. J.C., Hart, R.D., Peterson, B., De Carlo, E.H., Drupp, P.S., Hammar, T.R., 2014. Autonomous in situ measurements of seawater alkalinity. *Environmental Science & Technology* **48**, 9573-9581.

19. Lai, C.Z., DeGrandpre, M.D., Wasser, B.D., Branson, T.A., Clucas, D.S., Jaqueth, E.J., Benson, Z.D., Beatty, C.M., Spaulding, R.S., 2016. Spectrophotometric measurement of freshwater pH with purified meta-cresol purple and phenol red. *Limnology and Oceanography: Methods* **14**(12), 864-873.

20. Lai, C.Z., DeGrandpre, M.D., Wasser, B.D., Branson, T.A., Clucas, D.S., Jaqueth, E.J., Benson, Z.D., Beatty, C.M., Spaulding, R.S., 2017. Erratum: Spectrophotometric measurement of freshwater pH with purified meta-cresol purple and phenol red. *Limnology and Oceanography: Methods* **15**, 903.

21. Mosley, L.M., Husheer, S.L.G., Hunter, K.A., 2004. Spectrophotometric pH measurement in estuaries using thymol blue and *m*-cresol purple. *Marine Chemistry* **91**, 175-186.

22. Gabriel, M.D., Forja, J.M., Rubio, J.A., Gomez-Parra, A., 2005. Temperature and salinity dependence of molar absorptivities of thymol blue: Application to the spectrophotometric determination of pH in estuarine waters. *Ciencias Marinas* **31**(1B), 309-318.

23. Douglas, N.K. Byrne, R.H., 2017. Spectrophotometric pH measurements from river to sea: Calibration of mCP for $0 \leq S \leq 40$ and $278.15 \leq T \leq 308.15$ K. *Marine Chemistry* **197**, 64-69.

24. Dinauer, A., Mucci, A., 2017. Spatial variability in surface-water pCO_2 and gas exchange in the world's largest semi-enclosed estuarine system: St. Lawrence Estuary (Canada). *Biogeosciences* **14**, 3221-3237.

25. Gonski, S.F., 2016. *An evaluation of the performance of an ISFET pH sensor in a dynamic estuarine system*. University of Delaware. http://udspace.udel.edu/bitstream/handle/19716/21486/2016_GonskiStephen_MS.pdf?sequence=1. (Accessed 4 February 2018).

26. Martz, T., McLaughlin, K., Weisberg, S.B., 2015. Best practices for autonomous measurement of seawater pH with the Honeywell Durafet pH sensor. Southern California Coastal Water Research Project. California Current Acidification Network (C-CAN) Technical Report 861.

27. Bresnahan Jr., P. J., Martz, T. R., Takeshita, Y., Johnson, K. S., LaShomb, M., 2014. Best practices for autonomous measurements of seawater pH with the Honeywell Durafet. *Methods in Oceanography* **9**, 44-60.

28. Carter, B.R., Radich, J.A., Doyle, H.L., Dickson, A.G., 2013. An automated system for spectrophotometric seawater pH measurements. *Limnology and Oceanography: Methods* **11**, 16-27.

29. Raghuraman, B., Gustavson, G., Van Hal, R. E. G., Dressaire, E., Zhdaneev, O., 2006. Extended-range spectroscopic pH measurement using optimized mixtures of dyes. *Applied Spectroscopy* **60**(12), 1461-1468.

30. de Vargas Sansalvador, I. M. P., Fay, C. D., Cleary, J., Nightingale, A. M., Mowlem, M. C., Diamond, D., 2016. Autonomous reagent-based microfluidic pH sensor platform. *Sensors and Actuators B: Chemical* **225**, 369-376.

31. Dickson, A.G., Sabine, C.L., Christian, J.R. (Eds.), 2007. *Guide to Best Practices for Ocean CO_2 Measurements.* PICES Special Publication 3, 191 p.

32. DelValls, T.A., Dickson, A.G., 1998. The pH of buffers based on 2-amino-2-hydroxymethl-1,3-propanediol ('tris') in synthetic sea water. *Deep-Sea Research I* **45**, 1541-1554.

33. Dickson, A.G., 1993. pH buffers for sea water media based on the total hydrogen ion concentration scale. *Deep-Sea Research* **40**, 107-118.

34. Yao, W., Liu, X., Byrne, R.H., 2007. Impurities in indicators used for spectrophotometric seawater pH measurements: Assessment and remedies. *Marine Chemistry* **107**, 167-172.

35. Ramette, R. W., Culberson, C. H., Bates, R. G, 1977. Acid-base properties of tris(hydroxymethyl) aminomethane (tris) buffers in sea water from 5 to 40 ^{o}C. *Analytical Chemistry* **49**(6), 867-870.

36. Patsavas, M.C., Byrne, R.H., Liu, X., 2013a. Purification of meta-cresol purple and cresol red by flash chromatography: Procedures for ensuring accurate spectrophotometric seawater pH measurements. *Marine Chemistry* **150**, 19-24.

CHAPTER FIVE:

CO_2 SYSTEM INTERNAL CONSISTENCY ANALYSES OF FIELD DATA USING SPECTROPHOTOMETRIC pH_T DETERMINED WITH ESTUARINE mCP p(K_1e_2) MODEL

5.1 Abstract

Chapters Three and Four of this dissertation presented a p(K_1e_2) model for spectrophotometric pH_T measurement across a wide range of salinity ($0 \leq S \leq 40$) and temperature ($278.15 \leq T \leq 308.15$ K) using m-Cresol Purple (mCP) indicator. To evaluate the extent to which pH_T determined using this new p(K_1e_2) model accords with other CO_2 system measurements (TA and DIC), field data from two cruises were used to perform internal consistency analyses. Results showed that the new model for mCP produced pH_T that agreed well (RMSE ~0.01) with pH_T calculated from an empirically adjusted TA (TA^*) and DIC in the marine salinity range ($S \geq 20$); the model-produced pH_T agreed less well (RMSE ~0.07) with calculated pH_T at estuarine salinities ($0.5 < S < 20$). Calculated DIC and TA also yielded good agreement (RMSE ~3.8 μmol kg^{-1}) with measured DIC and TA^* in the marine salinity range, but the extent of agreement declined (RMSE ~9 μmol kg^{-1}) at estuarine salinities. However, the new model agreed well with the published models upon which they are based across the full salinity range (RMSE ≤ 0.008 for $0.5 < S \leq 40$). Uncertainties about the contributions of organic acids to TA and uncertainties in characterizations of carbonic acid dissociation constants (K_1 and K_2) complicate internal consistency analyses. These results point to a need for additional high-quality

CO_2 system data in the low- and estuarine-salinity range, not only for pH_T, but also for DIC, TA, and pCO_2, to determine the sources of offsets between measured and calculated parameters.

5.2 Introduction

Methodology for deriving the new estuarine mCP p(K_1e_2) model, hereinafter referred to as the Douglas and Byrne [1] model, is outlined in Chapter Three of this dissertation. Chapter Four subsequently provides a corrected iteration of this equation (Eq. 4.4), to be used with absorbance measurements either (a) made with purified mCP or (b) made with unpurified mCP and retrospectively corrected for absorbances of colorimetric impurities. The model is considered applicable over a broad range of salinity ($0 \leq S \leq 40$) and temperature ($278.15 \leq T \leq 308.15$ K).

To evaluate the model given in Eq. (4.4), internal consistency analyses can be performed to ascertain how closely the model's pH_T determinations agree with pH_T calculated from measured values of other CO_2 system variables. To gain a better understanding of marine CO_2 system changes attributable to ocean acidification, several carbon chemistry cruises have recently been undertaken to 'overdetermine' the CO_2 system by measuring three or more carbon-system master variables (DIC, TA, pH, and f_{CO2}). Because only two of the four parameters are needed in order to model the full CO_2 system, measuring three or more allows researchers to evaluate data quality, assess accuracy, and check for erroneous measurements. Overdetermination of the CO_2 system provides a valuable tool for refinement of measurements and models.

5.3 Methods

5.3.1 Sources of Field Data

For this internal consistency evaluation, two datasets from recent CO_2 system cruises along the west coast of North America have been employed. The 2013 West Coast Ocean

Acidification (WCOA13) cruise was a 17-day NOAA Ocean Acidification Program (OAP) cruise conducted between Seattle, Washington, and Moss Landing, California, using the NOAA Ship *Fairweather* (August 3–10, 2013) and the *R/V Point Sur* (August 21–29, 2013). Measurements of three CO_2 system parameters (DIC, TA, and pH_T) were performed at 76 sampling stations using discrete water samples collected in Niskin bottles at multiple depths throughout the water column. Conductivity-temperature-depth (CTD) casts and nutrient concentration measurements were also performed at each station [2].

The 2016 West Coast Ocean Acidification (WCOA16) cruise was a 34-day NOAA OAP cruise conducted between Baja California, Mexico, and Vancouver Island, Canada, from May 5 to June 7, 2016, using the NOAA Ship *Ronald H. Brown*. Measurements made during this cruise included the same suite of CO_2 system variables as those measured during WCOA13. Nutrients and CTD data were also collected. Many of the 132 sampling stations occupied during this cruise were the same as those occupied during WCOA cruises in 2007, 2011, 2012, and 2013 [3].

Data from both cruises spanned a wide range of salinities, including water samples from the Columbia River, where the salinities ranged from 0.1 to 15.1.

5.3.2 pH_T Measurements

Detailed descriptions of the methods used to measure DIC, TA, nutrients, temperature, and salinity can be found in Feely et al. [2] for WCOA13 and Alin et al. [3] for WCOA16. Briefly, DIC was measured coulometrically according to SOP 2 of Dickson et al. [4], and TA was measured using an open-cell titration according to SOP 3B of Dickson et al. [4]. Accuracy for both measurements was assessed using Certified Reference Materials (CRMs) provided by the Dickson laboratory (UCSD-SIO). Nutrients were measured according to the procedures of

Gordon et al. [5]. Temperature and salinity were determined using Sea-Bird temperature and conductivity sensors.

Measurements of pH_T are salient to our analyses and so are described here in detail. The pH_T samples were collected in 10-cm path length cylindrical cuvettes (~30 mL volume) and warmed for 30 minutes to a temperature of 298.15 K in a custom-made thermostatted cell warmer. All measurements were made using Agilent 8453 UV/Vis spectrophotometers thermostatted to 298.15 K. Using the Agilent ChemStation software package, absorbance blanks were taken at 434, 578, and 730 nm. Ten μL of 10-mM flash-purified mCP was added to each sample, and absorbance measurements were retaken at 434, 578, and 730 nm. Absorbance ratios, R, were calculated from these absorbance measurements, and pH_T at $T = 298.15$ K was calculated using the salinity of each sample according to the pH_T, $p(K_I e_2)$, and e_x algorithms of Liu et al. [6]. pH_T values were perturbation-corrected using the following empirical fit:

$$pH_T(corrected) = \left(1.006574 \times pH_T(calculated)\right) - 0.0508 \quad (5.1)$$

5.3.3 CO2SYS Analysis

All calculations using CO_2 system parameter pairings were performed using CO2SYS for MATLAB [7]. The program calculates the full suite of CO_2 system parameters for both input and output temperatures and pressures (i.e., shipboard and *in situ* conditions).

Data were divided into high-salinity ($S \geq 20$) and low-salinity ($S < 20$) subsets. For subsequent analyses, the data were screened according to their WOCE quality control (QC) designations. Because of the large size of the high-salinity dataset, only samples for which all measured variables carried a QC of 2 or 6, indicative of good or replicate data, respectively, were included in subsequent analyses. The low-salinity data subset was much smaller; therefore, low-salinity samples for which measured variables carried a QC of either 2 (good data), 3

(questionable data), or 6 (mean of replicates data) were included in subsequent analyses. Additionally, data from one station (WCOA13, station 133) were excluded from further analyses due to very large (>0.18) differences between measured and CO2SYS-calculated pH_T.

To demonstrate that small corrections in TA can bring about improved internal consistency, Patsavas et al. [8] determined that calculated TA underestimates measured TA by ~4 μmol kg^{-1} (0.18% of typical oceanic values). This empirical alkalinity correction was subtracted from the measured TA to account for a number of unknown measurement errors, including organic alkalinity and uncertainty in the equilibrium (K_1 and K_2) models. A similar correction of 4.56 ± 3.79 μmol kg^{-1} was made for the subset of WCOA13 and WCOA16 marine samples ($S \geq 20$) by calculating TA using the measured pH_T (according to Liu et al. [6]), DIC, and the K_1 and K_2 constant data of Mehrbach et al. [9] as refit by Lueker et al. [10]. This empirical correction, applicable for the combined high-salinity data from the two cruises, is comparable but slightly higher than the value Fassbender et al. [11] calculated for only the WCOA13 dataset, 3 ± 6 μmol kg^{-1}. The adjusted TA values are referred to hereinafter as TA^*; throughout the remainder of this chapter, the empirical adjustment applies only to measured TA values, and not to TA values calculated from DIC and pH_T. Appendix D shows the TA offset for WCOA13 and WCOA16 data with S ≥ 20.

For the data subset with $S \geq 20$, *R*-ratios were calculated using Eq. (5.1) along with the pH_T and $p(K_I e_2)$ models of Liu et al. [6]. These *R*-ratios were then used to calculate pH_T via the mCP $p(K_I e_2)$ model given in Eq. (4.4) (i.e., the updated Douglas and Byrne [1] model) and the e_x parameterizations of Liu et al. [6].

For the low-salinity data subset, raw absorbance data and *R*-ratios were available from both cruises. Therefore, it was not necessary to calculate *R*-ratios from reported pH_T values. *R*-

ratios were directly used to calculate pH_T according to Eq. (4.4). For all samples with $S < 20$, pH_T was also calculated using the Mosley et al. [12] model. Finally, for samples with $S \leq 0.5$, pH_f was calculated according to the algorithm of Lai et al. [13,14] and converted to pH_T within CO2SYS.

For internal consistency comparisons, pH_T was calculated using DIC and TA^*. TA was also calculated using DIC and pH_T. All calculations were performed at $T = 298.15$ K and $P = 1$ atm using the K_{HSO4} of Dickson [15] and the total boron (B_T) characterization of Uppstrom [16]. For the subset of data with $S \geq 20$, the K_1 and K_2 values of Mehrbach et al. [9] as refit by Lueker et al. [10] were used. For the subset of data with $S < 20$, the estuarine-range K_1 and K_2 values of Cai and Wang [17] were used.

5.4 Results

5.4.1 Spectrophotometric versus Calculated pH_T

Results of this internal consistency analysis for the combined WCOA13 and WCOA16 datasets are summarized in Table 5.1 using the same statistical parameters that were employed in the internal consistency analysis of Ribas-Ribas et al. [18]:

- Pearson's correlation coefficient (r), a measure of linear dependence between the two variables;
- Root mean squared error (RMSE), the square root of the mean of the squared differences between the pH_T calculated by the model listed in column 1 and the pH_T calculated by the model listed in column 2;
- Mean residual (MR) ± σ, the mean residual, given as the mean of the differences between the pH_T calculated by the model listed in column 1 and the pH_T calculated by the model listed in column 2, with an included uncertainty of one standard deviation (σ).

Residuals plots of ΔpH_T are shown as functions of pH_T (calculated using TA^* and DIC) for marine and estuarine samples in Figs. 5.1 and 5.2, respectively. Due to the small sample size of freshwater ($S \leq 0.5$) samples ($n = 4$, all of which are from WCOA13, station 44), subsequent discussion will focus on samples with $S > 0.5$.

Across both marine and estuarine salinity regimes, the Douglas and Byrne [1, Eq.(4.4)] $p(K_I e_2)$ model produces pH_T values that are in good agreement with those produced by published spectrophotometric pH_T models: within 0.004 of pH_T determined according to Liu et al. [6] and within 0.01 of pH_T determined according to Mosley et al. [12]. The larger differences between the pH_T values determined according to the Douglas and Byrne [1, Eq. (4.4)] and Mosley et al. [12] models arise from the presence of impurities in the mCP used to characterize the pK_I of Mosley et al. [12] (see Section 5.5.2). All spectrophotometric pH_T determinations correlate well with one another ($r > 0.99$).

Table 5.1 Summary of internal consistency statistics for calculations of pH_T. The Eq. (4.4) model is denoted as "DB."

pH_T Model 1	**pH_T Model 2**	***r***	**RMSE**	**MR ± σ**
Marine ($S \geq 20$, $n = 2136$)				
DB	Liu	1.0000	0.0013	-0.0013 ± 0.0002
DB	Mosley	1.0000	0.0053	-0.0052 ± 0.0010
Liu	Mosley	1.0000	0.0040	-0.0039 ± 0.0009
DB	TA*, DIC	0.9990	0.0101	-0.0017 ± 0.0100
Liu	TA*, DIC	0.9990	0.0101	-0.0017 ± 0.0100
Mosley	TA*, DIC	0.9990	0.0109	0.0036 ± 0.0103
Estuarine ($0.5 < S < 20$, $n = 18$)				
DB	Mosley	0.9998	0.0080	-0.0079 ± 0.0013
DB	TA*, DIC	0.7656	0.0731	0.0328 ± 0.0672
Mosley	TA*, DIC	0.7622	0.0773	0.0407 ± 0.0677
Freshwater ($S \leq 0.5$, $n = 4$)				
DB	Mosley	0.9988	0.0027	-0.0027 ± 0.0002
DB	Lai	0.9986	0.0170	-0.0170 ± 0.0002
Mosley	Lai	1.0000	0.0143	-0.0143 ± 0.0001
DB	TA*, DIC	-0.3070	0.3193	0.3192 ± 0.0058
Mosley	TA*, DIC	-0.3307	0.3219	0.3219 ± 0.0059
Lai	TA*, DIC	-0.3329	0.3362	0.3362 ± 0.0059

In the marine salinity range ($S \geq 20$), RMSEs between the spectrophotometric pH_T and CO2SYS-calculated pH_T are ~0.01, with respective RMSEs approximately equivalent for the 2013 and 2016 datasets. This difference between spectrophotometric and calculated pH_T is similar in magnitude to that determined by Ribas-Ribas et al. [18] for their spectrophotometric pH_T measurements using Thymol Blue.

In the estuarine salinity range ($0.5 < S < 20$), however, pH_T data comparisons exhibit more scatter. RMSEs between spectrophotometric and calculated pH_T are larger than for marine salinities and are ~0.07 for both the 2013 and 2016 cruise datasets. These larger differences also correspond to lower correlation coefficients between pH_T values determined via direct spectrophotometric measurements and CO2SYS calculations ($r \approx 0.77$ for the combined cruise dataset). This is true for pH_T determined with both the Mosley et al. [12] and Douglas and Byrne [1, Eq. (4.4)] models. The difference between spectrophotometric and calculated pH shows no discernible trend as a function of DIC, TA, pH_T, or salinity in this range. The scatter in the data reflects current challenges in modeling the CO_2 system in rivers and estuaries (see Section 5.5.1).

5.4.2 Measured versus Calculated TA

Internal consistency comparisons obtained using (a) TA^* and (b) TA calculated from measured DIC and spectrophotometric pH_T are given in Table 5.2. In general, parameter pairings involving pH or f_{CO2} tend to have better precision than those utilizing only TA and DIC [8]. Internal consistency between measured TA^* and TA calculated from DIC and pH_T (where $\Delta TA = TA^*(meas) - TA(calc)$) are shown for marine and estuarine conditions in Figs. 5.3 and 5.4.

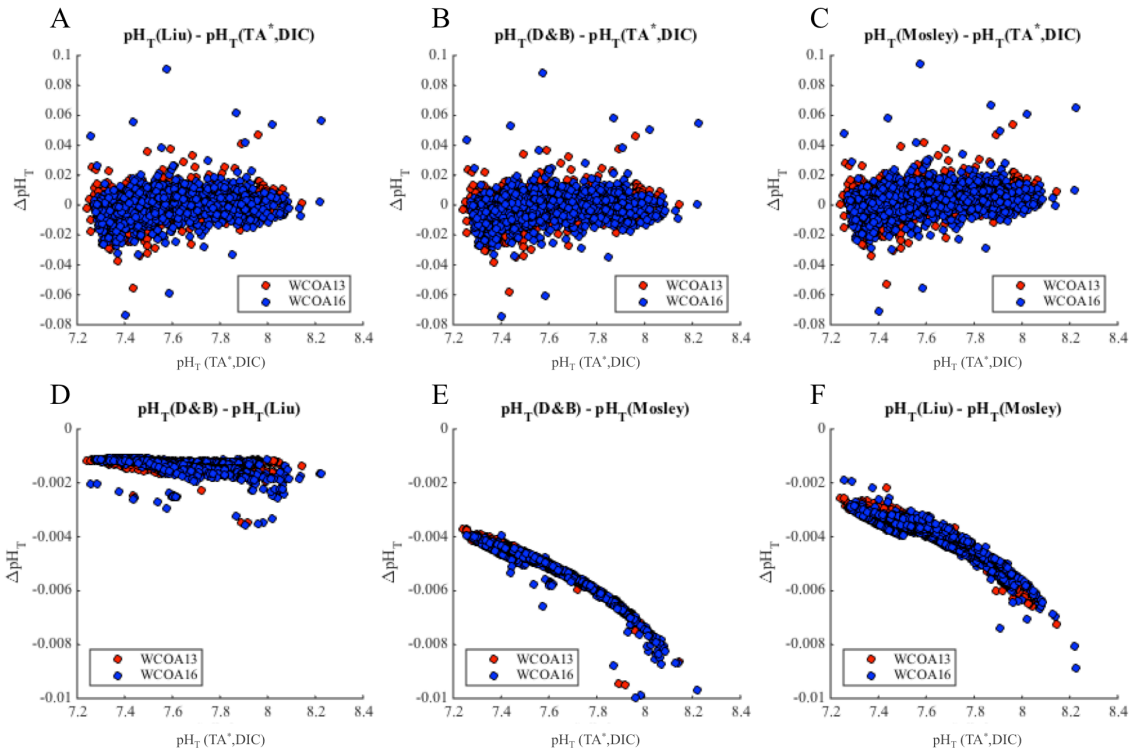

Fig. 5.1 Seawater ΔpH_T versus pH_T as calculated by TA^* and DIC. ΔpH_T is given for the following sets: (A) pH_T(Liu et al. [6]) – $pH_T(TA^*,DIC)$; (B) pH_T(Douglas and Byrne [1]) – $pH_T(TA^*,DIC)$; (C) pH_T(Mosley et al. [11]) – $pH_T(TA^*,DIC)$; (D) pH_T(Douglas and Byrne [1]) – pH_T(Liu et al. [6]); (E) pH_T(Douglas and Byrne [1]) – pH_T(Mosley et al. [11]); and (F) pH_T(Liu et al. [6]) – pH_T(Mosley et al. [11]).

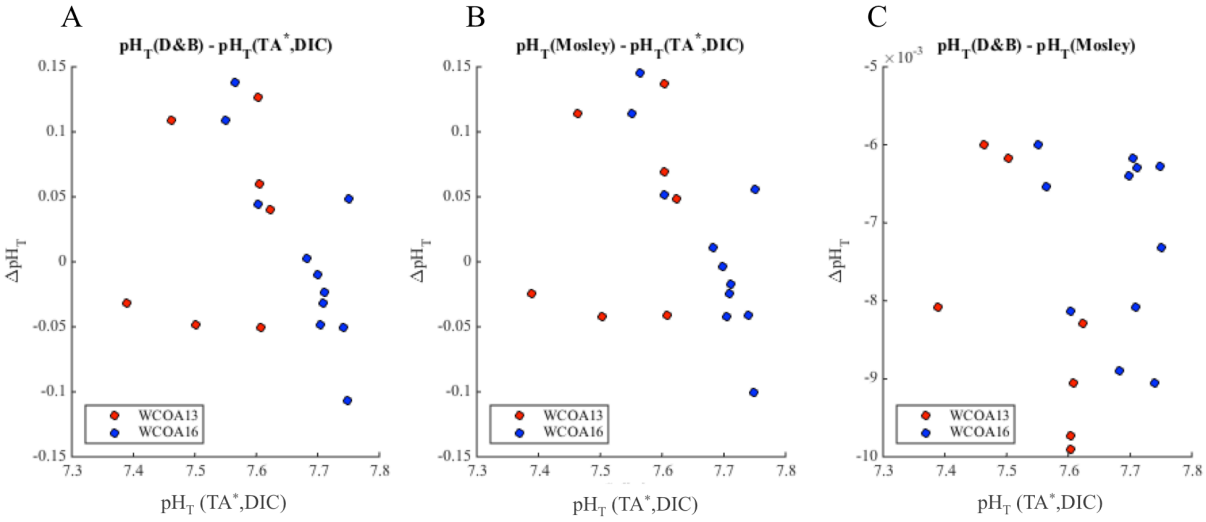

Fig. 5.2 Columbia River ΔpH_T versus pH_T (as calculated by TA^* and DIC). ΔpH_T is given for the following sets: (A) pH_T(Douglas and Byrne [1]) – $pH_T(TA^*,DIC)$; (B) pH_T(Mosley et al. [11]) – $pH_T(TA^*,DIC)$; and (C) pH_T(Douglas and Byrne [1]) – pH_T(Mosley et al. [11]).

Table 5.2 Summary of internal consistency statistics for calculations of TA. The Eq. (4.4) model is denoted as "DB."

TA_1	**TA_2**	***r***	**RMSE ($\mu mol\ kg^{-1}$)**	**MR ± σ ($\mu mol\ kg^{-1}$)**
Marine (S ≥ 20, n = 2136)				
TA*	TA (pH_{DB},DIC)	0.9986	3.7727	0.5025 ± 3.7400
TA*	TA (pH_{Liu},DIC)	0.9986	3.7927	0.0000 ± 3.7936
TA*	TA (pH_{Mosley},DIC)	0.9984	4.3483	-1.5740 ± 4.0544
Estuarine (0.5 < S < 20, n = 18)				
TA*	TA (pH_{DB},DIC)	0.9993	9.1862	-4.1892 ± 8.4124
TA*	TA (pH_{Mosley},DIC)	0.9993	9.7938	-5.1028 ± 8.6018

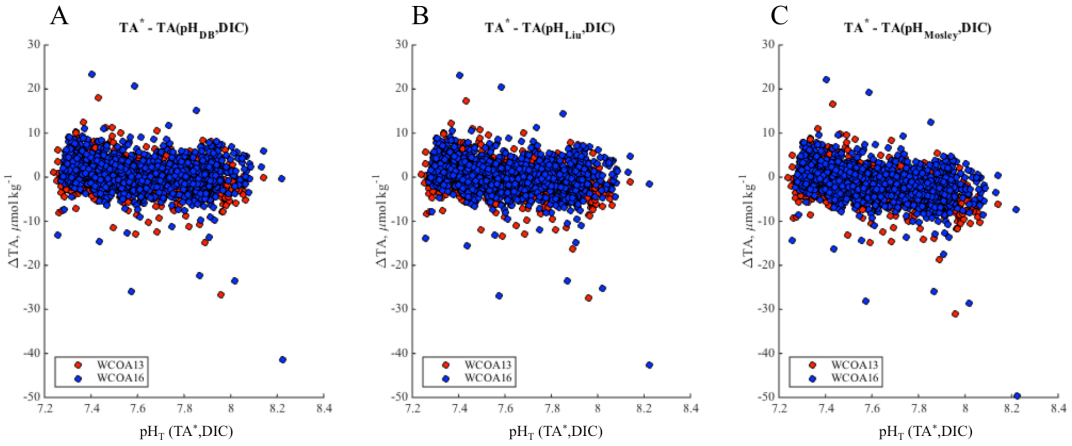

Fig. 5.3 Seawater ΔTA versus pH_T as calculated by TA^* and DIC. ΔTA is given for the following sets: (A) TA^* – TA(pH_{DB},DIC); (B) TA^* – TA(pH_{Liu},DIC); and (C) TA^* – TA(pH_{Mosley},DIC).

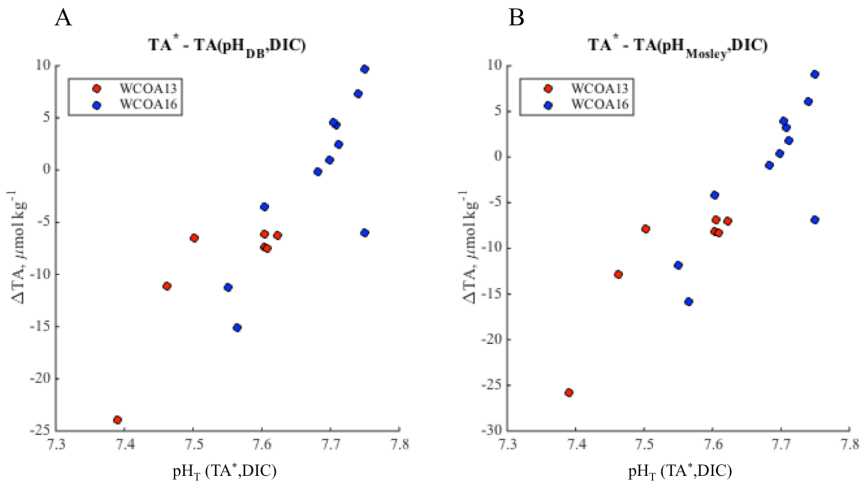

Fig. 5.4 Columbia River ΔTA versus pH_T (as calculated by TA^* and DIC). ΔTA is given for the following sets: (A) TA^* – TA(pH_{DB},DIC); and (B) TA – TA(pH_{Mosley},DIC).

For marine conditions all three spectrophotometric pH_T models performed well when paired with DIC and were able to achieve ΔTA values that were generally within the ±10 μmol kg^{-1} "weather" precision goal of the Global Ocean Acidification Observing Network (GOA-ON) [18]. However, RMSEs for ΔTA in the marine salinity range (~3.7 and 3.8 μmol kg^{-1}, respectively) were outside of the ±2 μmol kg^{-1} "climate" goal. Precision was degraded for estuarine calculations of ΔTA; RMSEs were ~9.2 μmol kg^{-1} for calculations using the Douglas and Byrne [1, Eq. (4.4)] pH_T model, and ~9.8 μmol kg^{-1} for calculations using the Mosley et al. [11] pH_T model. Typical precision was ±0.10% (2 μmol kg^{-1}) for direct DIC and TA^* measurements [3].

5.5 Discussion

5.5.1 Challenges of Measuring the Estuarine CO_2 System

While vital to our understanding of ocean acidification, monitoring of CO_2 system changes in coastal and estuarine environments presents a number of challenges due to the wide variability of CO_2 system parameters in these environments. Both natural and anthropogenic processes influence these changes, which can be large and occur on varied timescales, making accurate, precise measurements of the CO_2 system in these environments difficult [11,19–21].

Despite the large size of the WCOA13 and WCOA16 datasets (>2000 samples), the small number of samples in the Columbia River limits our ability to assess model accuracy in estuaries and freshwater environments. Larger, overdetermined estuarine datasets that include pH will enable increasingly refined internal consistency assessments. These datasets should also, when possible, employ pCO_2 measurements as an additional variable to calculate pH, and may benefit from redundant measurements of pH using spectrophotometry and either DuraFETs or spectrophotometrically calibrated electrodes [22,23].

Spectrophotometric pH_T samples from both the 2013 and 2016 cruises were corrected for indicator-induced perturbations using Eq. (5.1). The assumption that this empirical correction, which was determined for samples with marine salinities, would be applicable in lower-salinity waters is likely invalid, further complicating the low-salinity data and reducing its usefulness. For best accuracy, future spectrophotometric pH measurements in low-salinity waters should correct for indicator perturbations by either (a) determining a perturbation correction equation applicable for low-salinity samples, or (b) performing two indicator additions for each sample and regressing absorbance measurements taken after each addition. Because of the heterogeneous nature of samples in the nearshore environment, the second strategy is more rigorous. However, performing and measuring two indicator additions for each sample requires more time and thus may slow the pace of sample processing.

Sampling and measuring samples accurately in nearshore environments pose greater challenges than in marine environments. For spectrophotometric measurements, turbidity can have a deleterious effect on measurement quality due to light scattering. In addition, chromophoric dissolved organic matter (CDOM) weakly absorbs at the wavelengths used for spectrophotometric pH_T measurements [18]. Absorbance blanks largely compensate for these effects but cannot eliminate their significance.

Calculations involving low-salinity samples may be prone to errors due to assumptions about water composition. Estuarine dynamics complicate the CO_2 system: photosynthesis, remineralization, freshwater runoff, and tidal influences all affect carbon biogeochemistry. Although conservative ion concentrations can be determined from the salinity in seawater, ion-to-salinity ratios break down in freshwaters. Calcium, a quasi-conservative element in seawater, can be especially problematic in fresher waters, because its concentration is used to determine

Ω_A, the aragonite saturation state. When the calcium-to-salinity ratio breaks down in fresher waters, accurate determinations of Ω_A become difficult. Direct measurements of calcium concentrations using inductively coupled plasma-mass spectrometry (ICP-MS) can circumvent this problem for low-salinity samples [24].

5.5.2 Influence of Impurities on pH_T Determinations

Spectrophotometric pH_T values determined using the Mosley et al. [11] algorithm are consistently higher than pH_T using either the Liu et al. [6] or Douglas and Byrne [1, Eq.(4.4)] models. This is to be expected, as the mCP pK_I of Mosley et al. [11] was characterized using unpurified mCP. Impurity absorbances at 434 nm lower measured R values. The pK_I determined by Mosley et al. [12] is therefore artificially increased due to this suppression of R, such that any pH calculated using the Mosley et al. [12] pK_I algorithm will be spuriously high.

The magnitude of the offset between the purified [1,6] and unpurified [12] spectrophotometric pH_T models becomes larger at higher pH_T, as was observed in Douglas and Byrne [25] and is similar (~0.007 at $pH_T = 8.1$) to the offsets between pH_T measured with purified and unpurified indicators reported by Douglas and Byrne [25].

5.5.3 Uncertainties in the CO_2 System Models and Measurements

The CO2SYS software for MATLAB [7] currently offers six parameterizations for K_1 and K_2 applicable to estuarine conditions [17,26–30]. Further work to evaluate these estuarine K_1 and K_2 constants is needed, particularly in light of ocean acidification. Estuarine environments generally have higher f_{CO2} values than are observed in the open ocean [17,31,32] and are therefore subject to the errors in K_1 and K_2 characterizations that arise at $f_{CO2} > 600$ μatm [8,10,33,34]. For all WCOA13 and WCOA16 samples with $S < 20$, f_{CO2} calculated from TA and DIC was in excess of 550 μatm and was >600 μatm for all but one of these samples. Thus, it is

hypothesized that the scatter observed in this estuarine internal consistency analysis can be at least partially attributed to K_1 and K_2 model errors at high f_{CO2}. A study is underway in the Byrne lab to evaluate internal consistency of state-of-the-art measurements of all four CO_2 system parameters across a broad range of S,T, and f_{CO2} ranging from 200 to 2000 μatm toward the goal of redetermining K_1 and K_2 for a high-CO_2 world. Ideally, such future redeterminations of K_1 and K_2 should include characterization over both the marine and estuarine salinity ranges.

Dissolved organic matter has been cited as another possible cause for discrepancies in internal consistency calculations. In productive coastal environments, TA is affected by the presence of organic acids [35–38]. Organic alkalinity has only recently been identified as a potentially significant source of alkalinity, and both model-based [35] and experimental [36–38] approaches have been taken to quantify and characterize organic alkalinity. Rigorous determinations of organic alkalinity are preferable to empirical corrections, as organic alkalinity is merely one of many unknowns that should be explored and refined. Fassbender et al. [12] showed that for the 2011 and 2013 WCOA cruises, computational uncertainty of organic alkalinity is ~±5 μmol kg^{-1} and that therefore, on average, the organic alkalinity concentrations were not statistically distinguishable from zero for outer coastal samples. However, Yang et al. [37] found organic alkalinities as high as 41 μmol kg^{-1} in nearshore environments in west Florida, highlighting the heterogeneous nature of organic alkalinity as a contributor to TA. Because the models of the CO_2 system currently only consider inorganic alkalinity (e.g., carbonate, borate, phosphate, silicate alkalinities), the significance of organic alkalinity in coastal, estuarine, and riverine environments underscores the need for future models to take organic alkalinity into account.

5.6 Acknowledgments

The author wishes to thank the captains, officers, and crews of the NOAA Ship *Fairweather*, *R/V Pt. Sur*, and NOAA Ship *Ronald H. Brown*; the chief scientists of the WCOA13 and WCOA16 cruises: Dr. Richard Feely, Dr. Adrienne Sutton, Mr. Dana Greely, Dr. Simone Alin, Mr. Julian Herndon; and the scientific parties of the WCOA13 and WCOA16 cruises for their work that resulted in the two datasets used in this paper. N.K. Douglas received financial support from a University of South Florida Presidential Doctoral Fellowship through the Office of Graduate Studies. This work was also supported by two National Science Foundation grants, OCE 1220110 and OCE 1657894.

5.7 References

1. Douglas, N.K. Byrne, R.H., 2017b. Spectrophotometric pH measurements from river to sea: Calibration of mCP for $0 \leq S \leq 40$ and $278.15 \leq T \leq 308.15$ K. *Marine Chemistry* **197**, 64-69.
2. Feely, R.A., Alin, S.R., Hales, B., Johnson, G.C., Byrne, R.H., Peterson, William; Liu, Xuewu; Greeley, Dana (2015). Dissolved inorganic carbon, total alkalinity, pH and other variables collected from profile and discrete sample observations using CTD, Niskin bottle, and other instruments from NOAA Ship Fairweather and R/V Point Sur in the U.S. West Coast California Current System during the 2013 West Coast Ocean Acidification Cruise (WCOA2013) from 2013-08-05 to 2013-08-28 (NCEI Accession 0132082). Version 2.2. NOAA National Centers for Environmental Information. Dataset.
3. Alin, S.R., Feely, R.A. Hales, B. Byrne, R.H., Cochlan, W., Liu, X.; Greeley, D., 2017. Dissolved inorganic carbon, total alkalinity, pH, dissolved oxygen, nutrients, and other variables collected from profile and discrete sample observations using CTD, Niskin bottle, and other instruments from Ronald H. Brown in the West Coast of North America from Canada to Mexico from 2016-05-08 to 2016-06-06 (NCEI Accession 0169412). Version 1.1. NOAA National Centers for Environmental Information. Dataset.
4. Dickson, A.G., Sabine, C.L., Christian, J.R. (Eds.), 2007. *Guide to Best Practices for Ocean CO_2 Measurements.* PICES Special Publication 3, 191 p.
5. Gordon, L.I., Jennings, Jr., J.C., Ross, A.A., Krest, J.M., 1993. A suggested protocol for continuous flow automated analysis of seawater nutrients (phosphate, nitrate, nitrite and silicic acid) in the WOCE Hydrographic Program and the Joint Global Ocean Fluxes Study. *WOCE Operations Manual, Part 3*, 55 p.

6. Liu, X., Patsavas, M.C., Byrne, R.H., 2011. Purification and characterization of meta-cresol purple for spectrophotometric seawater pH measurements. *Environmental Science & Technology* **45**, 4862-4868.

7. van Heuven, S., Pierrot, D., Rae, J.W.B., Lewis, E., Wallace, D.W.R., 2011. MATLAB Program Developed for CO_2 System Calculations. ORNL/CDIAC-105b. Carbon Dioxide Information Analysis Center, Oak Ridge National Laboratory, U.S. Department of Energy, Oak Ridge, TN. doi: 10.3334/CDIAC/otg.CO2SYS_MATLAB_v1.1.

8. Patsavas, M.C., Byrne, R.H., Wanninkhof, R., Feely, R.A., Cai, W.-J., 2015. Internal consistency of marine carbonate system measurements and assessments of aragonite saturation state: Insights from two U.S. coastal cruises. *Marine Chemistry* **176**, 9-20.

9. Mehrbach, C., Culberson, C.H., Hawley, J.E., Pytokowicz, R.M., 1973. Measurement of the apparent dissociation constants of carbonic acid in seawater at atmospheric pressure. *Limnology and Oceanography* **18**, 897-907.

10. Lueker, T.J., Dickson, A.G., Keeling, C.D., 2000. Ocean pCO2 calculated from dissolved inorganic carbon, alkalinity, and equations for K_1 and K_2: validation based on laboratory measurements of CO2 in gas and seawater at equilibrium. *Marine Chemistry*, **70**(1), 105-119.

11. Fassbender, A.J., Alin, S.R., Feely, R.A., Sutton, A.J., Newton, J.A., Byrne, R.H., 2017. Estimating total alkalinity in the Washington coastal zone: Complexities and surprising utility for ocean acidification research. *Estuaries and Coasts* **40**, 404-418.

11. Mosley, L.M., Husheer, S.L.G., Hunter, K.A., 2004. Spectrophotometric pH measurement in estuaries using thymol blue and *m*-cresol purple. *Marine Chemistry* **91**, 175-186.

12. Lai, C.Z., DeGrandpre, M.D., Wasser, B.D., Branson, T.A., Clucas, D.S., Jaqueth, E.J., Benson, Z.D., Beatty, C.M., Spaulding, R.S., 2016. Spectrophotometric measurement of freshwater pH with purified meta-cresol purple and phenol red. *Limnology and Oceanography: Methods* **14**(12), 864-873.

13. Lai, C.Z., DeGrandpre, M.D., Wasser, B.D., Branson, T.A., Clucas, D.S., Jaqueth, E.J., Benson, Z.D., Beatty, C.M., Spaulding, R.S., 2017. Erratum: Spectrophotometric measurement of freshwater pH with purified meta-cresol purple and phenol red. *Limnology and Oceanography: Methods* **15**, 903.

14. Dickson, A.G., Wesolowski, D.J., Palmer, D.A., Mesmer, R.E., 1990. Dissociation constant of bisulfate ion in aqueous sodium chloride solutions to 250 ^{o}C. *Journal of Physical Chemistry* **94**(20), 7978-7985.

15. Uppstrom, L.R., 1974. The boron/chlorinity ratio of deep-sea water from the Pacific Ocean. *Deep Sea Research and Oceanographic Abstracts* **21**(2), 161-162.

16. Cai, W.-J., Wang, Y., 1998. The chemistry, fluxes, and sources of carbon dioxide in the estuarine waters of the Satila and Atlahama Rivers, Georgia. *Limnology and Oceanography* **43**(4), 657-668.

17. Ribas-Ribas, M., Rerolle, V.M.C., Bakker, D.C.E., Kitidis, V., Lee, G.A., Brown, I., Achterberg, E.P., Hardman-Mountford, N.J., Tyrrell, T., 2014. Intercomparison of

carbonate chemistry measurements on a cruise in northwestern European shelf seas. *Biogeosciences* **11**, 4339-4355.

18. Newton, J.A., Feely, R.A., Jewett, E.B., Williamson, P., Mathis, J., 2014. Global Ocean Acidification Observing Network: Requirements and Governance Plan. http://www.goa-on.org/docs/GOA-ON_plan_print.pdf.

19. Borges, A.V., 2011. Present day carbon dioxide fluxes in the coastal ocean and possible feedbacks under global change. *Oceans and the atmospheric carbon content*, eds. Duarte, P., Santana-Casiano, J.M. Dordecht: Springer Netherlands, 47-77.

20. Hoffmann, G.E., Smith, J.E., Johnson, K.S., Send, U., Levin, L.A., Micheli, F., Paytan, A., Price, N.N., Peterson, B., Takeshita, Y., Matson, P.G., Crook, E.D., Kroeker, K.J., Gambi, M.C., Rivest, E.B., Frieder, C.A., Yu, P.C., Martz, T.R., 2011. High-frequency dynamics of ocean pH: A multi-ecosystem comparison. *PLoS One* **6**, e28983.

21. Takeshita, Y., Frieder, C.A., Martz, T.R., Ballard, J.R., Feely, R.A., Kram, S., Nam, S., Navarro, M.O., Price, N.N., Smith, J.E., 2015. Including high-frequency variability in coastal ocean acidification projections. *Biogeosciences* **12**, 5853-5870.

22. Easley, R.A., Byrne, R.H., 2012. Spectrophotometric calibration of pH electrodes in seawater using purified m-cresol purple. *Environmental Science & Technology* **46**(9), 5018-5024.

23. Gonski, S.F., 2016. *An evaluation of the performance of an ISFET pH sensor in a dynamic estuarine system*. University of Delaware. http://udspace.udel.edu/bitstream/handle/19716/21486/2016_GonskiStephen_MS.pdf?sequence=1. (Accessed 4 February 2018).

24. Cai, W.J., pers. comm.

25. Douglas, N.K., Byrne, R.H., 2017a. Achieving accurate spectrophotometric pH measurements using unpurified meta-cresol purple. *Marine Chemistry* **190**, 66-72.

26. Roy, R.N., Roy, L.N., Vogel, K.M., Porter-Moore, C., Pearson, T., Good, C.E., Millero, F.J., Campbell, D.M., 1993. The dissociation constants of carbonic acid in seawater at salinities 5 to 45 and temperatures 0 to 45 ^{o}C. *Marine Chemistry* **44**(2), 249-267.

27. Goyet, C., Poisson, A., 1989. New determination of carbonic acid dissociation constants in seawater as a function of temperature and salinity. *Deep Sea Research Part A: Oceanographic Research Papers* **36**(11), 1635-1654.

28. Mojica Prieto, F.J., Millero, F.J., 2002. The values of $pK_1 + pK_2$ for the dissociation of carbonic acid in seawater. *Geochimica et Cosmochimica Acta* **66**(14), 2529-2540.

29. Millero, F.J., Pierrot, D., Lee, K., Wanninkhof, R., Feely, R., Sabine, C.L., Key, R.M., Takahashi, T., 2002. Dissociation constants for carbonic acid determined from field measurements. *Deep-Sea Research, Part I* **49**, 1705-1723.

30. Millero, F.J., 2010. Carbonate constants for estuarine waters. *Marine and Freshwater Research* **61**(2), 139-142.

31. Frankignoulle, M., Bourge, I., 1996. Atmospheric CO_2 fluxes in a highly polluted estuary (the Scheldt). *Limnology and Oceanography* **41**, 365-369.

32. Bakker, D.C.E., de Baar, H.J.W., de Wilde, H.P.J., 1996. Dissolved carbon dioxide in Dutch coastal waters. *Marine Chemistry* **55**, 247-263.

33. Lee, K., Millero, F.J., Byrne, R.H., Feely, R.A., Wanninkhof, R., 2000. The recommended dissociation constants for carbonic acid in seawater. *Geophysical Research Letters* **27**(2), 229-232.

34. Hoppe, C.J.M., Langer, G., Rokitta, S.D., Wolf-Gladrow, D.A., Rost, B., 2010. On CO_2 perturbation experiments: Over-determination of carbonate chemistry reveals inconsistencies. *Biogeosciences Discussion* **7**, 1707-1726.

35. Cai, W.-J., Wang, Y., Hodson, R.E., 1998. Acid-base properties of dissolved organic matter in the estuarine waters of Georgia, U.S.A. *Geochimica et Cosmochimica Acta* **62**(3), 473-483.

36. Hernández-Ayon, J., Zirino, A., Dickson, A.G., Camiro-Vargas, T., Valenzuela-Espinoza, E., 2007. Estimating the contribution of organic bases from microalgae to the titration alkalinity in coastal seawaters. *Limnology and Oceanography: Methods* **5**(7), 225-232.

37. Yang, B., Byrne, R.H., Lindemuth, M., 2015. Contributions of organic alkalinity to total alkalinity in coastal waters: A spectrophotometric approach. *Marine Chemistry* **176**, 199-207.

38. Muller, F.L, Bleie, B., 2008. Estimating the organic acid contribution to coastal seawater alkalinity by potentiometric titrations in a closed cell. *Analytical Chimica Acta* **619**(2), 183-191.

CHAPTER SIX:

CONCLUSIONS AND FUTURE STUDIES

6.1 Conclusions

6.1.1 Indicator Impurity Corrections

The ${}_{434}A_{\text{imp}}$ model presented in Chapter Two of this dissertation offers a new tool for researchers using unpurified mCP for spectrophotometric pH_T measurements. This straightforward model requires only a measurement of absorbances at high pH (~12) to determine the contribution of colorimetric impurities to the absorbance at the mCP acid peak (434 nm). The impurity absorbance (${}_{434}A_{\text{imp}}$) can then be used to correct measurements of samples in the natural pH range of seawater (7.0–8.3). The utility of this model is contingent upon impurities absorbing in the range of the mCP acid peak and negligibly in the range of the base peak, as observed by Yao et al. [1] and Liu et al. [2]. Because impurity contributions to absorbance can vary from one lot to another, the test should be performed any time a new lot of unpurified mCP is used.

6.1.2 p(K_1e_2*) Characterizations of mCP, TB, and CR Across the Estuarine Salinity Range*

Chapters Three and Four of this dissertation present new p(K_1e_2) models for mCP, TB, and CR applicable across a wide range of salinities ($0 \leq S \leq 40$) and temperatures ($278.15 \leq T \leq 308.15$ K) at atmospheric pressure. These equations combine a number of extant datasets and models that are applicable across more narrow ranges of salinity and temperature. All three new

models fit the extant datasets well: all data used to fit the new algorithms were within ±0.004 of fitted values for mCP; within ±0.0043 for TB, with one exception at $S = 40$, $T = 308.15$ K; and within ±0.0025 for CR. The new models are sufficient for shipboard or laboratory-based measurements of spectrophotometric absorbances using these indicators and provide a useful tool for making spectrophotometric pH measurements in nearshore, low-salinity waters where previous models were not considered applicable.

6.1.3 Internal Consistency of U.S. West Coast CO_2 System Cruise Datasets

Analyses of CO_2 system internal consistency from the 2013 and 2016 NOAA West Coast Ocean Acidification Cruise datasets showed that TA measurements in $S \geq 20$ waters are underestimated by between 4.5 and 5.0 μmol kg^{-1}, depending upon which p(K_1e_2) model is used to determine the spectrophotometric pH_T. The magnitude of this offset in TA is consistent with the findings of other internal consistency analyses in coastal systems [3,4]. This offset is thought to be largely due to the presence of organic alkalinity in productive coastal waters and uncertainties in characterizations of the CO_2 system dissociation constants (K_1 and K_2). When accounting for the ~5.0 μmol kg^{-1} difference between measured and calculated TA in waters where $S \geq 20$, internal consistency is improved.

However, samples collected from the Columbia River, where $S < 20$, exhibited poor internal consistency with large differences in calculated versus measured TA (RMSE ~9 μmol kg^{-1}). This poor internal consistency is attributed to the aforementioned uncertainties, as well as likely measurement error when correcting spectrophotometric pH_T samples for indicator-induced pH_T perturbations. The poor agreement between measured and calculated parameters in the estuarine salinity range highlights the need for large, carefully collected CO_2 system datasets in these waters so that individual sources of error can be explored and quantified.

6.2 Future Studies

Many challenges remain toward accurately measuring pH_T in both marine and estuarine waters, and work is ongoing toward this goal.

6.2.1 Calibration of Tris Buffer at Low Salinities

The estuarine $p(K_I e_2)$ models for mCP, TB, and CR presented in Chapters Three and Four of this dissertation have been constructed using datasets based on the pH of buffer solutions. Collaborative work among a number of laboratories around the world to calibrate Tris buffer in the estuarine salinity range is underway as part of the efforts of the Scientific Committee on Oceanic Research (SCOR) Working Group 145 [5]. Tris/Tris-HCl is the buffer chosen most frequently for laboratory measurements of marine pH [6], but a relative paucity of data for Tris calibration in the estuarine salinity range limits our ability to make robust estuarine pH measurements, especially at temperatures other than 298.15 K. Measurements of pH using Harned cells across a variety of salinities ($0 \leq S \leq 40$), temperatures ($273.15 \leq T \leq 323.15$ K), and Tris/Tris-HCl concentrations will provide a calibration of Tris applicable to these conditions, which will in turn be useful in the calibration of sulfonephthalein indicators [5].

6.2.2 Improved Standardization of mCP, TB, and CR

The mCP, TB, and CR models developed in Chapters Three and Four offer a interim models for the evaluation of spectrophotometric pH_T across a range of S and T until calibration experiments for these purified indicators can be performed in Tris buffers. The improved model for the pH_T of Tris buffer solutions at low salinities will enable more robust characterization of the equilibrium behavior of mCP. The pK_I [7] and $p(K_I e_2)$ [2] of mCP have been parameterized using Tris buffer solutions; the purified mCP model [2] has, in turn, been used to calibrate the $p(K_I e_2)$ of CR [8]. Work is underway at the National Institute of Standards and Technology

(NIST) to determine the pK_I of mCP using NMR spectroscopy. Harned cell and spectrophotometric measurements of mCP in Tris buffer solutions will also be used to more accurately characterize the pK_I of mCP [9]. A standardized pK_I determination for mCP across the full range of S and T will enable recalibrations of purified TB and CR.

6.2.3 Estuarine p(K_Ie_2) Model Evaluations for TB and CR

The p(K_Ie_2) models for TB and CR presented in Chapter Four have not yet been tested in marine or estuarine conditions. These models should be evaluated using field measurements of absorbances; field measurements of TA, DIC, and either f_{CO2} or pCO_2 will also enable calculations of thermodynamic internal consistency for pH measurements obtained according to the TB and CR models. For future internal consistency analyses in the estuarine salinity range, measurement data from carbon chemistry cruises can be archived for reevaluation when new carbonic acid dissociation constants are developed that are applicable for high-pCO_2 conditions.

6.2.4 Purification and Characterization of Sulfonephthalein Indicators

Easley and Place [10] have recently determined that seven different vendor-purchased sulfonephthalein indicators – mCP, TB, CR, Bromothymol Blue (BTB), Bromocresol Purple (BCP), Bromocresol Green (BCG), and Phenol Red (PR) – all contained impurity species. Currently, purifications have been performed for mCP [2, 11–13], TB [14], CR [11], and PR [12,13], but purification techniques should be developed for BTB, BCP, and BCG. Work is underway to characterize the p(K_Ie_2), e_1, and e_3/e_2 for TB across a range of S and T [14]. After purification, this work should also be performed for BTB, BCP, and BCG.

Because BCP is frequently used to measure TA [15,16] and its e_x's have only been given constant values with poor agreement among studies [15,17], parameterization is especially needed for BCP. Preliminary laboratory investigations point toward an e_3 of ~0.03 for BCP [14].

This relatively low e_3 value for BCP, as compared to other sulfonephthalein indicators, suggests that it may be strongly influenced by impurities. Spaulding et al. [18] report that the BCP used in a recent *in situ* analysis was only 90% pure and note that impurities can affect the molar absorptivity coefficient determination. For these reasons, the purification and characterization of BCP should be a priority.

Additionally, the effect of pressure on the p(K_1e_2) and e_x's of sulfonephthalein indicators should be determined [19], following the procedures outlined in Hopkins et al. [20] and Soli et al. [21]. This will enable these indicators' use in autonomous *in situ* instruments that can be deployed in marine and estuarine waters.

6.3 References

1. Yao, W., Liu, X., Byrne, R.H., 2007. Impurities in indicators used for spectrophotometric seawater pH measurements: Assessment and remedies. *Marine Chemistry* **107**, 167–172.
2. Liu, X., Patsavas, M.C., Byrne, R.H., 2011. Purification and characterization of meta-cresol purple for spectrophotometric seawater pH measurements. *Environmental Science & Technology* **45**, 4862–4868.
3. Fassbender, A.J., Alin, S.R., Feely, R.A., Sutton, A.J., Newton, J.A., Byrne, R.H., 2017. Estimating total alkalinity in the Washington coastal zone: Complexities and surprising utility for ocean acidification research. *Estuaries and Coasts* **40**, 404-418.
4. Patsavas, M.C., Byrne, R.H., Wanninkhof, R., Feely, R.A., Cai, W.-J., 2015. Internal consistency of marine carbonate system measurements and assessments of aragonite saturation state: Insights from two U.S. coastal cruises. *Marine Chemistry* **176**, 9-20.
5. Turner, D.R., Achterberg, E.P., Chen C-T.A., Clegg, S.L., Hatje, V., Maldonado, M.T., Sander, S.G., van den Berg, C.M.G., Wells, M. (2016). Toward a quality-controlled and accessible Pitzer model for seawater and related system. *Frontiers in Marine Science* **3**, 139.
6. DelValls, T.A., Dickson, A.G., 1998. The pH of buffers based on 2-amino-2-hydroxymethl-1,3-propanediol ('tris') in synthetic sea water. *Deep-Sea Research I* **45**, 1541-1554.
7. Mosley, L.M., Husheer, S.L.G., Hunter, K.A., 2004. Spectrophotometric pH measurement in estuaries using thymol blue and *m*-cresol purple. *Marine Chemistry* **91**, 175-186.

8. Patsavas, M.C., Byrne, R.H., Liu, X, 2013b. Physical-chemical characterization of purified cresol red for spectrophotometric pH measurements in seawater. *Marine Chemistry* **155**, 158-164.

9. Easley, R.A., Waters, J.F., Cai, W.J., 2018. OC14A-0392: ^{1}H-NMR study of acid-base equilibria of meta-cresol purple in artificial seawater tris buffers for oceanographic pH measurements. Abstracts of the 2018 Ocean Sciences Meeting, Portland, OR, 12 February 2018. <https://agu.confex.com/agu/os18/meetingapp.cgi/Paper/320499>.

10. Easley, R.A., Place, B.J., 2017. Mass spectra of sulfonephthalein pH indicator dyes and their impurities. *Journal of Research of the National Institute of Standards and Technology* **122**, 21.

11. Patsavas, M.C., Byrne, R.H., Liu, X., 2013a. Purification of meta-cresol purple and cresol red by flash chromatography: Procedures for ensuring accurate spectrophotometric seawater pH measurements. *Marine Chemistry* **150**, 19-24.

12. Lai, C.Z., DeGrandpre, M.D., Wasser, B.D., Branson, T.A., Clucas, D.S., Jaqueth, E.J., Benson, Z.D., Beatty, C.M., Spaulding, R.S., 2016. Spectrophotometric measurement of freshwater pH with purified meta-cresol purple and phenol red. *Limnology and Oceanography: Methods* **14**(12), 864-873.

13. Lai, C.Z., DeGrandpre, M.D., Wasser, B.D., Branson, T.A., Clucas, D.S., Jaqueth, E.J., Benson, Z.D., Beatty, C.M., Spaulding, R.S., 2017. Erratum: Spectrophotometric measurement of freshwater pH with purified meta-cresol purple and phenol red. *Limnology and Oceanography: Methods* **15**, 903.

14. Hudson-Heck, E., pers. comm.

15. Yao, W., Byrne, R.H., 1998. Simplified seawater alkalinity analysis: Use of linear array spectrometers. *Deep Sea Research Part I: Oceanographic Research Papers* **45**(8), 1383-1392.

16. Liu, X., Byrne, R.H., Lindemuth, M., Easley, R., Mathis, J.T., 2015. An automated procedure for laboratory and shipboard spectrophotometric measurements of seawater alkalinity: Continuously monitored single-step acid additions. *Marine Chemistry* **174**, 141-146.

17. Breland, J.A., Byrne, R.H., 1992. Determination of sea water alkalinity by direct equilibration with carbon dioxide. *Analytical Chemistry* **64**, 2306-2309.

18. Spaulding, R.S., DeGrandpre, M.D., Beck. J.C., Hart, R.D., Peterson, B., De Carlo, E.H., Drupp, P.S., Hammar, T.R., 2014. Autonomous in situ measurements of seawater alkalinity. *Environmental Science & Technology* **48**, 9573-9581.

19. Patsavas, M.C., 2014. *Improving spectrophotometric carbon system measurements.* University of South Florida.

20. Hopkins, A.E., Sell, K.S., Soli, A.L., Byrne, R.H., 2000. In-situ spectrophotometric pH measurements: the effect of pressure on thymol blue protonation and absorbance characteristics. *Marine Chemistry* **71**, 103-109.

21. Soli, A.L., Pav, B.J., Byrne, R.H., 2013. The effect of pressure on meta-Cresol Purple protonation and absorbance characteristics for spectrophotometric pH measurements in seawater. *Marine Chemistry* **157**, 162-169.

APPENDIX A

Copyright Permissions

Appendix A.1

Copyright permissions for Chapter Two

Copyright Clearance Center RightsLink®

Home | Create Account | Help

Title: Achieving accurate spectrophotometric pH measurements using unpurified meta-cresol purple

Author: N.K. Douglas,R.H. Byrne

Publication: Marine Chemistry

Publisher: Elsevier

Date: 20 March 2017

© 2017 Elsevier B.V. All rights reserved.

LOGIN

If you're a copyright.com user, you can login to RightsLink using your copyright.com credentials.

Already a RightsLink user or want to learn more?

Please note that, as the author of this Elsevier article, you retain the right to include it in a thesis or dissertation, provided it is not published commercially. Permission is not required, but please ensure that you reference the journal as the original source. For more information on this and on your other retained rights, please visit: https://www.elsevier.com/about/our-business/policies/copyright#Author-rights

BACK CLOSE WINDOW

Copyright © 2018 Copyright Clearance Center, Inc. All Rights Reserved. Privacy statement. Terms and Conditions.
Comments? We would like to hear from you. E-mail us at customercare@copyright.com

Appendix A.2

Copyright permissions for Chapter Three

APPENDIX B

Supporting Information for Chapter Three

Appendix B.1

Inputs used for polynomial fit of p(K_1e_2) across $0 \leq S \leq 40$ and $278.15 \leq T \leq 308.15$ K

For the p(K_1e_2) data calculated using the Lai et al. [1,2] and Liu et al. [3] models, S and T were equally spaced across their respective applicable ranges (T at intervals of 2 for Lai et al. [1,2]; S at intervals of 4 and T at intervals of 5 K for Liu et al. [3]). Weights were assigned to be inversely proportional to the number of values per source (n_{source}). A weight of 1 was arbitrarily assigned to the data calculated from Lai et al. [1,2] and other weights were calculated according to $W_{source} = (n_{Lai})\ (n_{source})^{-1}$.

Table B1.1 Inputs for polynomial p(K_1e_2) fit.

S	***T* (K)**	**p(K_1e_2)**	**Weight**	**Source**
0	281.15	8.463931	1	Lai et al. [1,2] calculated
0	283.15	8.443716	1	Lai et al. [1,2] calculated
0	285.15	8.423430	1	Lai et al. [1,2] calculated
0	287.15	8.403194	1	Lai et al. [1,2] calculated
0	289.15	8.383126	1	Lai et al. [1,2] calculated
0	291.15	8.363338	1	Lai et al. [1,2] calculated
0	293.15	8.343939	1	Lai et al. [1,2] calculated
0	295.15	8.325033	1	Lai et al. [1,2] calculated
0	297.15	8.306717	1	Lai et al. [1,2] calculated
0	299.15	8.289087	1	Lai et al. [1,2] calculated
0	301.15	8.272235	1	Lai et al. [1,2] calculated
0	303.15	8.256248	1	Lai et al. [1,2] calculated
20.00	278.15	7.940275	0.285714	Liu et al. [3], calculated
24.00	278.15	7.930115	0.285714	Liu et al. [3], calculated
28.00	278.15	7.922627	0.285714	Liu et al. [3], calculated
32.00	278.15	7.917812	0.285714	Liu et al. [3], calculated
36.00	278.15	7.915668	0.285714	Liu et al. [3], calculated
40.00	278.15	7.916196	0.285714	Liu et al. [3], calculated
20.00	283.15	7.875035	0.285714	Liu et al. [3], calculated
24.00	283.15	7.863559	0.285714	Liu et al. [3], calculated
28.00	283.15	7.854870	0.285714	Liu et al. [3], calculated
32.00	283.15	7.848970	0.285714	Liu et al. [3], calculated

36.00	283.15	7.845857	0.285714	Liu et al. [3], calculated
40.00	283.15	7.845532	0.285714	Liu et al. [3], calculated
20.00	288.15	7.811813	0.285714	Liu et al. [3], calculated
24.00	288.15	7.799001	0.285714	Liu et al. [3], calculated
28.00	288.15	7.789088	0.285714	Liu et al. [3], calculated
32.00	288.15	7.782076	0.285714	Liu et al. [3], calculated
36.00	288.15	7.777963	0.285714	Liu et al. [3], calculated
40.00	288.15	7.776750	0.285714	Liu et al. [3], calculated
20.00	293.15	7.750277	0.285714	Liu et al. [3], calculated
24.00	293.15	7.736113	0.285714	Liu et al. [3], calculated
28.00	293.15	7.724956	0.285714	Liu et al. [3], calculated
32.00	293.15	7.716807	0.285714	Liu et al. [3], calculated
36.00	293.15	7.711666	0.285714	Liu et al. [3], calculated
40.00	293.15	7.709533	0.285714	Liu et al. [3], calculated
20.00	298.15	7.690128	0.285714	Liu et al. [3], calculated
24.00	298.15	7.674596	0.285714	Liu et al. [3], calculated
28.00	298.15	7.662176	0.285714	Liu et al. [3], calculated
32.00	298.15	7.652869	0.285714	Liu et al. [3], calculated
36.00	298.15	7.646674	0.285714	Liu et al. [3], calculated
40.00	298.15	7.643591	0.285714	Liu et al. [3], calculated
20.00	303.15	7.631092	0.285714	Liu et al. [3], calculated
24.00	303.15	7.614179	0.285714	Liu et al. [3], calculated
28.00	303.15	7.600480	0.285714	Liu et al. [3], calculated
32.00	303.15	7.589994	0.285714	Liu et al. [3], calculated
36.00	303.15	7.582721	0.285714	Liu et al. [3], calculated
40.00	303.15	7.578661	0.285714	Liu et al. [3], calculated
20.00	308.15	7.572919	0.285714	Liu et al. [3], calculated
24.00	308.15	7.554614	0.285714	Liu et al. [3], calculated
28.00	308.15	7.539620	0.285714	Liu et al. [3], calculated
32.00	308.15	7.527937	0.285714	Liu et al. [3], calculated
36.00	308.15	7.519565	0.285714	Liu et al. [3], calculated
40.00	308.15	7.514504	0.285714	Liu et al. [3], calculated
0.06	298.15	8.210306	0.545454	Mosley et al. [4] data, corrected
0.13	298.15	8.177704	0.545454	Mosley et al. [4] data, corrected
0.27	298.15	8.132348	0.545454	Mosley et al. [4] data, corrected
0.54	298.15	8.082156	0.545454	Mosley et al. [4] data, corrected
1.01	298.15	8.027320	0.545454	Mosley et al. [4] data, corrected
1.50	298.15	7.986123	0.545454	Mosley et al. [4] data, corrected
2.00	298.15	7.953553	0.545454	Mosley et al. [4] data, corrected
3.04	298.15	7.909907	0.545454	Mosley et al. [4] data, corrected
4.03	298.15	7.876703	0.545454	Mosley et al. [4] data, corrected

4.98	298.15	7.852042	0.545454	Mosley et al. [4] data, corrected
7.51	298.15	7.801279	0.545454	Mosley et al. [4] data, corrected
10.00	298.15	7.766299	0.545454	Mosley et al. [4] data, corrected
14.99	298.15	7.718767	0.545454	Mosley et al. [4] data, corrected
20.02	298.15	7.685366	0.545454	Mosley et al. [4] data, corrected
20.26	298.15	7.684360	0.545454	Mosley et al. [4] data, corrected
24.98	298.15	7.666870	0.545454	Mosley et al. [4] data, corrected
30.01	298.15	7.653081	0.545454	Mosley et al. [4] data, corrected
30.03	298.15	7.653036	0.545454	Mosley et al. [4] data, corrected
35.02	298.15	7.644316	0.545454	Mosley et al. [4] data, corrected
35.04	298.15	7.644291	0.545454	Mosley et al. [4] data, corrected
39.99	298.15	7.640517	0.545454	Mosley et al. [4] data, corrected
39.99	298.15	7.640517	0.545454	Mosley et al. [4] data, corrected

Appendix B.2

References

1. Lai, C.Z., DeGrandpre, M.D., Wasser, B.D., Branson, T.A., Clucas, D.S., Jaqueth, E.J., Benson, Z.D., Beatty, C.M., Spaulding, R.S., 2016. Spectrophotometric measurement of freshwater pH with purified meta-cresol purple and phenol red. *Limnology and Oceanography: Methods* **14**(12), 864-873.
2. Lai, C.Z., DeGrandpre, M.D., Wasser, B.D., Branson, T.A., Clucas, D.S., Jaqueth, E.J., Benson, Z.D., Beatty, C.M., Spaulding, R.S., 2017. Corrigendum: Spectrophotometric measurement of freshwater pH with purified meta-cresol purple and phenol red. *Limnology and Oceanography: Methods*, doi: 10.1002/lom3.10210.
3. Liu, X., Patsavas, M.C., Byrne, R.H., 2011. Purification and characterization of meta-cresol purple for spectrophotometric seawater pH *measurements. Environmental Science & Technology* **45**, 4862-4868.
4. Mosley, L.M., Husheer, S.L.G., Hunter, K.A., 2004. Spectrophotometric pH measurement in estuaries using thymol blue and *m*-cresol purple. *Marine Chemistry* **91**, 175-186.

APPENDIX C

Supporting Information for Chapter Four

Appendix C.1

Corrected mCP p(K_1e_2) model test values.

Table C1.1 Corrected mCP p(K_1e_2) model test values.

Model	**Source**	**Equation**	**Test values (S = 35, T = 298.15 K, R = 1.0)**
pH_T	Liu et al. [1]	$pH_T = p(K_1e_2) + \log\left(\frac{R - e_1}{1 - R\frac{e_3}{e_2}}\right)$	7.66975
e_1	Liu et al. [1]	$e_1 = -0.007762 + 4.5174 \times 10^{-5}\, T$	0.00571
e_3/e_2	Liu et al. [1]	$e_3/e_2 = -0.020813 + 2.60262 \times 10^{-4}\, T + 1.0436 \times 10^{-4}\, (S - 35)$	0.05678
p(K_1e_2)	This work	$p(K_1e_2) = 5.567924 - 0.551542\, S^{0.5} + 0.126183\, S - 0.0290566\, S^{1.5} + 0.00363148\, S^2 - 0.000178371\, S^{2.5} + 53.204901\, S^{0.5}\, T^{-1} + 814.078293\, T^{-1}$	7.64685

Appendix C.2

References

1. Liu, X., Patsavas, M.C., Byrne, R.H., 2011. Purification and characterization of meta-cresol purple for spectrophotometric seawater pH *measurements. Environmental Science & Technology* **45**, 4862-4868.

APPENDIX D

Supporting Information for Chapter Five

Appendix D.1

Determination of TA^* offset

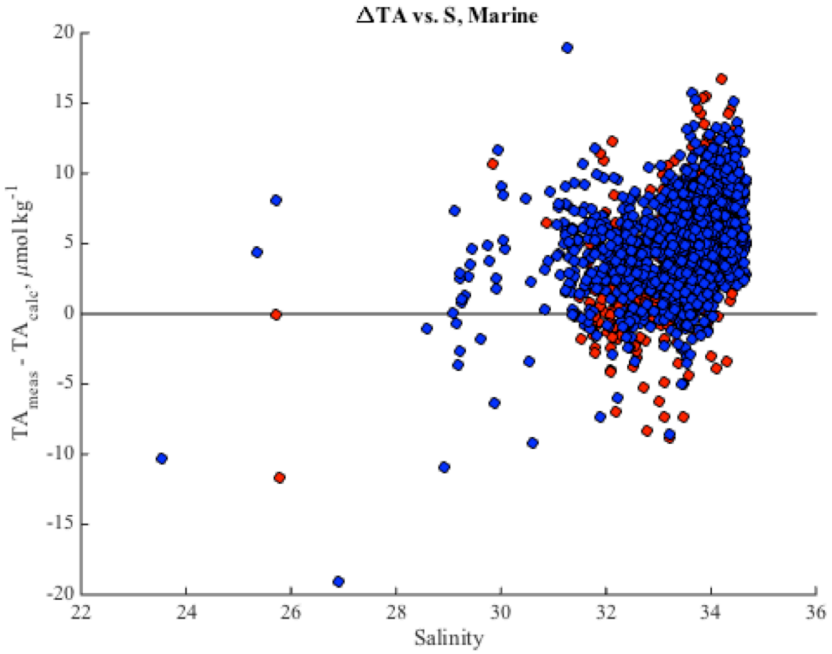

Fig. D1.1 ΔTA ($TA_{mes} - TA_{pH,DIC}$) vs. *S* for WCOA13 and WCOA16 data at marine salinities (*S* ≥ 20). Red points indicate WCOA13 data; blue points indicate WCOA16 data. The residuals are positive, with a mean offset of 4.5568 ± 3.7936 μmol kg^{-1}. This mean offset is used to calculate TA^*.